

Copyright  
by  
Oluwarotimi Folorunso  
2016

**The Thesis Committee for Oluwarotimi Folorunso Certifies that this is the approved  
version of the following dissertation:**

**Overexpression of Heat Shock Factor 1 Protects against Pathological  
Proteins in Neurodegenerative Diseases**

**Committee:**

---

James Lee, Ph.D., Chair

---

Anson Pierce, Ph.D., Mentor

---

Fernanda Laezza, Ph.D., M.D., Co-  
Mentor

---

Nigel Bourne, Ph.D.

---

Giulio Taglialatela, Ph.D.

---

Veronica Galvan, Ph.D.

---

---

David Niesel, Dean, Graduate School

**Overexpression of Heat Shock Factor 1 Protects against Pathological  
Proteins in Neurodegenerative Diseases**

**by**

**Oluwarotimi Folorunso, B.S.**

**Thesis**

Presented to the Faculty of the Graduate School of  
The University of Texas Medical Branch  
in Partial Fulfillment  
of the Requirements  
for the Degree of

**Doctor of Philosophy**

**The University of Texas Medical Branch  
October, 2016**

## Acknowledgements

I would like to thank my mentor, Dr. Anson Pierce for accepting me as a graduate student in his lab and supporting me through my thesis project. I am grateful for the opportunity. I have gained a lot of valuable experience.

I would like to thank Dr. James Lee and Dr. Fernanda Laezza for always believing in me and pushing me to be successful.

I would like to thank all of my committee members for their advice, patience and support, Dr. James Lee, Dr. Anson Pierce, Dr. Giulio Tagliatela, Dr. Fernanda Laezza, Dr. Nigel Bourne, and Dr. Veronica Galvan.

I would like to thank Dr. Mariano Garcia-Blanco for his support and provision of funds for me to complete my research work.

I would like to thank Dr. Shelton Bradrick for encouraging me and talking with me about my research work.

I would like to thank all the members of the Garcia-Blanco/Bradrick lab for allowing me to join their lab meetings, present and get feedback on my research work.

I would like to thank all of the members of Dr. Laezza's lab for their support, and I look forward to working with them as a postdoctoral fellow.

I am grateful to all the past members of the Pierce's lab, especially Dr. Pei-Yi Lin for her guidance and assistance with starting my thesis project and all her encouragements, and Samuel Umbaugh for his support.

I am thankful to everyone in the Biochemistry and Molecular Biology Program, in particular Dr. Tracy Toliver-Kinsky, JoAlice Whitehurst and Julie Quiroga who have supported me with my academic and research endeavors.

Lastly, I would like to thank my parents, siblings, cousins, friends, church members, and all the people I have met at UTMB.

# **Overexpression of Heat Shock Factor 1 Protects against Pathological Proteins in Neurodegenerative Diseases**

Publication No. \_\_\_\_\_

Oluwarotimi Folorunso, Ph.D.

The University of Texas Medical Branch, 2016

Supervisor: Anson Pierce

A classical feature of neurodegenerative disorders is the accumulation of protein aggregates, such as TAR DNA/RNA binding protein (TDP-43) and superoxide dismutase 1 (SOD1), which lead to neuronal dysfunction and loss. Therefore, molecules that maintain protein homeostasis may be beneficial therapeutic targets to correct the imbalance in protein folding and clearance in these disorders. Heat shock proteins (HSPs), such as HSP70 and HSP90 are molecular chaperones that maintain protein homeostasis and prevent neuronal death. HSPs are regulated by a stress-induced transcriptional factor, heat shock factor 1 (HSF1). HSF1 is inactive when in complex with HSP90 and becomes active once it is released from this interaction in the presence of misfolded proteins. Studies have shown that levels of multiple HSPs are reduced in the spinal cord of ALS patients, which suggests a decline in HSF1 activity, and could contribute to the accumulation of disease proteins. Targeted activation of HSF1 has raised tremendous interest as a potential target for therapeutic development. HSP90 inhibitors that target the HSF1-HSP90 complex, as well as drugs that are stress-induced HSF1 activators have been shown to prevent aggregation in neurodegeneration models; however, they also have toxic off-target effects. Furthermore, overexpression of constitutively active HSF1 reduced the accumulation of insoluble TDP-43 in cell culture; however, male mice overexpressing the active form had an infertility phenotype. This thesis reports that overexpression of wild-type HSF1 causes a robust induction of HSPs in response to proteotoxic stress, reduced toxicity and protected against TDP-43 and SOD1 disease-related pathology in cell culture and mice respectively. I have generated a new double transgenic mouse model to further investigate the protective mechanism of HSF1 overexpression against TDP-43 pathology, during the time of this work. The nuclear clearance of TDP-43 is a pathological phenotype seen in ALS and FTLTD, and my preliminary studies have shown that HSF1 induced a two-fold increase in nuclear TDP-43 in these double transgenic mice. These results have laid the framework for further research. This thesis provides new data supporting the therapeutic efficacy of targeting HSF1 levels for the treatment of TDP-43 proteinopathies and ALS.

## TABLE OF CONTENTS

List of Tables .....	xii
List of Figures .....	xiii
List of Illustrations .....	xv
List of Abbreviations .....	xvi
Chapter 1 Introduction .....	20
Neurodegenerative Diseases .....	20
Overview .....	20
Clinical Manifestation of neurodegenerative disease .....	21
Molecular pathways implicated in neurodegenerative diseases .....	22
Amyotrophic lateral sclerosis .....	25
Cu/Zn Superoxide dismutase (SOD1) .....	26
SOD1 in ALS .....	26
SOD1 Function .....	27
SOD1 Pathogenicity .....	27
Molecular pathways implicated in SOD1 .....	28
Tar DNA/RNA Binding protein (TDP-43) .....	28
TDP-43 in TDP-43 proteinopathies .....	28
TDP-43 Function .....	29
TDP-43 Pathogenicity .....	30
Molecular pathways implicated in TDP-43 .....	32
Heat shock factor 1 and neurodegenerative diseases .....	32
HSF1 Function .....	32
HSF1 Regulation .....	33
HSF1 Dysfunction in neurodegenerative diseases .....	34
HSF1 as a therapeutic target .....	35
Chapter 2 Heat shock factor 1 over-expression protects against exposure of hydrophobic residues on mutant SOD1 and early mortality in a mouse model of amyotrophic lateral sclerosis .....	38
INTRODUCTION .....	38

METHODS .....	42
SOD1 and HSF1 Transgenic Mice .....	42
BisANS assay .....	43
2D gel electrophoresis.....	44
Mass spectrometry .....	44
Western blotting.....	45
BisANS docking .....	46
Immunofluorescence microscopy .....	46
Statistical analysis .....	46
RESULTS .....	47
Soluble Mutant SOD1 in spinal cord extracts has increased surface hydrophobicity .....	47
Non-SOD1 proteins with altered surface hydrophobicity in soluble fractions of spinal cord from H46R/H48Q mice .....	50
BisANS docked to multiple sites around the metal binding region of H46R/H48Q SOD1 .....	52
SOD1 and chaperones enriched in detergent insoluble fractions .....	53
Effects of over-expression of HSF1 in H46R/H48Qx HSF1 mice .....	57
Discussion.....	61
CONCLUSION.....	68
Chapter 3 Overexpression of heat shock factor 1 maintains TAR DNA binding protein 43 solubility via induction of inducible heat shock protein 70 in cultured cells .....	70
INTRODUCTION .....	70
METHODS .....	73
Neuroblastoma Cell Culture .....	73
Primary Mouse Embryonic Fibroblast (MEF) Cells.....	74
Immunofluorescence Studies .....	74
Cell Lysate Collection and Preparation .....	75
Differential Detergent Fractionation.....	76
Antibody Characterization .....	77
Statistical Analysis.....	78
RESULTS .....	78

Enhanced heat shock response to TDP-43 overexpression.....	78
HSF1 overexpression prevents formation of TDP-43 puncta and maintains its solubility .....	80
HSF1 prevents accumulation of insoluble TDP-43 fragments .....	82
HSF1 protects against TDP-43 toxicity and proteotoxic stress .....	85
HSF1 activation does not enhance global protein turnover following proteasome inhibition .....	86
HSP70 is a major contributor to HSF1 mediated TDP-43 proteostasis...	88
DISCUSSION .....	91
Conclusion and Future Directions .....	94
PRELIMINARY STUDIES.....	94
METHODS .....	94
Generation of double transgenic mice (human HSF1 and human TDP-43) .....	94
Preparation of mouse brain lysate.....	95
Subcellular Fractionation.....	95
Real time-PCR.....	96
Western blotting.....	96
Behavioral Analysis.....	97
Statistical Analysis.....	97
RESULTS .....	98
DISCUSSION .....	104
CONCLUSION.....	107
FUTURE DIRECTIONS .....	108
REFERENCES .....	110



## **List of Tables**

Table 2.1: Protein identification and hydrophobic ratios.....	48
Table 3.1: List of antibodies used for experiments.....	76
Table 4.1: List of primer used for Real time-PCR.....	96

## List of Figures

Figure 2.1: Altered surface hydrophobicity of mutant SOD1 and non-SOD1 proteins in the spinal cords of symptomatic ALS mice. ....	49
Figure 2.2: BisANS docking SOD1. ....	50
Figure 2.3: Mutant SOD1 and chaperones co-fractionate in the detergent insoluble fractions. ....	51
Figure 2.4: Expression of HSF1 and distribution of HSPs in spinal cord. ....	53
Figure 2.5: Effect of HSF1 over-expression on body weight loss and healthspan of H46R/H48Q mice. ....	54
Figure 2.6: Effect of HSF1 over-expression on mutant SOD1 solubility. ....	55
Figure 2.7: Anterior horn region of lumbar spinal cord sections from mice at 220days. ....	56
Figure 2.8: Anterior horn region of lumbar spinal cord sections from mice at 220days. ....	60
Figure 2.9: Effects of HSF1 over-expression on measures of protein quality control in ALS. ....	61
Figure 3.1: Induction of HSPs. ....	79
Figure 3.2: Reduction of TDP-43-positive puncta. ....	81
Figure 3.3: HSF1 maintains TDP-43 solubility .....	83

Figure 3.4: HSF1 prevents accumulation of insoluble TDP-43 fragments. ....	84
Figure 3.5: HSF1 protects against CTF-induced toxicity.....	86
Figure 3.6: HSF1 activation does not increase global UPS activity and reduces induction of autophagy. ....	88
Figure 3.7: HSP70 inhibition reduces TDP-43 solubility and colocalizes with TDP- 43 pathology in human AD cortex.....	90
Figure 4.1: Total and subcellular localization of HSF1 in brain of TAR4/4 x HSF1 mice.....	98
Figure 4.2: Subcellular localization of SIRT1 in brain of TAR4/4 x HSF1 mice...	100
Figure 4.3: TDP-43 subcellular localization and levels in TAR4/4 x HSF1 mice..	101
Figure 4.4: Endogenous TDP-43 mRNA expression. ....	102
Figure 4.5: Increase in brain weight and no change in body weight.....	103
Figure 4.6: Wire hang test comparing TAR4/4 x HSF1 to TAR4/4. ....	104

## **List of Illustrations**

Illustration 1.1: Proteins associated with neurodegenerative diseases.....	21
Illustration 4.1: Generation of double transgenic mice overexpressing wild-type human TDP-43 and wild-type human HSF1 .....	95

## **List of Abbreviations**

AAV9	Adeno associated virus serotype 9
Actg1	cytoplasmic actin 2
AD	Alzheimer's disease
Ak1	adenylate kinase 1
Aldoc	fructose biphosphate aldolase C
ALS	amyotrophic lateral sclerosis
ANOVA	analysis of variance
ANS	1-Anilinonaphthalene-8-Sulfonic Acid
ATG7	Autophagy-related protein 7
BAG3	Bcl-associated athanogene 3
BCA	bicinchoninic acid
BisANS	4,4'-dianilino-1,1'-binaphthyl-5,5'-disulfonic acid
Cdc37	HSP90 co-chaperone/ cell division cycle protein 37
ChAT	choline acetyltransferase
CHIP	carboxyl terminus of Hsp70-interacting protein
CTF	C-terminal fragment
DTT	dithiothreitol
dpysl2	Dihydropyrimidinase-related protein 2
Eno1	alpha enolase
fALS	familial ALS
fFTLD	familial FTLD

FUS	fused in sarcoma
FTLD	frontotemporal lobar dementia
Gapdh	glyceraldehyde 3-phosphate dehydrogenase
GFP	green fluorescent protein
Gfap	glial fibrillary acidic protein isoform 1
HD	Huntington's disease
HDAC6	histone deacetylase 6
hnRNP	heterogeneous nuclear ribonucleoprotein
Hsc70	heat shock cognate 70
HSPs	heat shock proteins
HSP70	inducible heat shock protein 70
HSP90	heat shock protein 90
HSF1	heat shock factor 1
HSR	heat shock response
IRDye	infrared fluorescent Dye
KRIBB 11	N2-(1H-indazole-5-yl)-N6-methyl-3-nitropyridine-2,6-diamine
Ldhb	lactate dehydrogenase B-chain
LC3-II	membrane-bound microtubule-associated proteins 1A/1B light chain 3A
MALDI-TOF	matrix assisted laser desorption ionization time of flight
MEFs	mouse embryonic fibroblast
MG132	carbobenzoxy-Leu-Leu-leucinal
NES	nuclear exporting signal
NLS	nuclear localization signal

NMJ	neuromuscular junction
PanTDP-43	human and mouse TDP-43
PD	Parkinson's disease
P62	sequestosome-1
Pebp1	phosphatidylethanolamine-binding protein 1
Ppia	peptidyl prolyl isomerase A
Pgam1	phosphoglycerate mutase 1
Prdx6	peroxiredoxin 6
PI	propidium iodide
RRM	RNA recognition motif
SHSY5Y	Neuroblastoma
SIRT1	Sirtuin 1
SOD1	Cu/Zn superoxide dismutase 1
TAR4	hemizygous wild-type human TDP-43 overexpression transgenic mice
TAR4/4	homozygous wild-type human TDP-43 overexpression transgenic mice
TBST	Tris-buffered saline containing tween-20
TDP-43	TAR DNA binding protein 43
Thy1.2	T cell antigen 1 promote
TIA1	T Cell intracellular antigen-1
Tubb4b	Tubulin beta-4B chain
Ub-M-GFP	ubiquitin methionine GFP
Ub-R-GFP	ubiquitin arginine GFP
UCHL1	ubiquitin carboxy-terminal hydrolase L1

UPS	Ubiquitin Proteasome System
VER 155008	5'-O-[(4-Cyanophenyl)methyl]-8-[[[(3,4-dichlorophenyl)methyl]amino] – adenosine
WT	wild type
Ywhaz	14-3-3 protein zeta
Ywhag	14-3-3 gamma



# **Chapter 1 Introduction**

## **NEURODEGENERATIVE DISEASES**

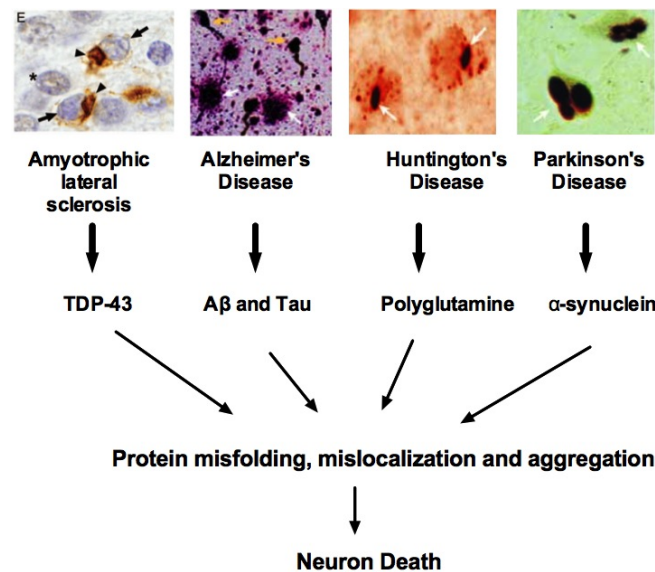
### **Overview**

Neurodegenerative disorders are characterized by gradual and permanent loss of neuronal activity or function that eventually leads to cell death. As the population ages and life expectancy increases, the prevalence of these diseases continues to increase dramatically. The prevalent neurodegenerative disorders are Alzheimer's disease (AD), Parkinson's disease (PD), Huntington's disease (HD) and amyotrophic lateral sclerosis (ALS). Today there are over five million people living with AD, one million with PD and 30 000 with ALS, in the United States. (Alzheimer's Association, PD Foundation, ALS Association) The socioeconomic burden of these devastating disorders is enormous and it is estimated that the cost of care for AD and other related dementias would be in excess of \$1 trillion in 2050 (Alzheimer's Association). There is no cure for these neurodegenerative disorders and the only drugs available target symptoms without addressing any of the mechanisms underlying the disease.

The classical feature of neurodegenerative disorders is the accumulation of soluble, functional proteins in aggregates in the brain and spinal cord. These disease-related protein aggregates can be found intracellularly in the cytosol, nucleus and endoplasmic reticulum as well as extracellularly [1].

The composition and conformation, cell types affected, as well as temporal and regional deposition of protein aggregates are distinguishing features between the various neurodegenerative diseases. (Figure 1.1) These differences likely underlie the variability

of clinical symptoms seen in patients, though the unifying characteristic of protein misfolding and dyshomeostasis among neurodegenerative disease could make therapeutic targets applicable to a variety of disorders.



Modified from Soto, 2003; Neumann, 2006

Illustration 1.1: Proteins associated with neurodegenerative diseases

Extracellular TAR DNA-binding protein 43 (TDP43) aggregates in ALS (arrow heads), extracellular amyloid plaques (amyloid beta) (white arrow) and intracytoplasmic hyperphosphorylated tau (yellow arrow) in AD, intranuclear polyglutamine in HD (white arrow) and intracytoplasmic alpha-synuclein aggregates in PD (white arrow).

### Clinical Manifestation of neurodegenerative disease

The clinical symptoms of neurodegeneration vary from motor defects to cognitive deficits, with many diseases showing multiple overlapping symptoms. The clinical manifestation of AD includes initial mild cognitive impairment eventually leading to

dementia, motor dysfunction and changes to personality. PD, on the other hand is commonly characterized as a movement disorder, with majority of patients also demonstrating cognitive symptoms including dementia, depression, anxiety, and hallucinations.

Chorea, dystonia, impaired postural reflexes, bradykinesia, cognitive decline, depression, obsessive-compulsive disorders and anxiety are associated with HD. Upper and lower motor neuron abnormalities and muscle atrophy are key features of ALS[2, 3] ; however, cognitive impairment is seen in some cases of ALS as well. Additionally, some patients develop both ALS and frontotemporal lobar dementia (FTLD) [2].

### **Molecular pathways implicated in neurodegenerative diseases**

The central theme of protein aggregation in these neurological disorders is linked to many underlying mechanism. Mitochondria are needed for ATP production, modulation of calcium flux is important for neuroplasticity, and apoptosis signaling[4]. Impaired mitochondrial dynamics can trigger oxidative stress, which is shown to alter protein conformation and could lead to aggregation[5].

Both autophagy and ubiquitin proteasome system (UPS), protein clearance pathways have been implicated in these disorders. Autophagy is important for the clearance of long-lived protein aggregated and recycling of damaged organelles [6]. Studies of post-mortem tissue have implicated autophagy as a critical factor for neurodegeneration [7]. Autophagy substrate, p62/sequestosome is present in ubiquitinated proteinaceous aggregates, and as such it is used as a marker for various neurodegenerative diseases[8, 9]. Mutations in autophagy genes, such as optineurin (OPTN) and p62, are causally linked to a small percentage of ALS [6, 10]. The UPS is

the degradative system for short-lived damaged proteins [11, 12]. The accumulation of ubiquitinated disease protein aggregates suggests a disruption of the UPS. Mutations in genes such parkin, ubiquitin ligase, and ubiquilin 2 (UBQLN2), ubiquitin shuttling protein are linked to PD[13] and ALS[14] respectively.

Recently, RNA homeostasis has emerged as an important mediator in neurodegenerative disorders. Various mutations in RNA binding proteins have been identified and linked as causative genes in certain cases of neurological disorders. Mutation to TARDBP (TAR DNA binding protein-43), fused in sarcoma (FUS) and others have all been identified in ALS [15]. Heterogeneous nuclear ribonucleoproteins (hnRNPs) A2B1 and A1, a RNA binding protein, in which mutations have been linked to multisystem proteinopathy and ALS [16]. These proteins are known to have low complexity domains (disorder regions) that are needed for their physiological function [17]. The presence of these regions makes them susceptible to aggregation [18].

One hypothesis is that age-related decline in the protein degradation machinery, and reduction in molecular chaperone levels makes protein susceptible to aggregation [19-22]. Heat shock proteins (HSP) are cellular chaperones that assist in the (re) folding and degradation of proteins [23, 24]. There is evidence showing that these proteins are decreased in ALS, AD and HD patients [20, 21, 25]. Heat shock proteins are differentially expressed in certain brain regions, which could predict the selective vulnerability of these areas[26]. Furthermore, neuronal and non-neuronal cells are shown to have different levels of HSPs, which may have implications for disease[27]. Mutations in HSP genes are associated with neuropathies, myopathies and retina degeneration [28]. HSP60 mutation is associated with axonal degeneration and hereditary spastic paraplegia

(SPG13)[29]. Mutations in several DNAJ proteins are linked diseases such as juvenile-onset Parkinsonism and cerebellar ataxia [30]. Furthermore, HSPB1 mutations are linked to axonal transport dysfunction in several neurological disease [28].

### **Mechanism of neuronal death**

Studying the mechanism of neuronal death in neurodegenerative diseases is challenging, as tissue for analysis is typically only available post-mortem at the late stages of the disease. For this reason *in vitro* and *in vivo* neurodegeneration models have been developed to better understand these pathways.

Apoptosis is a key cause of cell death in neurological disorders. Post-mortem tissue from AD patients shows increased levels of activated caspase-3, a marker for apoptosis[31]. In PD post mortem tissue, both the extrinsic and intrinsic apoptotic pathways are upregulated [32].

Excitotoxicity is a contributor to neuronal death through apoptosis. Accumulation of toxic aggregates is linked to calcium dyshomeostasis associated with numerous neurodegenerative diseases that cause aberrant neuronal firing eventually triggering apoptotic cell death [33]. Excess influx of calcium leads to hyperactive N-methyl-D-aspartate (NMDA), glutamate receptors seen in AD [34] and HD rodent models [35].

ER stress has also been shown to play a role in neuronal death. Accumulation of disease proteins can cause ER stress that induces downstream apoptotic cell death pathways in AD and ALS [36].

Autophagy is an uncommon cell death pathway. However, it is suggested that

mutations in autophagy genes, increased autophagy and defective clearance of autophagosomes could potentially initiate apoptotic events [37].

In summary, as disease progress there is a great deal of cross talk between cell death pathways, making it challenging to decipher how it initiates. There is some evidence in cell culture and animal models that disease-associated aggregated proteins are direct inducers of apoptosis [38].

### **Amyotrophic lateral sclerosis**

In 1869, French physician Jean-Martin Charcot defined ALS as a muscle degenerative disease [3]. It is called Lou Gehrig's disease in the United States [39]. In the United Kingdom, Australia and parts of Europe, motor neurone disease (MND) is used to define a group of disorders that includes ALS. ALS is a degenerative disease of upper and lower motor neurons and their axons in the brain and spinal cord, which leads to muscle degeneration, rapid progressive paralysis and death within three years of onset [2]. To date, there is no cure for ALS; however, there is only one FDA approved drug to treat this disease [40].

The two types of ALS, familial (fALS) and sporadic (sALS), comprise about 10% and 90% of all cases respectively [39]. The average age of onset varies between 50 to 65 years, while the prevalence doubles past the age of 80 [39]. However, 5% of cases have an early onset, before 30 years of age. Notably, the age of onset for fALS is about a decade earlier than sALS [39].

There are five core pathological subtypes of ALS and several underlying causal genes; these include ALS-SOD1 (superoxide dismutase 1), ALS-C9ORF72, (Hexanucleotide repeat expansion in C9ORF72) ALS-TDP-43, ALS-FUS (fused in sarcoma) and ALS-Guam.[41] Mutations in optineurin (OPTN), valosin-containing protein (VCP), ubiquilin 2 (UBQLN2), p62/sequestosome (SQSTM1), vesicle-associated

membrane protein-associated protein B (VAPB), charged multivesicular body protein 2B (CHMP2B), and profilin 1 (PFN1) are also linked to ALS [42]. In the past two years, two new genes have been discovered in ALS. TANK-binding Kinase 1 (TBK1) protein, which has a role in autophagy and immunity, and NIMA-related kinase 1 (NEK1), which plays a role in cell-cycle regulation[43].

There is some convergence of pathogenic mechanism of ALS and FTLD. FTLD is a type of dementia associated with changes in personality, language, behavior and cognitive (executive) function caused by neuronal loss in the frontal and temporal lobes of the brain [44]. Some patients with ALS show cognitive impairment (ALS-dementia) and about half of these develop FTLD[44]. FTLD has multiple subtypes, which include FTLD-tau, FTLD-DPR (dipeptide repeat protein), FTLD-UPS, FTLD-FUS and FTLD-TDP-43. C9ORF72 is an (GGGGCC) expansion repeat present in the C9ORF72 gene whose protein function is still unknown. It is associated with both fALS (~40%) and sALS (~10%), and fFTLD (25%) cases [45]. VCP mutations are responsible for 1-2% of fALS and FUS mutations are seen in 4% of fALS cases [46].

### **Cu/Zn Superoxide dismutase (SOD1)**

#### ***SOD1 in ALS***

The first disease causing SOD1 mutant was discovered in 1993 [3]. SOD1 mutation is seen in 20% of fALS and 3% of sALS [47]. To date, over 150 SOD1 mutations that have been discovered; however, the pathogenicity of all the mutants has not been completely studied [48]. SOD1 mutations were initially thought to disrupt its superoxide dismutase activity. Notably, not all mutations are associated with a reduction in SOD1 activity [49]. It is now widely accepted that SOD1 pathogenicity occurs through a toxic gain-of-function [50]. Mutant SOD1 is prone to aggregate and its presence in

humans has been replicated in rodent models, leading to selective loss of spinal motor neurons [51].

### ***SOD1 Function***

SOD1 is a 153 amino acid protein [47]. Its main function is to scavenge superoxides and turn them into molecular oxygen and hydrogen peroxide [3]. It is primarily localized to the cytoplasm and also to the nucleus, lysosomes, and inter-membrane space of the mitochondria [52]. It forms a homodimeric metalloenzyme with both zinc and copper ion catalytic site [52]. Its active form requires post-translational modification, acquisition of zinc and copper ion, disulfide bond formation and dimerization. Its metal binding function plays a limited role in its pathogenicity [53].

### ***SOD1 Pathogenicity***

In order to understand the toxicity of SOD1 alteration in disease, SOD1 knockout mice have been created [54]. Mice show variable results with a less overt neurodegenerative phenotype, and suggest that loss-of-function may only contribute to the disease and not initiate it [49]. On the other hand, overexpression of wild-type SOD1 in mice does not induce development of a motor phenotype [49]. Collectively, these two studies support the hypothesis for a gain-of-toxic function in ALS-SOD1. Using rodent models and patient samples there is evidence for neuronal and non-neuronal involvement in SOD1 pathogenicity. Expression of mutant SOD1 in glial cells showed aspects of ALS phenotype suggesting its contribution to the disease [55].



### ***Molecular pathways implicated in SOD1***

The presence of mutant SOD1 deposited in the outer membrane and matrix of mitochondria in the spinal cord of ALS patients has been implicated in mitochondrial dysfunction and toxicity [39]. In addition, mutant SOD1 has been shown to disrupt anterograde and retrograde axonal transport and induce toxicity [56].

Gliosis is implicated in SOD1 pathogenicity. There is an increase in activation of glial cells [57]. Surrounding mutant SOD1 neurons with wild-type glial cells protected them against cell death [5, 49].

Excitotoxicity associated with the reduction in astroglial glutamate transporter (EAAT2) has been observed in transgenic SOD1 mouse models and ALS patient tissue [58] [39].

### **Tar DNA/RNA Binding protein (TDP-43)**

#### ***TDP-43 in TDP-43 proteinopathies***

In 2006, there was the seminal discovery of immunoreactive TDP-43 RNA binding protein to be present in cytoplasmic ubiquitinated aggregates [59] Today, over 30 mutations have been discovered for TDP-43 [60]. Interestingly, most of these mutations cluster within the C-terminal region of the protein. TDP-43 mutations comprises of 1-3% of fALS cases, however, over 97% of ALS patients show accumulation of TDP-43 aggregates in both neurons and glial cells regardless of the genetic alterations [15]. This implies that mutations in other genes also trigger TDP-43 aggregation and highlights the importance of TDP-43.

### ***TDP-43 Function***

As its name implies, TDP-43 is a 43-kDa protein that is encoded by the TARBP gene. It is a conserved protein among different species and it is ubiquitously expressed. The presence of its two RNA recognition motifs, nuclear localization signal (NLS), nuclear export signal (NES) and the C-terminal disorder region suggests that it belongs to the heterogeneous nuclear ribonucleoproteins (hnRNPs) family [61].

TDP-43 is mainly located in the nucleus but shuttles between the two locations and is shown to have functions in both the nucleus and cytoplasm, where it has additional roles. Its nuclear functions have been thoroughly studied and they include transcription repression (mRNA targets), pre-mRNA maturation, splicing regulation of a large number of transcripts and microRNA biogenesis [41]. TDP-43 auto-regulates itself by binding to its own mRNA and tightly regulates its protein levels [62, 63]. More recently, its cytoplasmic functions were discovered to involve mRNA granule transport along axons to nerve terminals and this was shown in drosophila and induced pluripotent stem cells (iPS) from ALS patients (iPS) [64]. Furthermore, TDP-43 is involved in the formation of cytoplasmic stress granule (foci for repressed translation of mRNA) during cellular stress [65]. The disordered C-terminal domain of TDP-43 is needed for its physiological function in stress granule formation. However, this region has been shown to be involved in the accumulation of pathogenic TDP-43 aggregates [17, 18, 66].

In disease state, there is nuclear clearance of TDP-43 and cytoplasmic accumulation, fragmentation, aggregation and post-translational modifications. TDP-43 pathology is present in both the brain and spinal cord [67, 68].

TDP-43 pathogenicity has been debated between loss of function in the nucleus and cytoplasm, or a gain of toxic function, with evidence for both hypotheses [60, 64, 69].

### ***TDP-43 Pathogenicity***

#### *TDP-43 knockout*

TDP-43 knockout models have been generated to investigate whether TDP-43 toxicity in disease is due to a loss of function [69, 70]. Loss of TDP-43 function *in vivo* leads to phenotypes that suggest its may be a facet of disease pathogenicity. TDP-43 knockout in mice is embryonic lethal [70], however the heterozygous knock out only induce a mild phenotype as animals age [70]. Post-natal knockout of TDP-43 targeted specifically to motor neurons caused axonal and muscle atrophy, and motor dysfunction[69].

#### *TDP-43 cytoplasmic accumulation*

Nuclear clearance of TDP-43 and its cytoplasmic accumulation is seen in ALS, and is increased in the presence of mutations and cellular stress. Mice carrying a human TDP-43 transgene with a mutated NLS (hTDP-43 $\Delta$ NLS) signal showed loss of endogenous mouse TDP-43, cytoplasmic inclusions in many brain region, neuronal loss both in the brain and spinal cord, neuromuscular junction (NMJ) abnormalities, muscle atrophy, motor impairment loss of body weight and premature death[71]. Most importantly suppression of hTDP-43 $\Delta$ NLS expression after disease onset in these mice led to a rescue of endogenous nuclear TDP-43 protein, motor neuronal loss, motor impairment, NMJ abnormalities and an increase in lifespan[71].

#### *TDP-43 levels*

Overexpression of either the wild-type or mutant TDP-43 is pathogenic and displays a dose dependent toxicity. There is sufficient evidence showing that TDP-43 self-regulates its protein levels [62, 63]. In these overexpression models there is reduction in the

endogenous mouse TDP-43 protein levels, which makes defining the reason for the phenotype complex. Some studies have shown that lowering the endogenous mouse TDP-43 is not sufficient to cause a neurodegenerative phenotype. Meanwhile overexpression of wild-type hTDP-43 using a neuronal promoter Thy1.2, mouse prion promoter (brain and heart) or calcium/calmodulin dependent kinase CaMKII promoter (forebrain) all show variations in phenotypes such as upper and lower motor neuron degeneration, gliosis, rare TDP-43 inclusions, TDP-43 fragments and motor deficits, based on their levels and promoter region. [55, 72].

#### *TDP-43 fragments*

The contribution of TDP-43 pathology to disease is not completely understood. In cell culture, several laboratories including ours have shown that TDP-43 fragments are toxic to cells. Transgenic mice under the control of a Thy 1.2 promoter showed cognitive defects with no TDP-43 positive inclusions or degeneration [73], while AAV9 (adeno associated virus serotype 9) mediated transduction of TD-43 25kDa fragment showed some motor impairment[74].

#### *TDP-43 mutation*

The direct effect of TDP-43 mutations in animal models has been challenging to determine. Mouse models either overexpress wild-type or mutant human TDP-43, which cannot be directly compared due to varying levels of TDP-43 expression, which we now know, are critically important for toxicity [75]. However, one study showed that mutant

transgenic TDP-43 mice using a prion promoter drove pathology when crossed with wild-type TDP-43 [76]. The study reported the use of founder line with comparable levels of mutant or wild-type transgene accumulation.

#### *TDP-43 aggregation*

The role of TDP-43 aggregation in disease is unclear and its presence is not necessary for acquisition of a neurodegenerative phenotype in animal models. However, TDP-43 has been shown to trigger the accumulation of other ubiquitinated protein aggregates that could be toxic to the cells[72] and toxic oligomers have been detected in FTLN patients and transgenic mice[77].

#### *Molecular pathways implicated in TDP-43*

Levels of HSP70 and HSP40 in ALS patients and mouse models have been shown to be down regulated implying a disruption in their heat shock response pathway[20]. Recent studies show that TDP-43 accumulates in the mitochondria, which is increased by TDP-43 mutations. Importantly, suppression of TDP-43 localization to the mitochondria abolishes TDP-43 neurotoxicity[78]. A drug that targets the stress granule pathway was shown to reduce toxicity in an ALS drosophila model[79]. Additionally, elevated levels of ER stress have been detected in skin tissue from patients with TDP-43 mutation [80].

### **Heat shock factor 1 and neurodegenerative diseases**

#### *HSF1 Function*

The evolutionarily conserved heat shock proteins belong to a family of molecular chaperones that assist in protein folding, stabilization, transport and sorting, and disaggregation (protein homeostasis) under both physiological and pathological

conditions[81, 82]. Heat shock factor 1 (HSF1) is a highly conserved transcription factor for heat shock genes such as HSP110, 90, 70, 60, 40 and small HSPs families and other non-heat shock genes[82]. The synthesis of heat shock proteins under stressful conditions is known as the heat shock response (HSR), and it was first described as a biological response to elevated temperature[83]. HSF1 knockout mice lose the ability to induce the HSR, and are vulnerable to proteotoxic stress [24]. HSF1 knockout mouse fibroblast (MEFs) cells have a diminished ability to degrade ubiquitinated proteins [84].

Recent studies have focused on the role of HSF1 in non-HSP gene transcription [85], which includes regulation of cell survival genes [86]. HSF1 was recently discovered to induce neuroprotective pathway proteins, such as synaptic elements [87]

### ***HSF1 Regulation***

HSF 1 2, 3 and 4 all belongs to the HSF family [81]. HSF1 has multiple functional domains, which include an amino terminal helix-turn-helix DNA binding domain, a helical coiled-coil hydrophobic heptad repeat (HR-A/B) and a carboxy – terminal heptad repeat (HR-C), a regulatory domain (RD), and the transactivation domain[81]. The DNA-binding domain binds to nGAAn sequence within a cis- acting element referred to as the heat-shock element (HSE) on its DNA target. The heptad repeat domains regulate HSF1 trimerization. HR-A/B forms triple strand coiled-coil configuration and HR-C repeat prevent its spontaneous trimerization [81].

In the monomeric state, it forms a protein-protein complex with HSP90 and other proteins like p23 and cyclophilin where its activity is inhibited [88, 89]. HSF1 is activated by heat shock, accumulation of misfolded proteins, oxidative stress or other proteotoxic stresses. Misfolded proteins bind to HSP90, releasing HSF1 from its

inhibitory complex to be translocated into the nucleus where it is activated [82]. Furthermore, HSF1 activity is regulated by phosphorylation, sumoylation and acetylation. There are multiple phosphorylation sites on HSF1 [90]. Serine 303 and 307 are constitutively phosphorylated and are negative regulators of HSF1 activity. The most studied phosphorylation site for its activation is residue S326. Many kinases (such as CaMKII at S230) have been shown to phosphorylate HSF1 under different proteotoxic conditions [91-93]. Recent work has questioned the idea that HSF1 activation is driven by its phosphorylation with studies showing that HSF1 phosphorylation is not necessary for nuclear translocation and DNA binding. These results suggest that additional markers should be used when determining HSF1 activation [90]. Sirtuin 1 (SIRT1), a NAD-dependent histone deacetylase, positively regulates HSF1 binding. HSF1 is negatively regulated by p300 at lysine residue 80 in its DNA binding domain [94].

### ***HSF1 Dysfunction in neurodegenerative diseases***

Multiple laboratories have provided evidence showing HSF1 levels and the HSR, stress response system, are altered in cell culture, animal models and most importantly, post-mortem brain tissue in multiple neurodegenerative diseases [21, 22, 84, 95]. Synucleinopathy patients show reduced levels of HSF1. Cell culture and animal models of either wild-type or mutant  $\alpha$ -synuclein protein overexpression also show similar results. Furthermore, these cellular models show that there is an increase in HSF1 degradation regulated by NEDD4 [96]. HSF1 and HSP70 protein levels are significantly reduced in cell culture and knock-in polyglutamine expanded mouse models of HD [21]. HSF1 knock out mice showed some neurodegenerative phenotypes that include demyelination, enlarged lateral and third ventricle, gliosis and changes in

locomotive function that resembled PD, AD, and ataxia associating HSF1 dysfunction with varied neurodegenerative diseases [97] [84]. More recently, a TDP-43 mouse model was shown to have reduced HSF1 and HSPs (70 and 40) levels, while HSF1 levels were not reduced in ALS patients there was a significant reduction of HSP70 and HSP40 levels[20].

### ***HSF1 as a therapeutic target***

Most of the clinical trials and FDA-approved drugs for neurodegenerative diseases only target the symptoms of these diseases and not their underlying causes. Developing drugs that target protein misfolding might prove to be ideal in treating ALS and other neurodegenerative diseases. Overexpression or drug-induced activation of individual HSP proteins have been shown to have beneficial results in some neurodegenerative models while others had no effect. However, cell culture studies show that expression of multiple chaperones has an enhanced effect over individual chaperones [86, 98, 99]. We now know that HSPs work in hetero-complexes that are needed for their function, making HSF1 a better target. Various strategies have been used to target HSF1 to induce its activity, prolong its activity or lower the threshold of its activation.

### ***HSF1-HSP90 complex***

Several drugs have been used to target the HSF1-HSP90 complex, by inhibiting HSP90, and releasing HSF1. Well-known HSP90 inhibitors, which include geldanamycin and its derivatives, bind to the HSP90 ATP binding pocket and inhibit its activity. This drug has been shown to induce HSF1 –dependent chaperone genes. Geldanamycin has also been shown to reduce aggregation and toxicity in different cell culture models of



neurodegenerative diseases [100, 101], however high levels of HSP90 inhibitor are toxic, because of effects to HSP90 client proteins, which include kinases.

#### *HSF1 activation*

Celastrol is a quinone methide triterpene compound that has been suggested to bind to HSP90 C-terminal domain, and inhibits its interaction with Hsp90 co-chaperone Cdc37 protein [102]. It causes the activation of HSF1 and has shown protection beneficial effects against disease protein aggregation in neurodegenerative disease models such as AD mice; however, it can also be toxic [86, 103-105]. Its mode of action is not completely understood, but it is HSF1A is a benzyl pyrazole derivative, which induces HSF1-dependent chaperone proteins [86, 106]. Its mode of action is thought to be through altering protein chaperone complexes, but has been shown to alleviate polyglutamine dependent toxicity in flies [107].

#### *HSF1 overexpression*

There are some benefits to overexpression of constitutively active HSF1, it has been shown to effectively reduce insoluble and hyper-phosphorylated TDP-43 levels [20] and protects against polyglutamine aggregates in cell culture and mouse models[99]. However, overexpression of the constitutively active form of HSF1 caused infertility in male mice [108]. Previous work had suggested that overexpression of wild-type HSF1 had no amplified effect in protecting against proteotoxic insult [95]. However, our laboratory found that overexpression of the wild-type HSF1 protected against protein aggregates in multiple neurodegenerative disease models [109-111].

### *Post-translational modification*

Certain drugs prolong HSF1 activity with no effect on its activation. Sirtuin 1 (SIRT1), deacetylase, targets HSF1 and increases its activity by increasing access to bind to its target DNA[94]. Both drug-induced activation of SIRT1 using resveratrol [112], and SIRT1 overexpression [113] has shown beneficial effects against ALS phenotype in mutant SOD1 mice. SIRT1 strategy is useful but may have some off-target, given that is a deacetylase for multiple proteins.

## **Chapter 2 Heat shock factor 1 over-expression protects against exposure of hydrophobic residues on mutant SOD1 and early mortality in a mouse model of amyotrophic lateral sclerosis**

### **INTRODUCTION**

It has been proposed that exposure of hydrophobic surfaces increases the propensity of non-native proteins to oligomerize and form aggregates in a wide range of age-associated neurodegenerative diseases including amyotrophic lateral sclerosis (ALS), Alzheimer's (AD), Parkinson's (PD), and Huntington's diseases. ALS is the most common adult motor neuron disease characterized by progressive degeneration of motor neurons, which results in muscle atrophy and weakness, followed by paralysis and death. A number of different mutations in genes encoding Cu/Zn superoxide dismutase (SOD1) [114], TAR DNA binding protein 43 (TDP-43) [115], and 17 others are associated with familial forms of ALS (fALS), which make up 10% of total ALS cases. The first known genetic link to fALS was SOD1, which is responsible for 20% of familial cases, and over 150 mutations in SOD1 have been described [54]. SOD1 mutations can be grouped into two families based on their biophysical effects to the protein: pseudo-wild-type mutants which retain metal binding and enzyme activity, and metal binding region mutants such as H46R/H48Q, which have only partial to no metal binding ability and reduced or no enzyme activity [116, 117]. Despite being responsible for the disproportionation of superoxide radicals to oxygen and hydrogen peroxide, mutations in SOD1 are known to be toxic due to a gain of function rather than a loss of function [118]. Increased surface hydrophobicity of SOD1 mutants is a common feature [119, 120] and may be important

in gain of functionality through a structure-function relationship, however the degree to which soluble mutant SOD1 is misfolded *in situ* is unknown and difficult to measure using conventional assays. Changes in protein surface hydrophobicity are important because exposure of hydrophobic domains may facilitate the formation of new protein-protein interactions and aggregation of proteins which are observed in all cases of ALS. If allowed to persist *in vivo*, surface exposed hydrophobic domains could lead to formation of oligomers or seeding of amorphous or fibrillar protein aggregates that correlate with cellular toxicity [121, 122]. Importantly, substrate specificity of major heat shock proteins (HSPs) is dictated by sequence-specific hydrophobic amino acids that frequently occur in proteins but are usually buried and not surface-exposed [123-126]. Thus, exposed surface hydrophobicity is a significant recognition signal for HSP binding and subsequent re-folding or degradation by chaperones and co-chaperones via the ubiquitin proteasome system (UPS) [23] or autophagy [127].

Soluble, conformationally altered proteins and those with increased surface hydrophobicity are difficult to measure and screen for in biological samples without prior fractionation and purification, and available methods are not amenable to locating the specific domains where unfolding occurs. In addition, difficulties in replicating the off-pathway folding events that occur *in vivo* [128] make measuring conformationally altered species *in situ* advantageous. To address these difficulties, we have previously developed a novel fluorescence-based proteomic assay using 4,4'-bis-1-anilinonaphthalene-8-sulfonate (bisANS) that can detect changes in protein conformation on the basis of changes in protein surface hydrophobicity from soluble *in situ* tissue proteomes [129, 130]. Using this assay we have found that changes in protein conformation do occur in

skeletal muscle during ALS progression, experimental denervation, and muscle injury [129, 131, 132], and that the bisANS incorporation sites can be mapped onto proteins [132] for further targeting studies with conformation-specific antibodies [133], or other methods. In this study, we measure changes in surface hydrophobicity of proteins from the spinal cords of H46R/H48Q mice in order to examine the *in situ* surface hydrophobicity of soluble mutant SOD1 and non-SOD1 proteins from this model. By covalently labeling proteins with the conformation-sensitive dye bisANS, which fluoresces when it binds to apolar surfaces, we have found that the H46R/H48Q mutation in SOD1 provokes formation of high molecular weight SOD1 species with a lower solubility due to increased exposure of hydrophobic surfaces. Furthermore, we have uncovered changes in the surface hydrophobicity profile of 16 non-SOD1 proteins that are involved in energy metabolism pathways, cytoskeletal framework/cell mobility, signaling, and protein quality control systems.

Heat shock factor 1 (HSF1) is a 57kDa member of the HSF family, and is the major regulator of HSP expression [134]. Given that HSPs are cytoprotective and recognize exposed surface hydrophobicity in their selection of substrates, HSF1 is an attractive pharmacological target. Several pharmacological activators of HSF1 are known, and function through inhibition of the proteasome or negative regulators of HSF1, such as HSP90. The hydroxylamine compounds bimoclomol and arimoclomol prolong the activation of HSF1. Arimoclomol was tested on the G93A mouse model of ALS and it was found to increase lifespan by 22% [135] and is currently in phase 2/3 clinical trials for ALS [136]. The arimoclomol treated mice had elevated levels of HSP70 and 90 compared to untreated G93A mice, suggesting that HSP expression

through the HSF1 system was protective in ALS, however it is unknown whether metal binding region mutants will be protected by enhancing protein homeostasis. Riluzole, an FDA approved drug to treat ALS has been shown to increase latent HSF1 levels and enhance the heat shock response (HSR) [40, 137]. Importantly, increasing levels of HSF1 by the use of transgenes [138] or through glutamine and the CAAT enhancer-binding protein- $\beta$  (C/EBP- $\beta$ ) [139], are alternate ways to upregulate HSF1 and enhance the HSR due to titration of the HSF1 inhibitor HSP90. This is especially important for motor neurons, which are reported to have a high threshold for activation of HSF1 [95]. Several studies have shown that the over-expression of HSF1 extends lifespan and protects against various types of pathologies. For example, in *C. elegans* over-expression of HSF1 extends lifespan [140], while its inhibition shortens lifespan. Activation of HSF1 using the HSP90 inhibitor 17-N-allylamino-17-demethoxygeldanamycin (17-AAG) led to an extension in lifespan of a drosophila model of ALS, owing to the upregulation of the drosophila ortholog of  $\alpha$ B-crystallin [141]. We and others have demonstrated a protective role of HSF1 against protein misfolding and aggregation in other neurodegenerative diseases, including AD [110], Huntington's disease [99], and prion diseases [142]. Taken together, these studies confer the beneficial effects of an HSF1-based ALS therapy and an important role of the HSF1-mediated HSR in protecting against ALS.

We have created a transgenic mouse that over-expresses human HSF1 (HSF1<sup>+0</sup>) 2-4 fold in all tissues especially the CNS [138]. We have shown that HSF1<sup>+0</sup> mice have an enhanced HSR [138], and are protected from AD-like deficits in memory [143]. In the current study, the effect of HSF1 over-expression in a mouse model of ALS was

examined and found to significantly delay loss of bodyweight, disease onset, early disease, and survival in the 25<sup>th</sup> percentile suggesting that enhanced control of protein surface hydrophobicity by upregulating HSF1 is a potential target for the treatment of ALS and other proteinopathies.

## **METHODS**

### **SOD1 and HSF1 Transgenic Mice**

Mice were housed in a temperature and humidity-controlled vivarium at the Audie L. Murphy VA Hospital. Wild type transgenic human SOD1 (WT TG) mice were backcrossed to C57B6/J mice 4 times. The SOD1 H46R/H48Q mutant mice (H46R/H48Q) were generated by David Borchelt (line 139) [144] on a C3HeJ B6 background and backcrossed over 10 generations to a C57BL/6J background in our facility. HSF1<sup>+/-</sup> were derived and maintained on a C57BL/6 background, and the generation of these mice has been described previously [138]. Male H46R/H48Q breeders were mated with female HSF1<sup>+/-</sup> mice to generate mice for the survival cohorts, and the lifespans of the male breeders were monitored to ensure they did not deviate from parental lines due to mutant SOD1 copy loss. Offspring were genotyped to obtain double transgenic mice that contained both mutant H46R/H48Q and the HSF1 transgene (H46R/H48QxHSF1). Genotyping was performed by PCR using primers specific for the human SOD1 gene [114] and as previously described for the human HSF1 transgene [138]. Body weight measurements began when mice reached the age of 120 days and recording was performed bi-weekly until death (n=19/genotype). Disease onset was calculated as the day a mouse reached its maximal bodyweight, while early disease is defined as the day at which a 10% decrease in its maximal bodyweight was observed, and

survival is determined at the day at which a mouse is unable to right itself when place on its side for 30s [145, 146]. All procedures for handling animals in this study were reviewed and approved by the Institutional Animal Care and Use Committee (IACUC) of the Audie L. Murphy Memorial Veterans Hospital.

### **BisANS assay**

Covalent UV photolabeling of bisANS to proteins was performed essentially as described [132]. Briefly, soluble fractions (S1) of spinal cord tissue were isolated on ice by homogenization of tissue with 5 volumes of bisANS labeling buffer (50mM Tris 10mM MgSO<sub>4</sub> pH 7.4 plus protease inhibitors) followed by centrifugation at 100,000g for 1hr at 4°C. It has been shown that incubation of proteins with high dye:protein ratios of 100:1 or more can induce conformational changes in some proteins [147]. Therefore in all comparisons, we labeled 1mg/ml solutions of cytosolic protein with 200μM bisANS with a handheld 365nm UV lamp (UVP, Upland, CA) for 30 minutes on ice in a 96-well plate with non-mutant SOD1 over-expressing mice as controls. At this protein concentration it was estimated that the dye:protein ratio was approximately 8:1 based on abundance and molecular weights of Sypro Ruby spots in 2D gel profiles. BisANS labeled proteins were then precipitated 1:1 with 20% trichloroacetic acid. Precipitates were centrifuged at 4°C at 18,000g for 30min, and pellets were washed twice by disrupting with ice cold 1:1 ethanol:ethyl acetate. Cleaned pellets were dried and then dissolved in 6M urea, 4% CHAPS, 0.4% ampholytes. For SDS PAGE gels, 15μg of protein was diluted in 6X laemmli buffer and separated on 15% polyacrylamide gels. Following electrophoresis, gels were imaged for bisANS and stained with Sypro Ruby.



## **2D gel electrophoresis**

Following determination of protein concentration by BCA assay, 4 $\mu$ l of destreak reagent (GE Health) was added to 200 $\mu$ g of bisANS labeled protein, which was focused on 4-7 immobilized pH gradient (IPG) strips for 12hr. Focused IPG strips were then washed in equilibration buffer (50 mM Tris buffer pH 8.8, 6M urea, 30% glycerol, 2% SDS) containing 10mg/ml dithiothreitol (dTT) for 15 min followed by 25mg/ml iodoacetamide. Equilibrated strips were then separated on 15% polyacrylamide gels, placed in 10% methanol at 4°C, and visualized for bisANS fluorescence on a UV imager with a 365nm illumination source for 30 seconds (AlphaImager). 2D gels were placed in fixing solution (10% methanol 7% acetic acid) for 1hr and then stained in Sypro Ruby overnight with gentle agitation. Following destaining with fixing solution, gels were placed in doubly deionized water for 1hr and then imaged for Sypro Ruby fluorescence on a Typhoon 9410 imager (GE Health). BisANS and corresponding Sypro Ruby spots were matched and quantitated by densitometry using Imagequant (Molecular Dynamics). Hydrophobic ratios were determined by dividing the bisANS densitometric value by corresponding Sypro Ruby densitometric values. The mean hydrophobic ratios for each group were then compared using one-way ANOVA. Spots with significantly different hydrophobic ratios were picked using an ExQuest spot cutter (Biorad).

## **Mass spectrometry**

Picked spots were digested in gel with sequencing grade trypsin (promega) overnight at 37°C. Peptide digests were then spotted to a target with  $\alpha$ -cyano-4-hydroxycinnamic acid, and identified by matrix-assisted laser desorption ionization time of flight (MALDI-TOF) mass spectrometry (Voyager STR, Applied Biosystems). Peak lists were generated

by Data Explorer version 4.0.0.0 (Applied Biosystems) using advanced baseline correction peak width parameters of 32, flexibility of 0.5, and degree of 0.1; noise filter parameter of 0.7; gaussian smooth parameter of 5; noise reduction parameter of 2.00. Trypsin autocatalytic peaks were used to internally calibrate spectra, and were excluded from peak lists for Mascot database searches. Peptide mass fingerprints were then searched using Mascot (Matrix Science) and the NCBI nr 10/01/2012 database allowing 1 missed cleavage site. Variable modifications of carbamidomethylated cysteine and oxidation of methionine were included and a peptide mass tolerance of 100 ppm was used.

### **Western blotting**

Insoluble material remaining from homogenized spinal cords was sequentially extracted with detergents of increasing ionic strength as described previously [132]. In brief, after centrifugation of tissue homogenates at 100,000g the pellet was sonicated in bisANS labeling buffer to remove cytosolic proteins and re-pelleted at 100,000g for 30min. Next, pellets were extracted in the same buffer containing 0.5% Nonidet P40 by sonication and re-pelleted at 100,000g for 30min. This supernatant was termed P1. The remaining pellet was then sonicated in P1 buffer containing 0.25% SDS and 0.5% deoxycholate to isolate the P2 fraction, then P1 buffer containing 2% SDS and 0.5% deoxycholate to isolate the P3 fraction. Protein extracts were then boiled in non-reducing or reducing Laemmli buffer where indicated, and separated by 15% SDS PAGE followed by a 2hr wet transfer at 100V to polyvinylidene fluoride membranes (Biorad). Membranes were blocked in 5% milk Tris-buffered saline containing tween 20 (TBST) containing 20mM Tris, 137mM NaCl, and 0.4% tween 20 for 30min at room temperature. Membranes were incubated with sheep anti-human SOD1 (1:1000, Calbiochem), mouse anti-UCHL1 (1:5,000

Abnova#H00007345-M01), mouse anti-Hsp70 (1:10,000, Stressgen; SPA-810), rabbit anti-HSF1 (1:10,000 dilution, Stressgen;SPA-901), heat shock cognate 70 (Hsc70) (1:20,000 dilution, Stressgen SPA-815), rabbit anti-LC3 (1:2,500 dilution, Cell Signaling#2775), rabbit anti-CHIP (1:1000, Cell Signaling#2080), rabbit anti- $\alpha$ B-crystallin (1:2000, Abcam #ab13497), overnight at 4°C with gentle agitation.

### **BisANS docking**

BisANS was docked to SOD1 (dimeric WT metallated: [2C9V] or monomeric apo H46R/H48Q:[3GQF]) using Autodock Vina [148]. Docked pdb files were generated and rendered by RasMol version 2.7.5.2.

### **Immunofluorescence microscopy**

Mice were perfused transcardially with PBS and spinal cords were excised and fixed in PBS containing 4% paraformaldehyde at 4°C until processing. Lumbar regions of the spinal cord were imbedded in optimal cutting temperature compound and sectioned at 30 $\mu$ m and affixed to poly-D-lysine coated slides. Sections were blocked in 4% goat serum in TBST and stained with choline acetyltransferase (1:250), glial fibrillary acidic protein (1:500), SOD1 (1:500) Heat shock protein 70 (1:500), or  $\alpha$ B-crystallin (1:500) overnight at 4°C in 1% goat serum in TBST. Primary antibodies were visualized with secondaries conjugated with Alexa 350, 488, or 594 at 1:250 in 1% goat serum in TBST. Slides were imaged with an Olympus IX51 fluorescence microscope.

### **Statistical analysis**

2D gel data were analyzed for significance using one-way ANOVA. Post hoc tests were performed using Tukey's test at a significance value of 0.05. For those spots with

significantly different hydrophobic ratios compared to WT TG, the mean Sypro Ruby intensity and Western blot densitometric analyses were compared between WT TG and H46R/H48Q using a student's t test. Disease onset, early disease, and survival curves were compared using the log-rank test (Wilcoxon).

## **RESULTS**

### **Soluble Mutant SOD1 in spinal cord extracts has increased surface hydrophobicity**

In order to assess the global distribution of proteins with altered exposure of surface hydrophobicity in the spinal cords of symptomatic ALS mice, the soluble S1 fraction was labeled with bisANS and separated by 2D gel electrophoresis (Figure 2.1A). As shown in Figure 2.1B spots corresponding to human SOD1 were identified by MALDI-TOF mass spectrometry (Table 2.1) and further confirmed by Western blot using unlabeled spinal cord extracts as specific for SOD1 (data not shown). These spots specific for SOD1 were then quantitated for their bisANS fluorescence and normalized for protein by Sypro Ruby in order to determine their hydrophobicity ratio (Figure 2.1B and C). We observed that SOD1 separated into multiple spots with different isoelectric points, as previously shown by others in unlabeled extracts [149]. SOD1 spot numbers 153, 151, and 149 (Figure 2.1B&C) showed significant increases in the hydrophobic ratio compared to WT SOD1. Increased surface hydrophobicity of mutant SOD1 suggests that it may have increased propensities for aggregation and/or toxicity [150].

Table 1 Protein identification table and hydrophobic ratios

Protein Name	Accession #	Mass Values Searched	Mass Values Matched	Mowse Score	Probability of false hit	Percent Sequence Coverage	Fold H46R/H48Q /WT TG Sypro	Fold H46R/H48Q /WT TG BisANS:Sypro	P value
Heat shock cognate 71 kDa protein (Hsc70)	P63017	44	15	108	2.3e-06	28	1.43 (0.06)	1.37*	0.0001
		36	13	86	4.1e-04	25			
		85	19	96	3.4e-05	33			
		102	25	110	1.4e-06	37			
Dihydropyrimidinase-related protein 2 (Dpysl2)	O08553	27	9	70	1.5e-02	19	1.33 (0.16)	2.06*	0.0080
		52	12	71	1.2e-02	24	1.24 (0.31)	2.19*	0.0256
Glial fibrillary acidic protein isoform 1 (Gfap)	P03995	87	24	148	2.3e-10	46	0.95 (0.32)	1.91*	0.0119
Tubulin beta-4B chain (Tubb4b)	P68372	45	13	97	2.6e-05	27	1.25 (0.33)	2.08*	0.0062
Alpha-enolase (Eno1)	P17182	37	18	183	7.2e-14	42	0.99 (0.98)	3.08*	0.0118
Actin, cytoplasmic 2 (Actg1)	P63260	76	16	101	1.1e-05	45	1.62 (0.01)	0.84	0.0467
		29	9	80	1.5e-03	30	1.63 (<0.01)	0.72*	0.0020
Fructose-bisphosphate aldolase C (Aldoc)	P05063	33	15	138	2.3e-09	45	1.13 (0.65)	1.13	0.0128
		65	16	116	3.6e-07	46	0.96 (0.92)	2.98*	0.0189
L-lactate dehydrogenase B chain (Ldhb)	P16125	35	9	76	3.5e-03	20	1.00 (0.99)	1.67*	0.0284
		46	10	77	2.6e-03	28	1.11 (0.64)	1.21	0.7792
Phosphoglycerate mutase 1 (Pgam1)	Q90BJ1	37	9	85	4.5e-04	46	1.64 (0.20)	2.07*	0.0136
		29	11	125	4.6e-08	52	1.42 (0.16)	1.14	0.6404
14-3-3 zeta (Ywhaz)	P63101	67	13	80	1.6e-03	35	3.25 (<0.01)	0.35***	0.0006
14-3-3 protein gamma (Ywhag)	P61982	55	12	78	2.3e-03	31	2.26 (<0.01)	0.47***	0.0001
Peroxiredoxin-6 (Prdx6)	O08709	39	15	135	4.6e-09	53	1.48 (0.02)	0.75*	0.0442
Ubiquitin carboxy-terminal hydrolase L1 (Uchl1)	Q9R0P9	40	10	75	4.2e-03	42	2.28 (0.02)	0.55*	0.0141
		28	10	90	1.6e-04	42	2.11 (0.04)	0.57**	0.0006
Adenylate kinase isoenzyme 1 (Aki1)	Q9R0Y5	15	6	73	7.6e-03	37	1.33 (0.48)	0.59*	0.0113
Phosphatidylethanolamine-binding protein 1 (Pebp1)	P70296	15	6	82	8.1e-04	48	1.82 (0.04)	0.66*	0.0179
		12	5	70	1.5e-02	36	1.36 (0.20)	0.85	0.6637
Peptidyl-prolyl cis-trans isomerase A (Ppia)	P17742	56	18	113	7.2e-07	57	0.76 (0.37)	1.62	0.0356
		48	14	91	1.1e-04	40	1.11 (0.76)	4.44**	0.0106
Human Cu, Zn Superoxide Dismutase (SOD1)	P00441	40	8	76	7.0e-03	47	0.42 (<0.01)	1.75*	0.0241
		14	6	80	2.2e-03	28	0.52 (0.04)	1.13	0.0335
		36	8	67	4.6e-02	34	0.45 (0.01)	2.08**	0.0051
		28	7	74	9.2e-03	38	0.63 (0.13)	1.46*	0.0046

Protein IDs and gene names (in parentheses) are shown as well as fold-changes in their respective hydrophobic ratios and abundance with respect to matched WT TG spots. Statistical significance is indicated by asterisks \*p = 0.05, \*\*p = 0.01, \*\*\*p < 0.01 for ANOVA tests and p values of student's t test are reported in parentheses.

Table 2.1: Protein identification and hydrophobic ratios

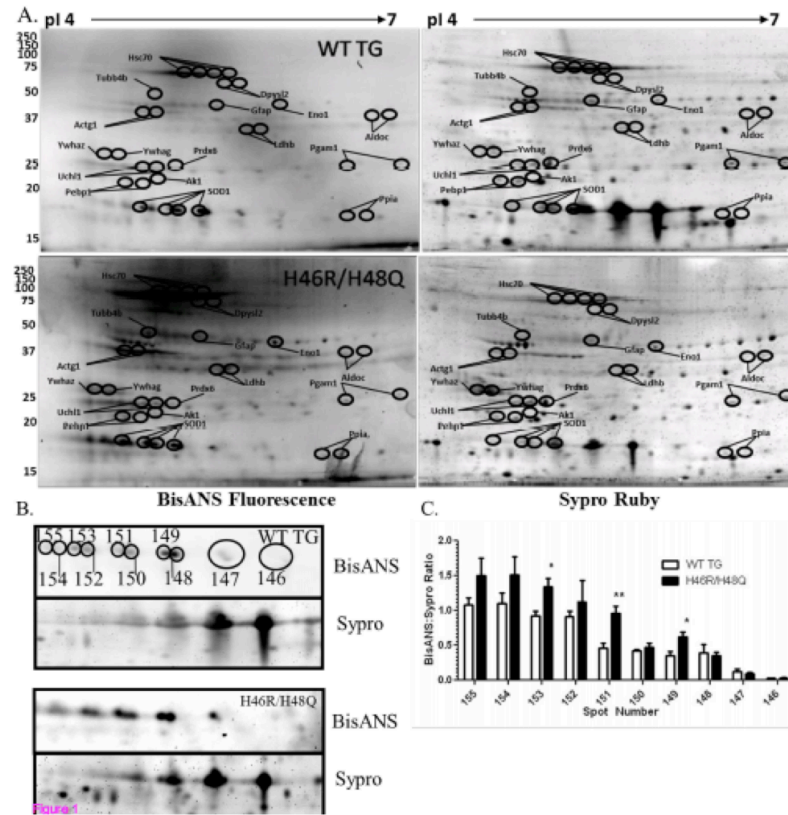


Figure 2.1: Altered surface hydrophobicity of mutant SOD1 and non-SOD1 proteins in the spinal cords of symptomatic ALS mice.

Representative 2D gels of wild type transgenic human SOD1 (WT TG, n = 8) and H46R/H48Q (n = 12) with molecular weights (left axis) and isoelectric points (pI, upper axis). Spots that significantly differed from WT TG in hydrophobic ratio are circled and annotated based on the gene names of their accession numbers identified by MALDI-TOF mass spectrometry. B) Enhanced region of 2D gels containing WT SOD1 and H46R/H48Q mutant SOD1 proteins. BisANS fluorescence and corresponding total protein stained with Sypro Ruby are shown. Quantitated SOD1 spots are shown with numbered ellipses and correspond to the quantitated hydrophobic ratio shown in C). Bars represent the mean hydrophobic ratio  $\pm$  standard deviation of 10–8 mice per group. \*p < 0.05, \*\*p < 0.01 by one-way ANOVA.

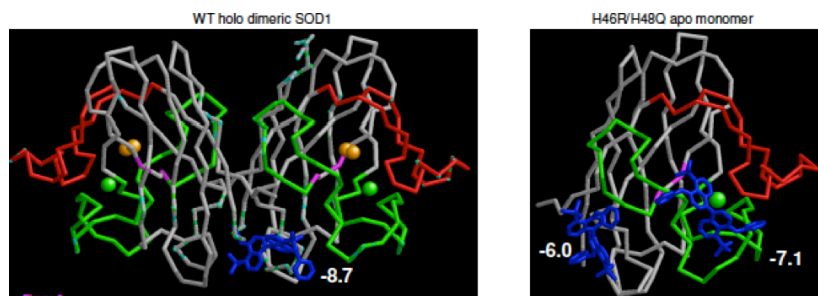


Figure 2.2: BisANS docking SOD1.

BisANS (blue) docked with WT human SOD1[2C9V] and H46R/H48Q [3GQP]. The zinc loop (aa49-84) is colored green, and electrostatic loop (aa121-144) is colored red. Amino acids 46 and 48 are colored magenta, copper ions (orange), and zinc ions (green). Binding energies are given for bisANS binding sites in kcal/mol. H46R/H48Q possess a binding site for bisANS in the metal binding region, whereas holo WT dimeric SOD1 does not.

### **Non-SOD1 proteins with altered surface hydrophobicity in soluble fractions of spinal cord from H46R/H48Q mice**

Since the toxic gain of function acquired by mutations in SOD1 may also alter non-SOD1 proteins in the spinal cord, we quantitated the non-SOD1 spots in the bisANS labeled extracts separated by 2D gels shown in Figure 2.1. We observed conformational alteration in a number of non-SOD1 proteins, and their fold changes in protein level and hydrophobicity ratio with respect to non-mutant WT mice were examined (Table 2.1 and Figure 2.1).

We examined one of the non-SOD1 proteins ubiquitin carboxyl hydrolase L1 (UCHL1) in more detail, due to its role in maintaining mono-ubiquitin pools and abundance in

spinal cord. Changes in UCHL1 surface hydrophobicity were found to correlate with a dimeric state in recombinant human UCHL1 separated by size exclusion chromatography into monomeric and dimeric states (data not shown).

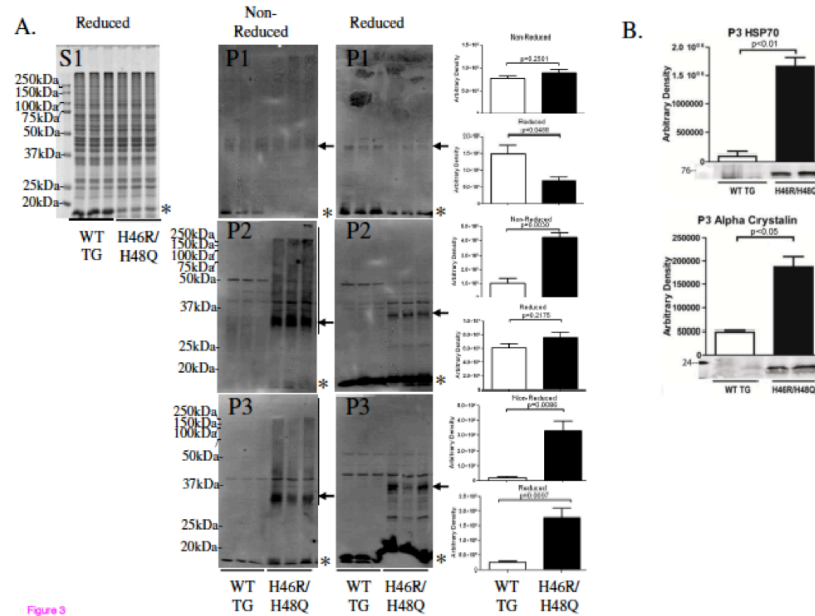


Figure 2.3: Mutant SOD1 and chaperones co-fractionate in the detergent insoluble fractions.

Spinal cord extracts were subjected to differential detergent extraction and A) the soluble fraction was electrophoresed under reducing and denaturing conditions and stained with Coomassie (S1) and P1-P3 fractions were immunoblotted for SOD1 under non-reducing or reducing conditions (P1-P3). Asterisks indicate the position of the monomeric SOD1. High molecular weight reactivity to the SOD1 antibody was detected in the H46R/H48Q extracts but not WT TG (indicated by vertical bar). High molecular weight reactivity to SOD1 diminished with addition of a reducing agent, however a band corresponding to dimeric SOD1 persisted and is indicated by an arrow. B) Inducible heat shock protein 70



and  $\alpha$ Bcrystallin co-fractionated with mutant SOD1 in the detergent insoluble fractions of spinal cord. \* $p = 0.05$ , \*\* $p = 0.01$ , Bars represent the mean of 6 mice  $\pm$  SD.

### **BisANS docked to multiple sites around the metal binding region of H46R/H48Q SOD1**

In order to investigate possible binding sites of bisANS in WT or mutant SOD1, crystal structures of dimeric WT holo human SOD1 [2C9V] and monomeric H46R/H48Q apo SOD1 [3GQF] were docked with bisANS (Figure 2.2), as WT holo SOD1 is known to exist as a dimer, while H46R/H48Q has been reported to be poorly metallated and can exist as a monomer [151, 152]. As shown in Figure 2.2, bisANS (colored blue) had one energetically and geometrically favorable binding site between WT SOD1 monomers, but H46R/H48Q had multiple possible binding sites around the copper binding (colored green) and electrostatic loops (colored red) of SOD1, which have been reported to be disordered in H46R/H48Q SOD1[151]. These data were consistent with *in situ* data (Figure 2.1) showing that H46R/H48Q had a greater degree of exposed surface hydrophobicity than wild-type, likely due to instability and greater exposure of the metal binding region in SOD1.

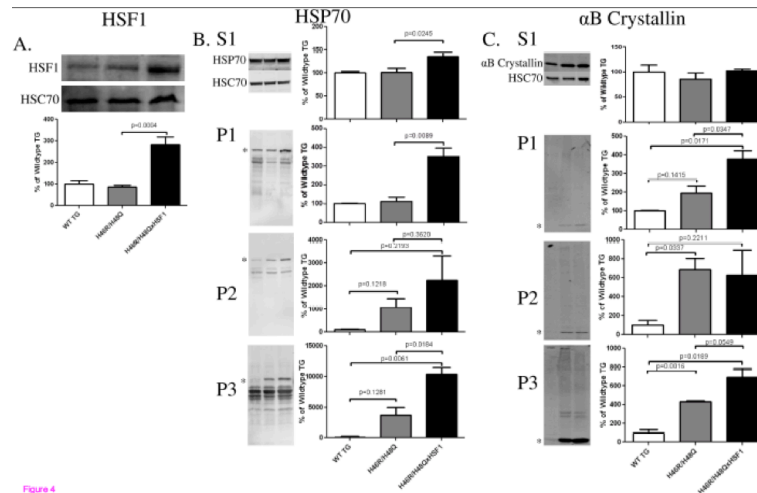


Figure 4

Figure 2.4: Expression of HSF1 and distribution of HSPs in spinal cord.

A) Western blot of HSF1 in spinal cord homogenates from normal and symptomatic control mice normalized with HSC70, demonstrating the over-expression of HSF1 in H46R/H48QxHSF1 mice compared to H46R/H48Q littermates. B) Spinal cords were extracted with detergents of increasing ionic strength as described in the methods. S1 and P1-3 extracts were immunoblotted for inducible HSP70 (B) or  $\alpha$ B-crystallin (C). Asterisks are given at the position of the expected monomeric protein. p is indicated by brackets, bars represent the mean of 6 mice  $\pm$  SD.

### SOD1 and chaperones enriched in detergent insoluble fractions

In order to determine whether the solubility of mutant SOD1 correlated with the observed differences in hydrophobicity, we examined spinal cord extracts for the presence of SOD1 by differential detergent extraction (Figure 2.3A). In the Coomassie stained soluble S1 fraction, SOD1 migrates as a monomer under reducing and denaturing SDS page at 17kDa, and differences in levels of SOD1 between WT TG and H46R/H48Q are

affected by both transgene copy number and solubility. Mutant SOD1 formed high molecular weight bands in the P2 and P3 fraction (Figure 2.3A, arrow), and showed high molecular weight smearing corresponding to SOD1 (Figure 2.3A, vertical bar and asterisk), which was partially resolved by reducing the sample with dTT. In pellet 3, we also observed a dramatic increase in the level of chaperones such as HSP70 and  $\alpha$ B-crystallin, suggesting that these chaperones were bound to mutant SOD1 as has been shown with other SOD1 mutants[153] (Figure 2.3B).

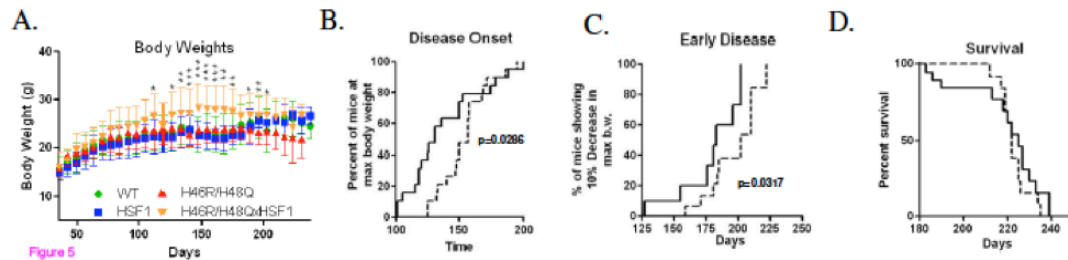


Figure 2.5: Effect of HSF1 over-expression on body weight loss and healthspan of H46R/H48Q mice.

H46R/H48Q mice (Solid line)  $n = 20$  and H46R/H48QxHSF1 (dashed line)  $n = 19$ .

- A) Beginning at 3 weeks of age, weekly averages of body weight are plotted for the survival cohort for WT (green circles), HSF1 (blue squares), H46R/H48Q (red triangles), and H46R/H48QxHSF1 (gold triangles). Asterisks indicate significant differences in H46R/H48QxHSF1 vs. H46R/H48Q at the \* $p < 0.05$ , \*\* $p < 0.01$ , and \*\*\* $p < 0.001$  level.
- B) Disease onset was determined as the time animals reached their maximum bodyweight. C) Early disease was defined as a drop of 10% of the mouse maximal weight
- D) disease duration was calculated by subtracting the survival time from disease onset. E)

Survival was defined as the point at which animals could not right themselves within 30s after being placed on their side.

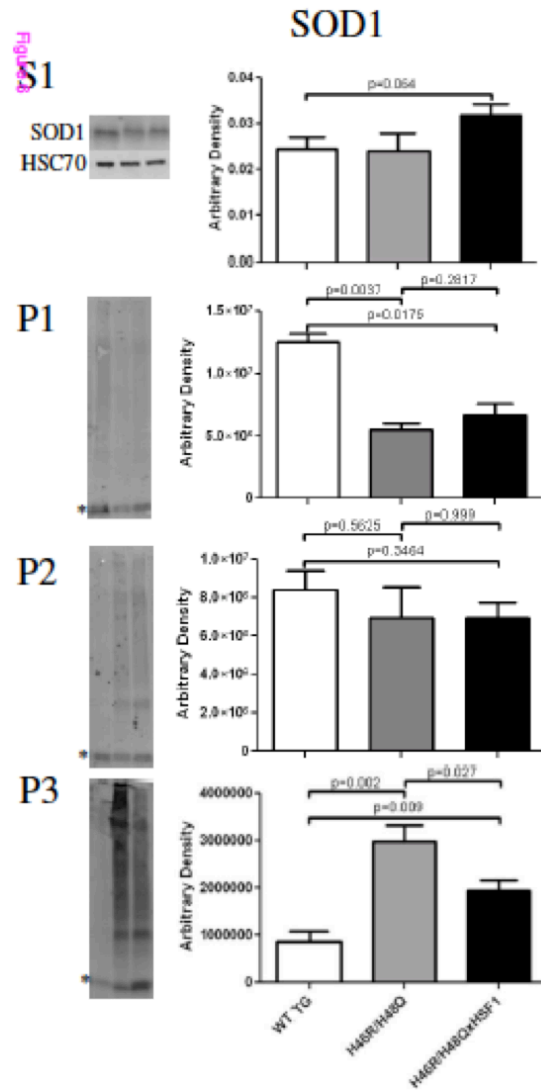


Figure 2.6: Effect of HSF1 over-expression on mutant SOD1 solubility.

SOD1 in the soluble S1 and detergent soluble fractions P1-P3. Asterisks are given at the position of the expected monomeric SOD1. Bars represent an n = 6 +/- SD.

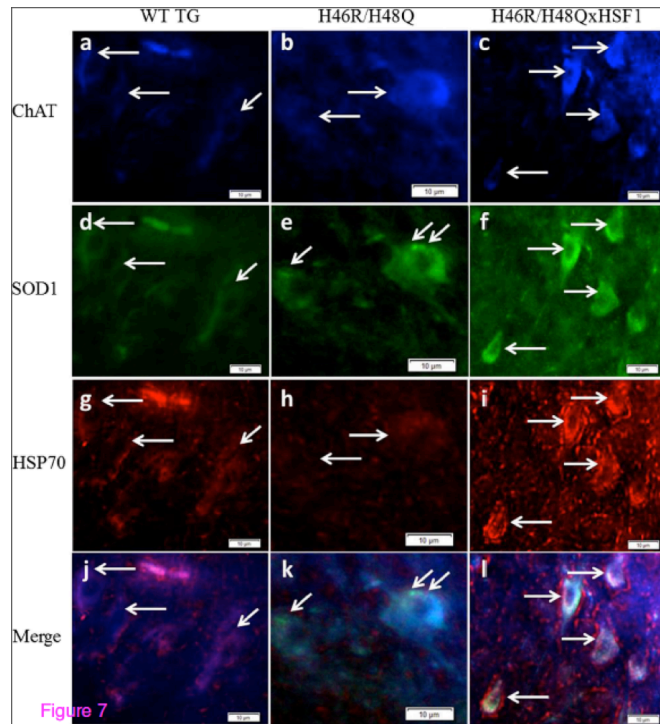


Figure 2.7: Anterior horn region of lumbar spinal cord sections from mice at 220days.

Motor neuron choline acetyltransferase (ChAT) positive cells (a-c, arrows) co-localized with SOD1 positive staining (d-f, arrows). H46R/H48Q mice exhibited small intracellular perinuclear SOD1 reactive punctae (e, arrows), while H46R/H48QxHSF1 tissues had a more even intracellular distribution of SOD1 staining (f). This corresponded with differences in HSP70 distribution to SOD1 reactive punctae in H46R/H48Q mice (h) while in contrast, colocalization with ChAT reactive cells in H46R/H48QxHSF1 mice was stronger (i). Scale bar represents 10μm.

### **Effects of over-expression of HSF1 in H46R/H48Qx HSF1 mice**

Because chaperones and HSPs bind to exposed surface hydrophobic domains to assist protein re-folding or degradation, mutant H46R/H48Q SOD1 mice were crossed with the HSF1<sup>+/-</sup> transgenic mice (H46R/H48QxHSF1) in order to determine the effects of HSF1 upregulation on disease progression of ALS. H46R/H48QxHSF1 were identified by PCR, and HSF1 over-expression was verified by Western blot of spinal cord extracts (Figure 2.4A) in mice at 222days. HSF1 expression in the H46R/H48QxHSF1 symptomatic mice was three-fold higher ( $p=0.0004$ ) in the spinal cord compared to H46R/H48Q and WT TG littermates. Soluble levels of chaperones HSP70 (Figure 2.4B) but not  $\alpha$ B-crystallin (Figure 2.4C) were elevated in the spinal cords of H46R/H48QxHSF1 mice, while levels of HSP70 and  $\alpha$ B-crystallin were elevated in the P1 and P3 fractions of the spinal cord, indicating a more robust HSR in H46R/H48QxHSF1 mice. Differences in HSP70 and  $\alpha$ B-crystallin could be detected in total homogenates as early as 197d in H46R/H48QxHSF1 compared to WT TG controls. Disease progression can be followed by weight loss, and has been reported as a reliable marker of healthspan, as well as symptom and disease onsets in ALS mouse models. Hence, the body weights for H46R/H48Q and H46R/H48QxHSF1 cohorts were followed. H46R/H48QxHSF1 mice ( $n=19$ ) maintained body weights significantly better overall when compared to H46R/H48Q mouse littermates ( $n=20$ ) (Figure 2.5A). Disease onset, the period of time when mice reached their maximum body weight, was also significantly delayed by over-expression of HSF1 ( $p=0.0286$ , Figure 2.5B). Initiation of early disease was calculated for H46R/H48QxHSF1 and H46R/H48Q littermates using body weights as described in the Methods. Compared to the H46R/H48Q littermates, the percentage of

H46R/H48QxHSF1 mice that underwent early symptoms of the disease was significantly delayed ( $p=0.0317$ ) compared to H46R/H48Q (Figure 2.5C). While overall survival was unaffected (Figure 2.5D), survival of the 25<sup>th</sup> percentile was significantly different ( $p=0.017$ ). Ubiquitous over-expression of HSF1 protected H46R/H48Q against ALS as evidenced by their improved body weight retention and delayed disease onset, symptom onset, and early survival. Also, over-expression of HSF1 led to a non-significant increase ( $p=0.064$ ) in soluble mutant SOD1 and significantly reduced its levels in detergent insoluble fractions by 34% ( $p=0.027$ ) (Figure 2.6). These data suggest that overexpression of HSF1 may have altered the solubility of SOD1 and improved protein homeostasis in motor neurons. To examine this, spinal cords were sectioned and the lumbar region was examined (Figure 2.7). As shown, the distribution of SOD1 in motor neurons was altered by overexpression of HSF1, as choline acetyltransferase (ChAT) positive motor neurons contained fewer SOD1 puncta and exhibited a more uniform staining for SOD1 in cell bodies compared to H46R/H48Q. This corresponded to a more intense staining for HSP70 in ChAT positive motor neurons compared to H46R/H48Q tissues. Likewise,  $\alpha$ B-crystallin staining showed a striking change in its distribution in the H46R/H48Q tissues going from a diffuse pattern as seen in WT TG tissues to a more punctate nuclear pattern as seen in the large SOD1 positive cell bodies in the H46R/H48Q spinal cord (Figure 8). Overexpression of HSF1 appeared to restore this shift to resemble the appearance of WT TG. In addition to motor neurons, GFAP positive astrocytes also contributed a major portion of the HSP70 and  $\alpha$ B-crystallin staining.

One possible explanation for the restoration of SOD1 solubility in tissues of H46R/H48QxHSF1 mice could be explained by enhanced chaperone-mediated turnover

of mutant SOD1. Mutant SOD1 has been shown to be degraded by both the proteasome and macroautophagy [154]. Since HSF1 could affect induction of macroautophagy, we next examined levels of membrane-bound microtubule-associated proteins 1A/1B light chain 3A (LC3-II). Levels of LC3-II protein remained elevated in H46R/H48QxHSF1 mice as observed in H46R/H48Q (Figure 2.9A), while normalized levels of p62 were also unchanged by HSF1 overexpression indicating that rates of macroautophagy were not affected. The carboxyl terminus of Hsp70 interacting protein (CHIP) is an important co-chaperone that has been shown to play a role in the polyubiquitination and proteasomal degradation of mutant SOD1 when bound to Hsp/Hsc70 [155]. To determine whether HSF1 over-expression would enhance CHIP expression, the expression levels of CHIP in the spinal cords from H46R/H48QxHSF1 mice were examined by Western blot. Levels of CHIP were significantly decreased ( $p=0.001$ ) following mutant SOD1 over-expression, likely due to a shift in protein turnover in ALS away from the UPS, which was prevented by over-expression of HSF1 (Figure 2.9B).



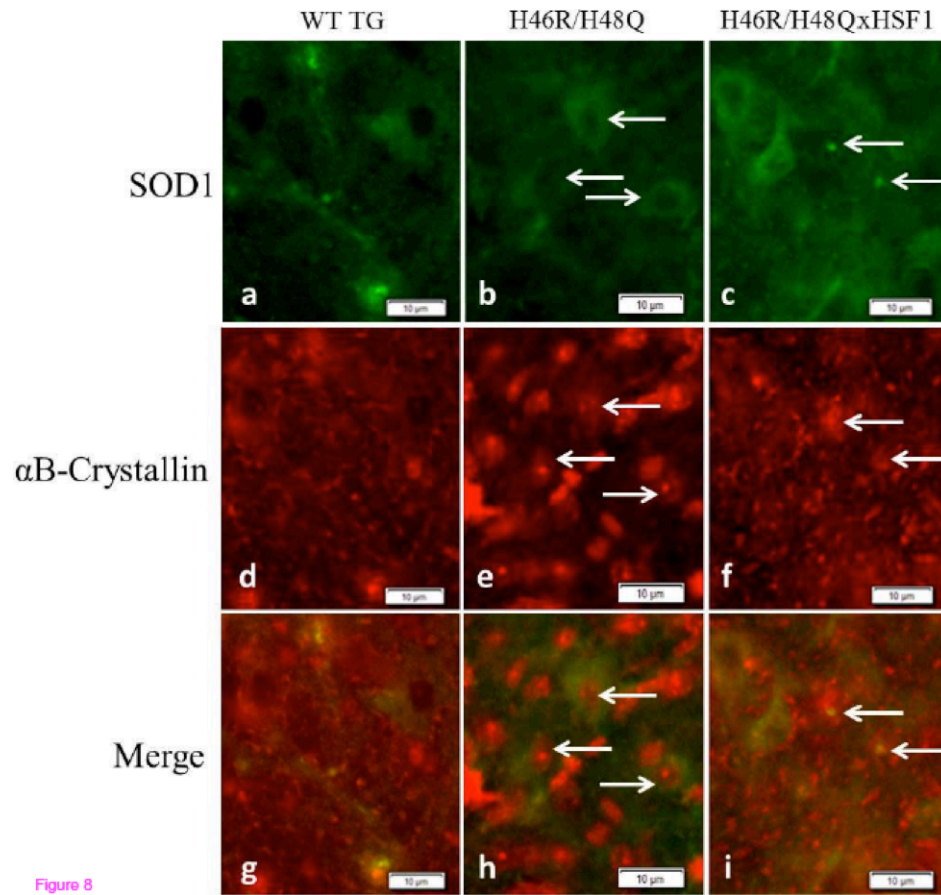


Figure 8

Figure 2.8: Anterior horn region of lumbar spinal cord sections from mice at 220days.

$\alpha$ B-crystallin staining was diffuse throughout WT TG and H46R/H48QxHSF1 tissues (d,f) and co-localized diffusely with small SOD1 positive punctae in H46R/H48Q vs.

H46R/H48QxHSF1 tissues (f, arrows). Strikingly,  $\alpha$ B-crystallin staining appeared more punctate and localized to cell nuclei of SOD1 expressing cells (e,h, arrows) in

H46R/H48Q tissues. Scale bar represents 10  $\mu$ m.

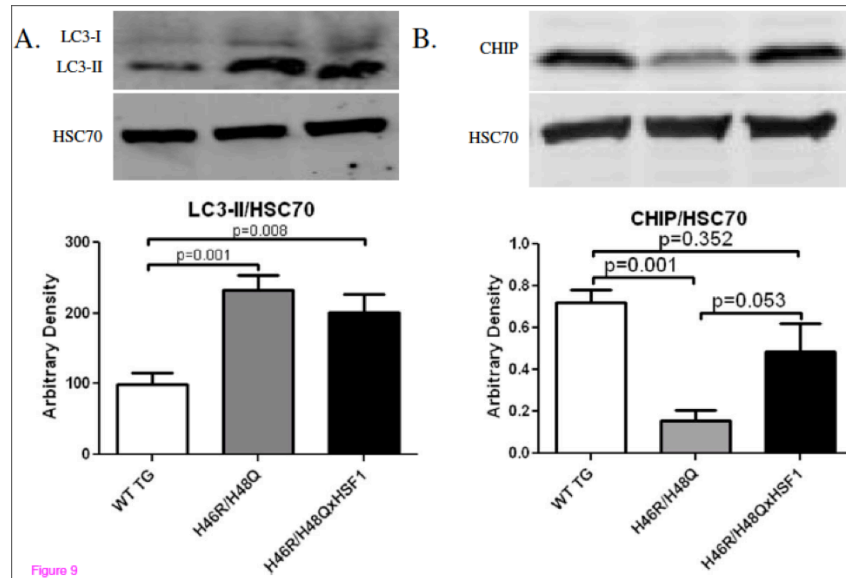


Figure 2.9: Effects of HSF1 over-expression on measures of protein quality control in ALS.

Whole spinal cords were homogenized in 2%SDS and immunoblotted for A) LC3-II or B) CHIP and normalized with Hsc70. Bars represent an  $n = 6 \pm$  SD.

## Discussion

A change in protein surface hydrophobicity can be an important indicator to determine alterations in protein structure, and thus indicative of losses or toxic gain of protein function. Exposure of protein surface hydrophobicity and disordered regions in proteins have been reported to precede aggregation [150], and to be an important intrinsic quality of proteins that can determine whether they are aggregation prone or capable of forming amyloid using bioinformatic approaches [122]. In addition to intrinsic hydrophobicity, proteins expose hydrophobic residues on their surface through post-translational modifications, mutations, or oxidative damage, which may not be predicted with bioinformatic approaches alone. SOD1 contains a greek key  $\beta$ -barrel which can be

exposed or unfold due to SOD1 mutations near the metal binding region, and conformation-specific antibodies targeting this site can detect SOD1 in neuronal tissues of human familial and sporadic ALS patients [156, 157]. The bisANS related compound ANS has similar properties to bisANS and has been used to show that the point in time at which amyloidogenic proteins exhibit their greatest toxicity correlates with a surge in surface hydrophobicity [158]. Increased surface hydrophobicity of the SOD1 mutant studied here *in situ* and by others has been described using different *in vitro* techniques [119, 120, 128, 151]. In this proteomic study, we have utilized a covalent photolabeling approach with the hydrophobic dye bisANS to monitor the surface hydrophobicity of mutant SOD1 and other non-SOD1 proteins in the spinal cord of H46R/H48Q mice.

Consistent with several studies looking at the hydrophobicity of G93A or single mutant H46R or H48Q SOD1 using similar hydrophobic dyes *in vitro* [150, 158], we observed alterations and an overall increase in soluble SOD1 surface hydrophobicity of previously reported isoelectric species of SOD1 [149] in the H46R/H48Q double mutant of SOD1 *in situ*. Our *in situ* analysis of the conformationally altered proteome shows for the first time only a fraction of the total SOD1 soluble pool exhibits these properties, and that the degree of exposed surface hydrophobicity is varied among isoelectric species of SOD1. These differences in surface hydrophobicity are important, and could reflect different conformational states that each mutant undergoes *in vivo* during symptomatic stages of ALS, metallation status of the protein [117], or may identify species of SOD1 that are most toxic. We found that the metal binding region appeared to be the most plausible target of bisANS in mutant SOD1 (Figure 3), and this can be confirmed by

identification of the specific bisANS incorporation site(s) using mass spectrometric methods in future studies.

The surface hydrophobicity detected by bisANS correlated with the insolubility of mutant SOD1 and the presence of high molecular weight species of SOD1 in detergent insoluble fractions, which was partially dependent upon disulfide bonds or mixed disulfides. While the species of mutant SOD1 detected here with bisANS were soluble species, the conformational alterations in SOD1 alluded to by changes in surface hydrophobicity may be indicative of toxic gain of function. Interestingly, increases in surface hydrophobicity of WT SOD1 as detected by ANS correlate with a gain in SOD1's ability to bind, cleave DNA or RNA, and induce its aggregation [159, 160]. Mutant SOD1 has also been shown to display increased binding to neurofilament (NFL) mRNA [161], and to alter RNA homeostasis by binding to Hu antigen R and T-cell internal antigen 1 (TIA1) related protein [162], two key players in modulating stress granule formation and mRNA stability along with TDP-43. However it is unknown whether the increased hydrophobicity associated with the SOD1 mutants studied here enhances these reported gains of function in SOD1. Further studies are required to elucidate the direct impact that increased protein surface hydrophobicity has on toxic gains of function in SOD1. Aggregates in spinal cords of ALS patients as well as in the mice used in this study have been reported to contain various chaperones such as HSP70 and  $\alpha$ B-crystallin [153], intermediate filament proteins, and others [163], supporting the idea that interventions that enhance proteostasis might be beneficial in ALS.

Since SOD1 mutations and aggregation are only observed in some ALS cases, there is good reason to suspect that the toxic effects of mutant SOD1 may be indirect and

involve non-SOD1 proteins. For this reason, we also examined the changes in surface hydrophobicity of soluble non-SOD1 proteins in the spinal cords from symptomatic ALS mice. We found sixteen non-SOD1 proteins with significantly altered surface hydrophobicity, and these could be separated into groups such as energy metabolism, cytoskeletal organization, protein quality control, and signaling based upon their reported functions.

Although too numerous to discuss all, a few of the proteins in Table 1 deserve some discussion. Several glycolytic proteins are “moonlighting proteins” and perform functions outside of glycolysis with implications for neurodegenerative disease [132, 164]. Changes in surface hydrophobicity in glycolytic enzymes correlate well with clinical and experimental observations that defects in energy homeostasis are a common feature in subsets of ALS patients [132, 165, 166]. In our study, we detected alterations in surface hydrophobicity of several glycolytic enzymes and proteins important in energy homeostasis including alpha-enolase, fructose-bisphosphate aldolase C, L-lactate dehydrogenase B chain, phosphoglycerate mutase 1, and adenylate kinase 1.

Alexander disease is a neurodegenerative disease caused by mutations in the glial fibrillary acidic protein (GFAP), leading to aggregates of GFAP and chaperones called Rosenthal fibers [167]. We detected significant increases in the surface hydrophobicity of GFAP, but whether the changes in GFAP hydrophobicity observed in this study were indicative of aggregation in ALS is unknown.

Defects in protein homeostasis and quality control are hypothesized as important mechanisms in neurodegenerative diseases [168]. The constitutive chaperone Hsc70, which is involved in several aspects of protein homeostasis, has been shown to bind to

mutant SOD1 via interaction with CHIP to promote mutant SOD1 degradation, and is found in spinal cord aggregates from both mice [153] and humans [163]. In this study, surface hydrophobicity of Hsc70 in H46R/H48Q was significantly increased compared to WT transgenic littermates. This is consistent with the finding that increases in ANS binding are associated with thermal denaturation of Hsc70 [169]. Another chaperone, peptidyl-prolyl cis trans isomerase A (PPIA) also known as cyclophilin A, is an immunophilin that binds cyclosporine A and catalyzes the conversion of peptidyl-prolyl bonds from cis to trans. Over-expression of cyclophilin A has been found to protect cells from mutant SOD1-induced cell death [170], and to aggregate with Hsc70 and 14-3-3 gamma in G93A mice [163]. It is plausible that the alterations we observed in surface hydrophobicity correlate with these activities of cyclophilin A, although it has not been directly tested.

UCHL1 is an abundant protein in motor neurons, and deletions in the 7<sup>th</sup> and 8<sup>th</sup> exons cause gracile axonal dystrophy in mice, characterized by motor/behavior abnormalities and shortened lifespan [171]. UCHL1 is a monoubiquitin binding protein with weak ubiquitin hydrolase activity that may function in maintaining monoubiquitin pools [172]. UCHL1 has been shown to form dimers that enhance a ubiquitin-ubiquitin ligase activity [173]. In the same study this activity was associated with increased aggregation of  $\alpha$ -synuclein in a cell model system of PD. Thus, it would appear that dimerization of UCHL1 promotes a gain of function activity that is detrimental under certain circumstances. In our study, we observed a decrease in surface hydrophobicity of UCHL1 (Figure 1, Table 1) that correlated with a similar decrease in surface hydrophobicity of UCHL1 between monomeric and dimeric forms *in vitro* (Supplemental

Figure 2A and B). These data suggest that in ALS dimerization of UCHL1 is favored. Whether decreased surface hydrophobicity of UCHL1 translates into increased ubiquitin-ubiquitin ligation, or local depletion of the monoubiquitin pool remains to be determined.

The surface hydrophobicity of the signaling proteins 14-3-3 gamma and zeta isoforms were found to be significantly decreased. Originally highlighted in the brain for their roles in activating tryptophan and tyrosine hydroxylases, 14-3-3 proteins were later proven to have diverse functions mostly as scaffolding proteins, and have been implicated in a variety of neurodegenerative diseases [174]. With regards to ALS, 14-3-3 proteins have been shown to modulate NFL mRNA stability [175] and assist in targeting misfolded proteins to aggresomes by linking Bcl-associated athanogene 3 (BAG3) to histone deacetylase 6 (HDAC6) [176, 177]. A triple phospho-mimetic mutant S58E/S184E/T232E has been linked to decreased bisANS incorporation in purified human 14-3-3 zeta [178]. Phosphorylation of Serine 58 in 14-3-3 zeta has been characterized as a molecular switch for induction of apoptotic cell death [179]. Therefore, in addition to its solubility being affected in ALS mice [163], changes observed in surface hydrophobicity of 14-3-3 in this study may be indicative of its phosphorylation.

Misfolded proteins are associated with exposed surface hydrophobicity, and the proteins that we identified with altered hydrophobicity likely represent metastable proteins that are easily misfolded during proteotoxic stress. Strikingly, Xu et al recently examined proteins that became insoluble in the brains of mice expressing mutant forms of amyloid precursor protein[180]. Many of the same proteins that we found misfolded here in the spinal cord of ALS mice were also found to be insoluble in the brains of mice modeling AD, supporting a connection to the misfolding we have measured using

bisANS and the downstream aggregation process that occurs during proteotoxic stress. Misfolded proteins and proteins with exposed hydrophobicity are recognized by chaperones on the basis of surface hydrophobicity. Since we observed increases in surface hydrophobicity of mutant SOD1 and 16 other non-SOD1 proteins in the spinal cord of H46R/H48Q mice, we set out to determine whether over-expression of HSF1 would be protective against SOD1 mutant-mediated ALS and alteration in proteome surface hydrophobicity. As expected, over-expression of HSF1 was detected in the spinal cord of H46R/H48QxHSF1 mice by Western blot, and led to an increase in the solubility of SOD1. HSF1 over-expression led to a robust induction of HSP70 and  $\alpha$ B-crystallin as detected in some soluble and insoluble fractions which could be detected as early as 197 days. However, HSP induction was not able to completely reverse SOD1 aggregation. Co-localization of HSPs by immunofluorescence and increased co-fractionation of HSP70 and  $\alpha$ B-crystallin with SOD1 in insoluble fractions measured here, and the observations that these HSPs bound to mutant SOD1 *in vivo* by others [153] suggests they were associated with aggregated SOD1. Immunofluorescence of H46R/H48Q mice also detected an increased number of cells with nuclear localized  $\alpha$ B-crystallin staining and speckles that were absent in double transgenic mice (Figure 2.8e,h). Recently nuclear localization of  $\alpha$ B-crystallin has been shown to be associated with stress and associates with the survival of motor neuron complex[181]. Association of  $\alpha$ B-crystallin with alpha 7 subunits of the 20S proteasome suggest it could also be involved in facilitating turnover of bound aggregates [182]. This is supported by the observations that differences in protein homeostatic machinery were detected in the UPS associated co-chaperone CHIP, but not macroautophagy of H46R/H48QxHSF1 mice. ALS is a multifactorial disorder



affecting multiple cell types and physiological phenotypes, and these are reflected in transgenic mouse models of ALS[183]. H46R/H48QxHSF1 maintained a 3-fold increase in HSF1 expression throughout the study, which led to retention in body weight and delay in disease onset, early disease, and survival of the 25<sup>th</sup> percentile with exception of overall survival of the experimental cohorts (Figure 2.5). Motor neuron death is an early event in the disease process, and are responsible for the timing and early symptoms in ALS [184], while astrocytes[185] and microglia[186] are responsible for disease progression suggesting that HSF1 over-expression had a primarily beneficial effect on motor neurons, but not on astrocytes or microglia.

## **CONCLUSION**

We show that changes in surface hydrophobicity as detected by bisANS relate to important gains or losses of function in soluble SOD1 and the non-SOD1 proteins we identified. Importantly, this study demonstrates that soluble fractions of mutant SOD1 are indeed misfolded and exhibit increased surface hydrophobicity, which correlates with the insolubility of mutant SOD1 and may be indicative of toxic gain of function. In future studies, mapping the bisANS incorporation sites to the isoelectric species of mutant SOD1 and the other non-SOD1 proteins that were altered will enable these domains to be targeted in order to determine their possible roles in ALS. Furthermore, the bisANS fluorescent-based assay used here can be applied as part of a high-throughput screening approach to identify compounds/drugs that interfere with the exposure of hydrophobic surfaces of metastable proteins or prevent aggregation. Over-expression of HSF1 was associated with maintenance in bodyweight, delayed disease onset, progression, and early survivorship. These data indicate that there is a functional and survival benefit to over-expression of HSF1 and enhancing the heat shock response, and validates therapeutic

strategies aimed at activating HSF1 for ALS models. This is the first study to demonstrate that over-expression of full-length HSF1 is beneficial in ALS, and further shows that increasing HSF1 protein may be an additional strategy to activate HSF1 rather than by inducing proteotoxic stress or inhibiting HSP90. **(This chapter contains previously published work in [109])**

# **Chapter 3 Overexpression of heat shock factor 1 maintains TAR DNA binding protein 43 solubility via induction of inducible heat shock protein 70 in cultured cells**

## **INTRODUCTION**

TDP-43 is a 43-kDa nuclear protein that contains two RNA recognition motifs (RRM1 and 2) and a C-terminal disordered region, and ubiquitinated inclusions containing TDP-43 are detected in the cytoplasm and nucleus of both neurons and glial cells in TDP-43 proteinopathies such as amyotrophic lateral sclerosis (ALS) and a subset of frontotemporal dementia (FTD) [59, 67]. Mutations in the C-terminal region are genetically linked to a subset of ALS cases [187]. Histologically, TDP-43 is mislocalized and depleted from its nuclear location to the cytoplasm in 97% of ALS cases, 51% of FTD, and 57% of Alzheimer's disease, where it accumulates and is proteolytically cleaved to form C-terminal fragments [188-190]. Studies depleting TDP-43 in cells and animal models have shown a substantial impact on mRNA splicing as well as proteomic signatures, supporting a loss of function role for TDP-43 toxicity [62, 191, 192]. Meanwhile, the presence of TDP-43 (full length), C-terminal fragments (CTF), and higher molecular weight TDP-43 species are found in the detergent insoluble fraction of brains and spinal cords of patients with TDP-43 proteinopathies[67], and could possibly spread in a non-random fashion in a prion-like manner[193], supporting a gain of function mechanism of toxicity. Various studies have shown that caspase-mediated processing represents one of the mechanisms of generating the TDP-43 fragments [194-196]. The roles of these CTFs (25 and 35kDa) in TDP-43 pathogenesis have been

investigated. Accumulation of CTFs causes cognitive deficits in a TDP-43 mouse model[73] and *in vitro* it forms cytoplasmic aggregates and is toxic[197]. Irrespective of whether a loss of function or gain of function mechanism is driving toxicity, maintaining TDP-43 solubility remains an essential therapeutic target, and systems that eliminate/reduce insoluble neurotoxic TDP-43 species address both possible mechanisms, and could alleviate pathogenesis or decrease the spreading of the disease.

Due to the importance of protein homeostasis in various neurodegenerative diseases much focus has been placed on the regulation of HSP expression as a therapeutic strategy for protein conformational diseases[198]. To contend with protein misfolding the cell recruits HSPs to assist in refolding misfolded proteins, catalyze solubilization, or eliminate misfolded proteins via interaction with two major pathways of protein degradation the Ubiquitin Proteasome System (UPS) or macroautophagy. HSPs consist of families of proteins classified by their molecular weight and are up regulated in cells during times of stress. Because motor neurons have a high threshold for activation of HSP genes and depend on peripheral HSPs produced by the neighboring cells, such as astrocytes, they are more susceptible to stress[199].

Previously, we have shown that overexpression of heat shock factor 1(HSF1), the master transcription factor for HSPs has protective effects in ALS and AD mouse models [109, 143]. HSF1 increased the solubility of mutant SOD1 concomitant with delayed disease onset[109], and amelioration of AD-like cognitive impairment, respectively[143]. Other studies have shown that multiple HSPs are responsible for TDP-43 homeostasis and metabolism. For example, Jackrel et al engineered HSP104/105 from yeast that solubilizes TDP-43 aggregates and prevents TDP-43 associated toxicity[200]. HSP90 has

been shown to be important in TDP-43 turnover via its co-chaperone Cdc37 [201], and HSP70 and its co-chaperone HSP40 are constitutively bound to TDP-43 and interact with its disordered C-terminus and are important in preventing TDP-43 aggregation [202]. Therefore, since multiple HSP's regulate TDP-43 homeostasis, an attractive target to affect global TDP-43 homeostasis may be HSF1, which drives the expression of these HSPs and many others. Along these lines, other studies have demonstrated that pharmacologic activation of HSF1 can protect against the aggregation and toxicity of exogenously expressed TDP-43 fragments or transgenes[203], however these small molecules operate by inducing proteotoxic stress themselves, typically by inhibiting HSP90, which have been shown to disrupt HSP90:TDP-43 interactions[201] as well as many other HSP90 clients. Therefore, we sought to investigate the role of enhancing HSF1 via overexpression without the use of pharmacologic activators in an effort to elucidate its role in maintaining TDP-43 solubility and maintaining its homeostasis. Importantly, arimoclomol an HSF1 co-activator that amplifies the HSR without causing proteotoxic stress is currently in phase II/III trials for treatment of ALS patients bearing SOD1 mutations [135] and one of the effects of riluzole, the only FDA approved drug to treat ALS has been shown to increase latent HSF1 levels and enhance heat shock response[204].

In our study, we investigate the role of HSF1 in TDP-43 homeostasis. We show a robust heat shock response to TDP-43 overexpression in human HSF1 overexpressing mouse embryonic fibroblasts (HSF1<sup>+/+</sup> MEF) as determined by increases in HSP70 and 90 protein levels. We see that HSF1 prevents the accumulation of TDP-43 positive puncta. In addition, we show that HSF1 prevents the transition of TDP-43 from a soluble

to insoluble state. We show that HSF1 prevents the accumulation of pathogenic TDP-43 fragments and protects against their toxicity. We confirmed this by demonstrating that HSF1 and/or HSP70 ATPase inhibition exacerbated TDP-43 insolubility, and that genetic knockout of HSF1 accelerated TDP-43 fragmentation as well as significantly decreased its solubility, indicating that HSF1 and its transcriptional targets play an important role in preserving TDP-43 solubility and proteostasis.

## **METHODS**

### **Neuroblastoma Cell Culture**

Undifferentiated SH-SY5Y cells were cultured in Dulbecco's modified Eagle's medium (DMEM/F12 50/50) supplemented with 10% fetal bovine serum, 1% penicillin-streptomycin. Cells were transfected with a human non-mutant heat shock factor 1 cDNA in a pCMV-AC vector (2.5 $\mu$ g HSF1 SC321225, Origene) using lipofectamine 2000 reagent (Invitrogen) in a 1:3 DNA:lipofectamine ratio according to manufacturer's instructions. HSF1 transfected cells were selected using G418 (400 $\mu$ g/mL) selection agent (Cellgro). Stably transfected HSF1 overexpressing cells (HSF1-SH-SY5Y) were treated with 10 $\mu$ M MG132 (Sigma-Aldrich) for 6, 12, or 24 hours or with DMSO as a control for transfected and non-transfected cells. In some experiments, cells were pre-treated with 10 $\mu$ M N2-(1H-indazole-5-yl)-N6-methyl-3-nitropyridine-2,6-diamine (KRIBB 11) an HSF1 inhibitor (Calbiochem) for 30 minutes and then treated with 10 $\mu$ M MG132 for 24hrs and compared to cells treated with 10 $\mu$ M MG132 alone. For HSP70 inhibition experiments, cells were treated with 10 $\mu$ M 5'-O-[(4-Cyanophenyl)methyl]-8-[[[(3,4-dichlorophenyl)methyl]amino]-adenosine (VER 155008), an HSP70 inhibitor (TORCIS bioscience) and then 10 $\mu$ M MG132 for 24hrs, and compared to cells treated

with 10 $\mu$ M MG132 alone. To assess ubiquitin proteasome activity, SH-SY5Y cells were stably transfected with ubiquitin-arginine-GFP (Ub-R-GFP) and ubiquitin-methionine-GFP (Ub-M-GFP in a pN1 vector[11] using the same conditions as above. For celastrol experiments, cells were treated with 0.1 $\mu$ M celastrol for 1hr and allowed to recover for 5hrs, followed by treatment with 10 $\mu$ M MG132 for 6 and 24hrs.

### **Primary Mouse Embryonic Fibroblast (MEF) Cells**

MEFs were obtained from neonatal mouse skin and tails, 1–3 days of age as described[138]. Briefly, skin and tails were digested in DMEM/F12 50/50 plus 10%FBS plus collagenase overnight in a petri dish at 37°C. Cells were dislodged by pipetting up and down from skin and tail, centrifuged at 500g and resuspended in DMEM/F12, counted, and plated in a T-75 flask. MEFs were obtained from both wild-type (C57Bl/6J background) and human HSF1 overexpressing mice that were derived on a C57Bl/6 background and described previously, [138]. Briefly, mice overexpress human HSF1 mRNA and protein with its endogenous promoter in all tissues 2-4 fold above endogenous mouse Hsf1. MEF experiments were performed with passage 1–3 cells. MEFs were seeded in 6-well plates at  $0.25 \times 10^6$ /well and transfected with 2.5 $\mu$ g wild-type human TDP43 with tdTOMATOHA tag constructs [205] using lipofectamine 2000 (Invitrogen). HSF1 Knockout (HSF1<sup>-/-</sup>) MEFs were a kind gift of Benjamin Ivor, Medical College of Wisconsin[206] and were treated with 10  $\mu$ M MG132 (Sigma-Aldrich) for 6 or 12 hrs.

### **Immunofluorescence Studies**

MEFs were seeded onto glass coverslips at  $0.25 \times 10^6$  cells/well in 6-well dishes and then transfected with wtTDP-43 tdTOMATOHA using lipofectamine. After 12hrs cells were washed and fixed in 2% paraformaldehyde in phosphate buffered saline (PBS). Cells were mounted on microscope slides using vectashield-mounting medium with DAPI (Vectorlabs Burlingame, CA). Human control and AD tissues were acquired from the Oregon Brain Bank. Tissues were sectioned on a cryostat at 10 $\mu$ m thickness, fixed and stained with HSP70 (Stressgen SPA-810, RRID# AB\_2039260) at 1:50, rabbit anti-TDP-43 (C-terminal) polyclonal antibody (T1580, Sigma Aldrich RRID#: AB\_2532125) at 1:50 and antibody signals were detected using secondary goat anti-mouse Alexa 488 (Invitrogen RRID#: AB\_10566286) at 1:100 and rabbit Alexa 594 1:100 (Invitrogen, RRID#: AB\_10561549). Lipofuscin fluorescence was blocked by a subsequent incubation in 0.1% solution of Sudan Black for 10 minutes prior to mounting.

Cells and tissues were imaged using Olympus wide field fluorescence microscope. Post-processing including uniform contrast and brightness adjustments performed equally across all comparative images. Puncta associated with tdTOMATO fluorescence were quantitated using Image J.

### **Cell Lysate Collection and Preparation**

After wtTDP-43 tdTOMATOHA transfection, MEFs were washed with cold PBS, and scraped in cold RIPA buffer with 5% SDS plus phosphatase inhibitor cocktail 2 (Sigma) and protease inhibitor cocktail set 1 (Calbiochem). For celastrol experiments, cells were washed with cold PBS and scraped in cold RIPA buffer with 2% SDS. For both experiments, cell lysates were sonicated and protein concentration was determined by the bicinchoninic acid (BCA) assay (Pierce). Equal amounts of protein (50 $\mu$ g/sample) were



resolved on 15% SDS-PAGE. The following antibodies were used; mouse anti-GFP 1:3000 (Pierce Thermo, MA5-15256 RRID# AB\_10979281), rabbit anti-ATG7 1:10000 (abcam, ab133528, RRID#: AB\_2532126), rabbit anti-LC3B 1:1000 (Thermo Scientific Pierce, PA5-17224 RRID# AB\_10987450), HSP90 1:10000 (Stressgen, SPA-846 RRID# AB\_1659604), HSP70 1:10000 (Stressgen, SPA-810 RRID# AB\_2039260). Antibody signals were detected with IRDye 680LT 1:15,000 (LiCor, Cat#926-68020 RRID# AB\_10706161) or IRDye 800CW 1:20,000 (LiCor, Cat#926-32211 RRID# AB\_621843) conjugated secondary antibody using an odyssey imager (LI-COR).

**TABLE I. Primary Antibodies Used**

Antigen	Description of immunogen	Source, host species, catalog No., clone No., RRID	Concentration used (WB)
HSP90	Human Hsp90	Stressgen, rabbit polyclonal, SPA-846, AB_1659604	1:10,000
HSP70	Native human Hsp70 protein	Stressgen, mouse monoclonal, ADI-SPA-810, C92F3A-5, AB_2039260	1:10,000
TDP-43	Synthetic peptide corresponding to aa 355–369 of human TDP-43 conjugated to KLH	Sigma, rabbit polyclonal, T1580, AB_2532125	1:1,000
Caspase-3	Raised against aa 1–277 representing full-length procaspase-3 of human origin	Santa Cruz Biotechnology, rabbit polyclonal, sc-7148, AB_637828	1:200
$\alpha$ -Tubulin	$\alpha$ -Tubulin <i>Tetrahymena thermophila</i> and <i>Tetrahymena pyriformis</i> (mixture)	DSHB, mouse monoclonal, 12G10, AB_528498	1:10,000
LC3B	Synthetic peptide corresponding to residues near the amino terminus of LC3B	Pierce, rabbit polyclonal, PA5-17224, AB_10987450	1:1,000
ATG7	Synthetic peptide corresponding to residues in the human Apg7 protein	Abcam, rabbit polyclonal, ab133528, EPR6251, AB_2532126	1:10,000
GFP	GFP from the jellyfish <i>Aequorea victoria</i> N-terminal peptide-KLH conjugated	Thermo Scientific, mouse monoclonal, MA5-15256, GF28R, AB_10979281	1:3,000

Table 3.1: List of antibodies used for experiments

### Differential Detergent Fractionation

After treatment with MG132, MEFs and SH-SY5Y cells were scraped in cold PBS, pelleted, and lysed in RIPA buffer. Cell lysates were centrifuged at x 100 000g for 30

min at 4 °C. Supernatants were collected as the RIPA soluble fraction. The resulting pellets were washed with RIPA buffer by sonication and centrifugation at x 100 000g for 30 min at 4 °C. RIPA insoluble pellets were then dissolved in urea buffer (7 M urea, 2 M thiourea, 4% CHAPS, 30 mM Tris, pH 8.5), and centrifuged at x 100 000g for 30 min at 22 °C and the RIPA-insoluble supernatant was collected. The protein concentration of the RIPA soluble fraction was determined by bicinchoninic acid (BCA) assay (Pierce). Equal amount of RIPA-soluble protein (50µg/sample) and equal volume of RIPA-insoluble fraction were resolved by 15% SDS-PAGE and transferred to PVDF membranes (Bio-rad). Following transfer, PVDF membranes were blocked in 5% powdered milk and incubated with the following antibodies overnight at 4°C; rabbit anti-TDP-43 C-terminal specific polyclonal antibody (T1580, Sigma Aldrich RRID#: AB\_2532125), mouse anti-HSP70/HSP72 1: 5000 (Stressgen SPA-810 RRID#: AB\_2039260), rabbit anti-caspase-3 1:200 (Santa Cruz, sc-7148 RRID#: AB\_637828), mouse anti-alpha tubulin 1:10,000 (Iowa bank, 12G10 RRID#: AB\_528498). Antibody signals were detected with IRDye 680LT (1:15,000) or IRDye 800CW (1:20,000) conjugated secondary antibody using an odyssey imager (LI-COR).

### **Antibody Characterization**

Please see Table 1 for a list of all antibodies used.

Anti-HSP70 antibody recognized the expected molecular weight (~70kDa) and anti-HSP90 antibody recognized the expected molecular weight (~90kDa) on western blots from MEFs (Pierce et al. 2010). HSF1<sup>-/-</sup> MEFs showed no induction of HSP70 after MG132 stress. In SH-SY5Y cells treatment with HSF1 inhibitor showed reduction in HSP70 and HSP90 bands as expected. Anti-GFP antibody detects expected 26kDa band

(Dantuma et al. 2000). No bands were detected in control cells that were not transfected with ub-R-GFP construct. A significant increase in the GFP band was detected after proteasome inhibition in ub-R-GFP stable-expressing SH-SY5Y cells treated with proteasome inhibitor MG132. Anti-ATG7 antibody recognized a band at 75kDa molecular weight (manufacturer's datasheet). Anti-LC3B antibody recognized bands at ~14 and 16kDa molecular weights and shows a pattern of expected decrease in band size with MG132 treatment. Anti-TDP-43 (C-terminal) antibody recognized TDP-43 at ~43kDa in both MEFs and SH-SY5Y cells. As expected, the C-terminal specific TDP-43 antibody recognized C-terminal 35kDa and 25kDa fragments produced after MG132 treatment. The anti-caspase-3 antibody recognized two bands p11 and p20 bands (manufacturer's datasheet)

## **Statistical Analysis**

Data were expressed as mean  $\pm$  SEM. Evaluation of differences within two groups were evaluated by Student's *t*-test using IBM SPSS statistics version 20.0 (SPSS, Inc., Armonk, NY). Difference were considered statistically significant at values of  $p < 0.05$

## **RESULTS**

### **Enhanced heat shock response to TDP-43 overexpression**

To assess whether HSF1 overexpression affects the heat shock response to TDP-43 overexpression, we utilized MEF's from HSF1<sup>+/-</sup> mice which overexpress a native human HSF1 roughly 4-fold that is not constitutively active[138]. We transfected HSF1<sup>+/-</sup> MEFs with human TDP-43 tagged with the fluorescent protein TdTomato. TDP-

43 overexpression alone had no effect on HSP70 (Figure 3.1A) and HSP90 (Figure 3.1B) protein levels in wild-type MEFs 12hrs post TDP-43 transfection compared to non-transfected MEFs. In contrast, there was a significant induction of HSP70 (Figure 3.1A) and HSP90 (Figure 3.1B) in HSF1<sup>+/-</sup> MEFs at 12hrs post TDP-43 transfection compared to non-transfected HSF1<sup>+/-</sup> MEFs. We observed a 2 and 1.5 fold induction of HSP70 (Figure 3.1A) and HSP90 (Figure 3.1B) in HSF1<sup>+/-</sup> MEFs compared to WT MEFs at 12hrs post TDP-43 transfection, respectively (Figure 3.1). Eventually at 24 hours, WT MEFs responded to TDP-43 overexpression through significant induction of HSP70 and 90. This demonstrates that WT cells are somewhat refractory to a TDP-43 overexpression induced heat shock response, and shows that HSF1 sensitizes cells to TDP-43 stress, however it is unknown whether overexpression of HSF1 altered TDP-43's propensity to aggregate.

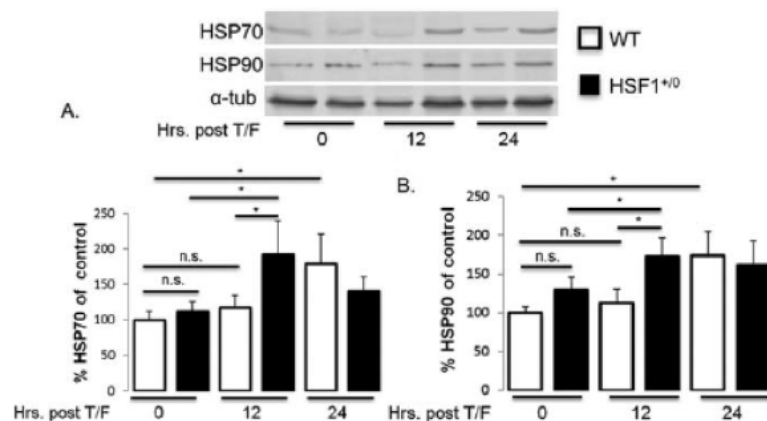


Figure 3.1: Induction of HSPs.

Induction of HSPs. Primary mouse embryonic fibroblasts from human HSF1-overexpressing mice (HSF1<sup>+/-</sup> MEFs) and WT MEFs (as controls) were transfected with tdTomato-tagged human WT TDP-43. A: Immunoblot for HSP70 and HSP90 at 12 and

24 hr post-transfection compared with controls. Bars represent mean  $\pm$  SEM;  $n \geq 9$  per group. \* $P < 0.05$ ; n.s., not significant.

### **HSF1 overexpression prevents formation of TDP-43 puncta and maintains its solubility**

Because overexpression of wild-type TDP-43 has been shown to model TDP-43 pathology *in vitro* [205], we analyzed transfected cells for TDP-43 positive puncta. At 12hrs post TDP-43 transfection TDP-43 positive puncta were observed in WT, however HSF1 overexpression led to a significant ( $p < 0.05$ ) 2.5-fold reduction in TDP-43 positive puncta in HSF1<sup>+/-</sup> MEFs compared to WT MEFs (Figure 3.2).

The proteasome inhibitor MG132 has been shown to drive the accumulation of TDP-43 into stress granules and cytosolic inclusions and promote fragmentation of the TDP-43 C-terminus [195, 207]. In order to determine whether HSF1 had an effect on stress-induced accumulation of detergent insoluble TDP-43 in un-differentiated SH-SY5Y cells, we developed a stable line of HSF1 overexpressing SH-SY5Y cells and treated them with MG132. Western blot data showed that treatment of SH-SY5Y cells with 10 $\mu$ M MG132 caused a significant reduction in the level of TDP-43 soluble in 0.1% SDS RIPA buffer compared to the non-treated cells (Figure 3.3A). To test whether HSF1 was responsible for maintaining the solubility of TDP-43, we treated SH-SY5Y cells with the HSF1 inhibitor KRIBB II (N2-(1H-indazole-5-yl)-N6-methyl-3-nitropyridine-2,6-diamine) which impairs the recruitment of elongation factors needed to promote HSP gene expression[208], and inhibits the induction of HSP70 in response to MG132 (Figure 3.3B). Pre-treatment with 10 $\mu$ M KRIBB II followed by 10 $\mu$ M MG132 significantly reduced RIPA soluble TDP-43 compared to MG132 alone, and a 2-fold reduction

compared to non-treated cells (Figure 3.3C). To corroborate the above results, we treated HSF1 knockout (HSF1<sup>-/-</sup>) MEFs with 10 $\mu$ M MG132 for 6hrs and 12hrs. We first examined the heat shock response to MG132 stress. We show that HSP70 induction was prevented in HSF1<sup>-/-</sup> MEFs even after 12hrs of MG132 treatment (Figure 3.3D). We then investigated the effect of HSF1 knockout on TDP-43 solubility, and show that TDP-43 solubility was not altered in HSF1<sup>-/-</sup> MEFs alone (Figure 3.3D), but when HSF1<sup>-/-</sup> MEFs were treated with MG132 we observed a significant ( $p<0.05$ ) 1.5-fold reduction in RIPA soluble TDP-43 compared to WT MEFs treated with MG132 at 6hrs (Figure 3.3D). At 12hrs post MG132 treatment we see significant ( $p<0.01$ ) 13-fold reduction in RIPA soluble TDP-43 in HSF1<sup>-/-</sup> MEFs compared to WT MEFs (Figure 3.3D) and even observe soluble 35kDa and 25kDa fragments of TDP-43.

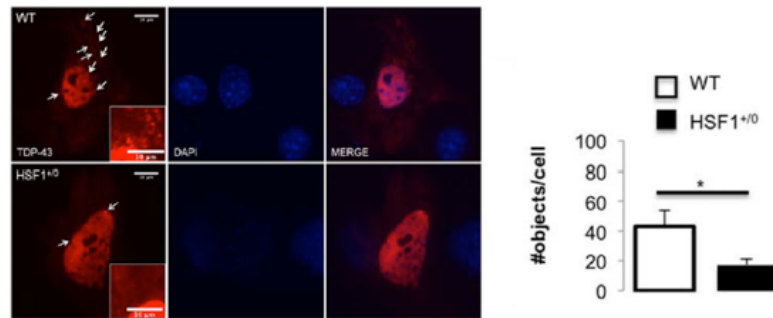


Figure 3.2: Reduction of TDP-43-positive puncta.

WT and HSF1<sup>+/0</sup> MEFs were transfected with a wtTDP-43 tdTomato HA construct. Cells were fixed in 2% paraformaldehyde 12 hr posttransfection. **Left:** Fluorescence microscopy images of tdTomato-tagged TDP-43-transfected cells show positive puncta (red, arrows); DAPI was used to stain cell nuclei (blue). For the **inset** images, a region of the cytosol was enlarged, and the intensity was uniformly and linearly increased by 100%

to show cytosolic features. **Right:** ImageJ was used to quantify TDP- 43 puncta per cell. Bars represent mean  $\pm$  SEM; n= 26 cells per group. \*P < 0.05.

### **HSF1 prevents accumulation of insoluble TDP-43 fragments**

Accumulation of detergent soluble and insoluble fragments has been shown to contribute to the pathogenicity of TDP-43 *in vitro* and *in vivo*. MG132 has been shown to trigger TDP-43 fragmentation and activation of caspase-3 [195, 207]. To investigate whether HSF1 prevents the accumulation of TDP-43 fragments we examined the levels of TDP-43 fragments in the detergent insoluble (urea soluble) fraction after MG132 treatment in HSF1 overexpressing SH-SY5Y cells compared to control. At basal levels, we see a significant reduction in TDP-43 35kDa fragments (TDP-35) in the HSF1 SH-SY5Y cells compared to controls in the urea fraction (Figure 3.4A). A significant 10-fold increase in TDP-35 fragment was seen in SH-SY5Y cells treated with 10 $\mu$ M MG132 compared to non-treated, but no increase in TDP-35 was observed in treated versus non-treated HSF1 SH-SY5Y cells (Figure 3.4A).

Conversely, we see the accumulation of both TDP-35 and TDP-25 fragments in MG132 treated HSF1<sup>-/-</sup> MEFs in the RIPA soluble fraction (Figure 3.3A) and in the urea fraction compared to control (Figure 3.4B). In aggregate, the distinct comprehensive effects of HSF1 on the soluble and insoluble pools of TDP-43 and its fragments in response to MG132 with time are shown in SH-SY5Y cells overexpressing HSF1 (Figure 3.4C) and in HSF1<sup>-/-</sup> MEFs (Figure 3.4D). We show that HSF1 overexpressing SH-SY5Y cells treated with 10 $\mu$ M MG132 had a significantly lower level of cleaved caspase-3 (Figure 3.4E), suggesting that HSF1 overexpression might be cytoprotective.

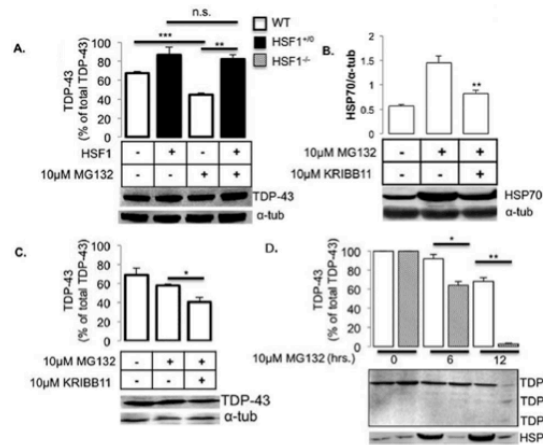


Figure 3.3: HSF1 maintains TDP-43 solubility

Western blot of TDP-43 (C-terminal specific antibody) from the RIPA-soluble fraction.

A: SH-SY5Y and SH-SY5Y cells transfected with human HSF1 were treated with 10  $\mu$ M proteasome inhibitor MG132 for 24 hr. B,C: SH-SY5Y cells were treated with 10  $\mu$ M HSF1 inhibitor KRIBB11 for 30 min or DMSO, followed by 10  $\mu$ M MG132 for 24 hr, and immunoblotted for HSP70 (B) or TDP-43 (C). D: WT and HSF1<sup>-/-</sup> MEFs were treated with MG132 for 6 and 12 hr and immunoblotted for TDP-43 or HSP70. All cell lysates were dissolved in 0.1% SDS RIPA buffer and centrifuged at 100,000g. All immunoblots show endogenous RIPA-soluble TDP-43 with a C-terminal-specific antibody. Bars represent mean  $\pm$  SEM; n=3 per group. \*P < 0.05, \*\*P < 0.01, \*\*\*P < 0.001; n.s., not significant.



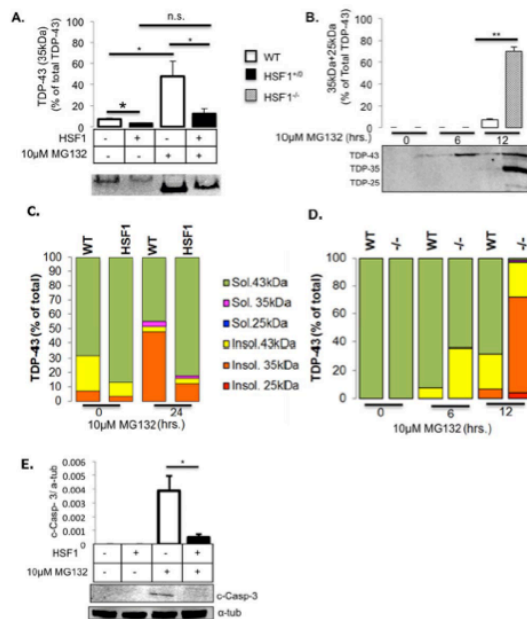


Figure 3.4: HSF1 prevents accumulation of insoluble TDP-43 fragments.

Western blot of TDP-43 (C-terminal-specific antibody) from the RIPA-insoluble fraction.

A: SH-SY5Y cells overexpressing human HSF1 were treated with 10 μM MG132 for 24

hr. B: HSF1<sup>-/-</sup> and WT MEFs were treated with 10 μM MG132 for 6 and 12 hr. Cell

lysates were collected in 0.1% SDS RIPA buffer and centrifuged at

100,000g. The insoluble pellets were washed twice in 0.1% SDS RIPA buffer and

dissolved in 7 M urea, 2 M thiourea, and 2% CHAPS and centrifuged at 100,000g

(supernatant was collected as urea fraction). C,D: C-terminal TDP-43-specific bands at

43 and 35 kDa in the soluble and insoluble fractions were immunoblotted in the same

detection

antibody and quantitated and expressed as a percentage of the total TDP-43 signal.

Graphs show all TDP-43 species for both RIPA-soluble and RIPA-insoluble fractions

from nontransfected control SH-SY5Y (WT) and HSF1-SH-SY5Y (C) and WT and

HSF1<sup>-/-</sup> MEFs after 10  $\mu$ M MG132 treatment (D). E: Cleaved caspase-3 immunoblot in HSF1

transfected SH-SY5Y cells treated with 10  $\mu$ M MG132 for 24 hr. Bars represent mean  $\pm$  SEM; n=3 per group. \*P < 0.05, \*\*P < 0.01; n.s., not significant, Student's t-test.

### HSF1 protects against TDP-43 toxicity and proteotoxic stress

To determine if HSF1 activation protects against toxicity induced by TDP-43 C-terminal fragments (CTF) as described previously we transfected SH-SY5Y cells with a TDP-43 CTF (a.a. 216- 414) fused with EGFP (CON4) following pre-treatment with 0.1 $\mu$ M celastrol to activate HSF1. Our results show that HSF1 activation prevented cells from undergoing early and late apoptosis as detected by PI/annexin-V double staining using flow cytometry (Figure 3.5A&B). These findings were also supported by observing a significant reduction in toxicity after MG132 treatment in HSF1 overexpressing SH-SY5Y cells compared to control non-treated cells (Figure 3.5C).

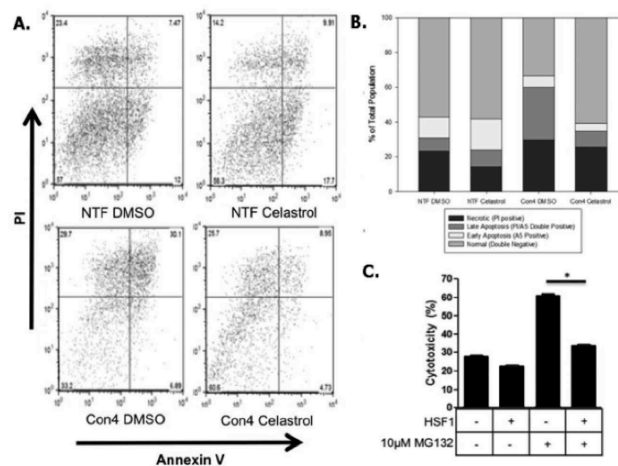


Figure 3.5: HSF1 protects against CTF-induced toxicity.

HSF1 was pharmacologically activated by treating SH-SY5Y cells with 0.1  $\mu$ M celastrol for 1 hr, and cells were allowed to recover for 5 hr. Cells were then transfected with EGFP-tagged TDP-43 CTF (Con4). A: Cells were fixed after 48 hrs and sorted by fluorescent-activated cell sorting. Propidium iodide and annexin V double staining were used to detect apoptotic cells, and their proportions are displayed (B). C: Lactate dehydrogenase assay was used to measure cell toxicity in HSF1-transfected SH-SY5Y cells treated with 10  $\mu$ M MG132 for 12 hrs. Bar represents mean  $\pm$  SEM; n = 3 per group. \*P < 0.05.

#### **HSF1 activation does not enhance global protein turnover following proteasome inhibition**

Next, we wanted to investigate the mechanism of HSF1 mediated protection against stress-induced insolubility of TDP-43. Accumulation of TDP-43 into ubiquitin-positive inclusions in ALS and FTLN brains have implicated the ubiquitin proteasome system UPS in TDP-43 degradation or pathogenesis [209, 210]. We used a GFP reporter system that allows us to quantify global rates of UPS proteolysis[11]. Two constructs that have ubiquitin fused to GFP (Ub-R-GFP and Ub-M-GFP) were used to develop a stable line in SH-SY5Y cells. Upon ubiquitin cleavage Ub-R-GFP is rapidly degraded by the proteasome, but not Ub-M-GFP[11]. Stably transfected SH-SY5Y cells were pretreated with 0.1 $\mu$ M celastrol and then MG132 for 24hrs. MG132 led to significant accumulation of the Ub-R-GFP reporter, however no difference in GFP protein levels was detected in

cells pre-treated with 0.1 $\mu$ M celastrol and MG132 compared to MG132 alone (Figure 3.6A). Autophagy has been suggested to play a role in TDP-43 homeostasis [211, 212] and HSF1 has been shown to upregulate ATG7, a key regulator of macroautophagy [213]. To test whether HSF1 protects against proteasome inhibition by activating macroautophagy we first pretreated SH-SY5Y cells with 0.1 $\mu$ M celastrol and then 10 $\mu$ M MG132 and measured the protein levels of microtubule-associated protein light chain 3 (LC3-I & LC3-II) (Figure 3.6B). We see a significant up-regulation of LC3II protein levels after 10 $\mu$ M MG132 treatment compared to control non-treated cells. However, we show that LC3II levels were significantly reduced in cells pretreated with celastrol followed by MG132 compared to MG132 only, indicating that HSF1 activation blunts the induction of autophagy induced by MG132. No significant differences were detected in either ATG7 levels between celastrol treated vs. MG132 treated alone (figure 3.6C), or in p62 levels (data not shown) indicating that upregulation of autophagy or autophagic flux, respectively are not mechanisms of protection being offered by HSF1 in the context of MG132, and that HSF1 activation is more preventive than restorative in this model.

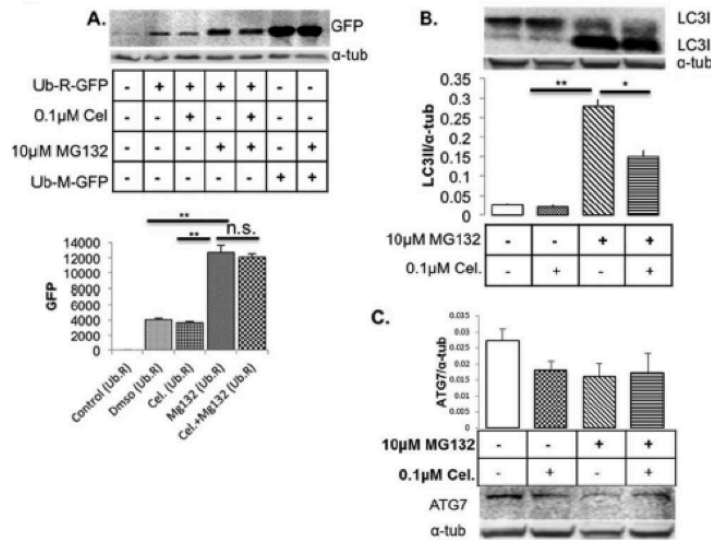


Figure 3.6: HSF1 activation does not increase global UPS activity and reduces induction of autophagy.

Ub-R-GFP stably transfected and nontransfected SH-SY5Y cells were pretreated with 0.1  $\mu$ M celastrol for 1 hr and allowed to recover for 5 hr. Cells were then treated with 10  $\mu$ M MG132 for 24 hr and harvested for immunoblot. A: Immunoblot for GFP at 6 hr. B: Immunoblot for LC3-II normalized by  $\alpha$ -tubulin. C: Immunoblot for ATG7. Bars represent mean  $\pm$  SEM; n = 3.

\*P < 0.05, \*\*P < 0.01; n.s., not significant.

### HSP70 is a major contributor to HSF1 mediated TDP-43 proteostasis

We have shown that HSP70 induction during TDP-43 stress is more sensitive in cells overexpressing HSF1 compared to WT cells (Figure 3.1). To confirm that HSP70 plays a significant role in maintaining TDP-43 solubility we treated SH-SY5Y cells

with 10 $\mu$ M VER155008 a known HSP70 ATPase inhibitor. First we show that VER155008 alone does not affect TDP-43 solubility (Figure 3.7A) but when SH-SY5Y cells are treated with both MG132 and 10 $\mu$ M VER155008 we see a significant reduction in RIPA soluble TDP-43 compared to MG132 alone, and a further decrease compared to control non-treated cells (Figure 3.7A).

Conversely, we see a significant increase in TDP-43 in the urea fraction in SH-SY5Y cells treated with both VER155008 and MG132 compared to MG132 alone (Figure 3.7A). Surprisingly, we did not detect any difference in the urea soluble 35kDa TDP-43 fragment (Figure 3.7A). To assess the potential clinical relevance of the relationship between HSP70 and TDP-43, we examined the colocalization of HSP70 with TDP-43 pathology in cortical layers II/III of AD patients compared to age-matched controls. Using immunofluorescence microscopy we show the presence of TDP-43 positive puncta and co-localization of HSP70 with TDP-43 pathology in AD tissues compared to control (Figure 3.7B).

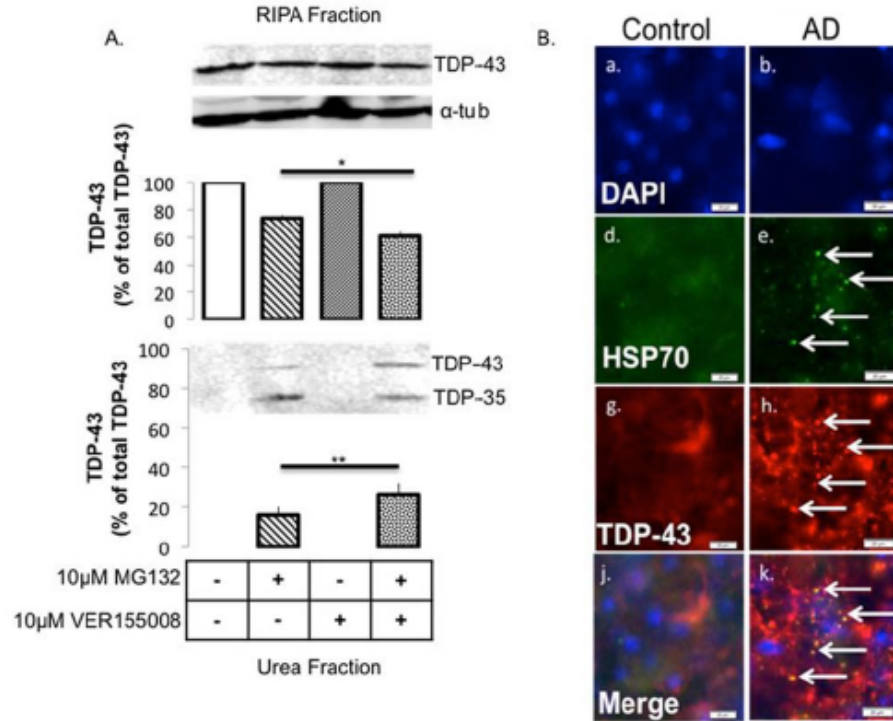


Figure 3.7: HSP70 inhibition reduces TDP-43 solubility and colocalizes with TDP-43 pathology in human AD cortex.

Western blot of TDP-43 (C-terminal-specific antibody) from the RIPA-soluble and -insoluble fraction (urea fraction). SH-SY5Y cells were treated with 10  $\mu$ M VER155008, an HSP70 inhibitor, and then with 10  $\mu$ M MG132 for 24 hr. Cell lysates were dissolved in 0.1% SDS RIPA buffer and centrifuged at 100,000g, and the supernatant was collected as the RIPA-soluble fraction. Pellets were washed twice with 0.1% SDS RIPA buffer and then dissolved in 7 M urea, 2 M thiourea, and 2% CHAPS and centrifuged at 100,000g. Supernatant was collected as RIPA-insoluble (urea) fraction. **A:** Immunoblot for TDP-43 of 0.1% SDS RIPA-soluble fraction. In graph, bars represent mean  $\pm$  SEM; n = 3. **\*\*P** < 0.01. **B:** Immunofluorescence staining shows TDP-43- and HSP70-positive cells in layer II/III of cortex from control or AD brain.

## DISCUSSION

We have previously shown that human HSF1 overexpressing mice (HSF1<sup>+/0</sup>) have an enhanced heat shock response[138], are protected against AD-like memory deficits [143], and show delayed disease onset in an ALS mouse model [109] that correlated with an increase in HSPs (such as HSP70) at the protein level. This study shows that enhancing HSF1 without pharmacologically inducing proteotoxic stress is protective against TDP-43 induced aggregation and toxicity in a human neuronal-like system. Using different cellular models that overexpress a non-mutant human HSF1 transgene, we demonstrate that HSF1 overexpression lowers the threshold of the heat shock response to TDP-43 overexpression and concurrently prevents the accumulation of TDP-43-positive puncta in response to TDP-43 overexpression or MG132 induced proteotoxic stress (Figure 3.1 and 3.2). Although we have not confirmed that these puncta are exclusively TDP-43 aggregates, previous studies have shown that the presence of TDP-43 during stress in cytoplasmic foci or stress granules could become pathogenic seeds[214]. Insoluble TDP-43 has been shown to have prion-like properties and can aggregate in a self-templating manner [198]. The current data indicates that HSF1 enhances the heat shock response to prevent the stress-induced transition of detergent soluble TDP-43 to detergent insoluble TDP-43 (Figure 3.3). The results suggest that the mechanism by which HSF1 protects against TDP-43 insolubility is, at least in part, upregulation of HSP70 and dependent upon its ATPase activity; however, other HSPs or factors could be involved. Although the dissociation constant of the HSP70 inhibitor used is lowest for HSP70, its affinity to other HSPs cannot be entirely ruled out, therefore



other HSPs such as HSP90 could contribute to the protective effects. We examined the global activity of protein degradation pathways including ubiquitin proteasome system (UPS) and macroautophagy. We did not observe any increase in the global UPS activity with celastrol, an HSF1 activator before MG132 stress (Figure 3.6A). Our results confirm a previous study that showed no change in proteasome activity in constitutively active HSF1 stress induced cells[215]. Although no difference was detected in global rates of UPS-mediated degradation, targeted degradation of specific substrates, such as TDP-43, could be altered by HSF1. Our findings are also consistent with the observation that, in neurons, newly synthesized proteins are the population of proteins most susceptible to MG132-mediated insolubility [216]. Autophagy is thought of as a late stage event that is activated for clearance of long-lived aggregated proteins. Given that autophagy has been shown to be required for clearance of TDP-43 macroaggregates[12, 210] and that HSF1 can upregulate the expression of a regulator of autophagy ATG7[217], we hypothesized that HSF1 might be driving TDP-43 turnover via induction of autophagy. However, autophagy was found to be induced less in HSF1 activated cells subjected to stress, suggesting that HSF1 activation induces the production of HSPs that prevent the accumulation of newly synthesized proteins and TDP-43 aggregates, making cells less dependent on macroautophagy during proteasome inhibition (Figure 3.6B), this was supported by our observation that inhibition of the ATPase activity of HSP70 significantly worsened TDP-43 solubility.

Clearance of TDP-43 pathology has been shown to be advantageous; disease progression was slowed, and motor improvement followed after mutant human TDP-43 gene expression was switched off in both a TDP-43 rat and a mouse model [218, 219].

Here we show that HSF1 overexpression protects against TDP-43 pathology by preventing the accumulation of insoluble and truncated forms of TDP-43 (35kDa and 25kDa fragments). We show that HSF1 possibly protects against caspase-mediated cleavage of TDP-43 by simultaneously preventing caspase-3 activation during stress (Figure 3.3). Our results were confirmed by inhibiting HSF1 activity or knocking out the HSF1 gene, which exacerbated TDP-43 insolubility. Next, we showed that HSP70 co-localizes with TDP-43 pathology in the cortex of AD patients, indicative of a biological significance between HSP70 and TDP-43 in humans.

In conclusion, we show that HSF1 can prevent the conversion of TDP-43 from a soluble species to an insoluble one by up regulation of its chaperones such as HSP70 and not through enhancing global activity of the UPS or autophagy. This study demonstrates how HSF1 could play a preventive role in TDP-43 insolubility in response to proteotoxic stress; it will next be important to determine whether activation of HSF1 in a model system that contains established TDP-43 pathology would also be protective. Given that arimoclomol is currently undergoing phase II/III clinical trials for ALS patients with SOD1 mutations, these studies suggest that Arimoclomol or similar activators could be applicable to the remaining ALS patient population and other TDP-43 proteinopathies.

**(This chapter contains previously published work in [111])**

## **Conclusion and Future Directions**

### **PRELIMINARY STUDIES**

#### **METHODS**

##### **Generation of double transgenic mice (human HSF1 and human TDP-43)**

Mice overexpressing human TDP-43 were purchased from the Jackson Laboratory, stock number 012836 (The Jackson Laboratory, Bar Harbor, Maine, USA). Briefly, TDP-43 transgene was designed with the human TARDBP gene driven by a mouse Thy1 (neuronal) promoter and SV40 polyadenylation site[72]. TAR4 mice were bred to B6SJLF1/J. Mice overexpressing human HSF1 were generated by our laboratory and maintained on a C57BL/6J background. Briefly BAC clone 2274G4 (Invitrogen) contains the entire human HSF1 gene[220]. TAR4 mice were crossed with hHSF1<sup>+/-</sup> mice, TAR4 x hHSF1<sup>+/-</sup> offspring was crossed with hHSF1<sup>+/-</sup> mice or wild-type mice (C57BL/6J background). The next generation offspring was crossed with hHSF1<sup>+/-</sup> mice or wild-type mice (C57BL/6J background). This was done six times to generate a congenic strain before experiments were performed (Illustration 4.1). All animals were genotyped before and after studies were conducted.

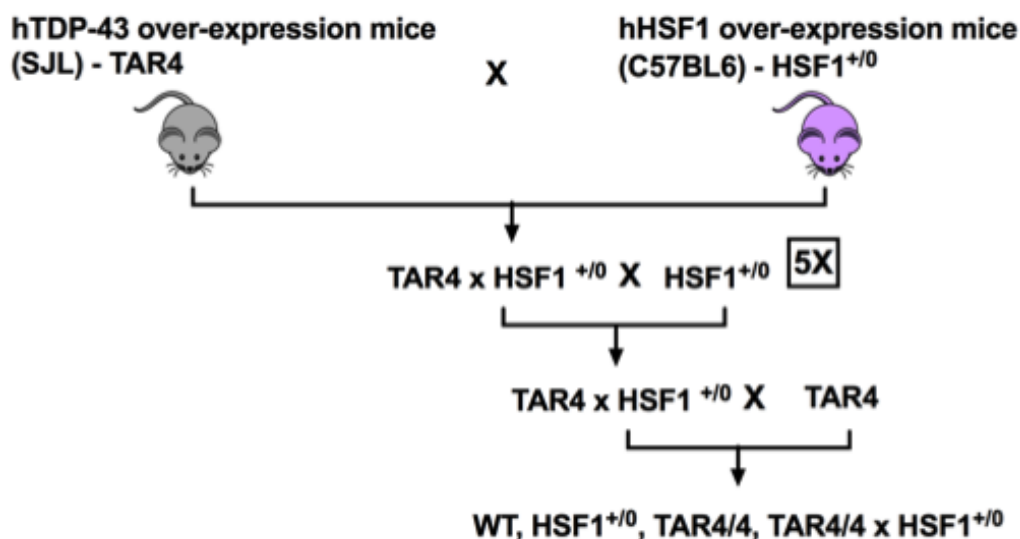


Illustration 4.1: Generation of double transgenic mice overexpressing wild-type human TDP-43 and wild-type human HSF1

### Preparation of mouse brain lysate

Sagittal half brain tissue was homogenized in 10x v/w 2% SDS RIPA buffer (50mM Tris, 150mM NaCl, 1% NP-40, 0.5% deoxycholate) containing 1x protease inhibitor cocktail 1 (CALBIOCHEM) and phosphatase inhibitor cocktail 2 (Sigma) [221]. Following centrifugation, BCA assay (Pierce) was used to determine protein concentration of RIPA-soluble fraction [221].

### Subcellular Fractionation

Subcellular fractionation was slightly modified from previous studies[72]. Frozen tissues were weighed and homogenized in buffer containing 10mM HEPES, 10mM NaCl, 1mM KH<sub>2</sub>PO<sub>4</sub>, 5mM NaHCO<sub>3</sub>, 5mM EDTA, 1mM CaCl<sub>2</sub>, 0.5 mM MgCl<sub>2</sub> (7.5x v/w). After 10mins on ice, 2.5M sucrose (0.375x v/w) was added. Next, tissues were homogenized and centrifuged at 6,300 xg for 10mins [221]. The supernatant was defined as the non-

nuclear fraction. The pellet was washed three times in TSE buffer (10mM Tris, 300mM sucrose, 1mM EDTA, 0.1% Nonidet P-40) 10x v/w), homogenized, and centrifuged at 4000 xg for 5mins [221]. Finally the pellet was re-suspended in RIPA with 2% SDS (5x v/w) as the nuclear fraction).

### Real time-PCR

Total RNA was extracted from one hemisphere brain tissues using TRIzol® reagent (Invitrogen). RNA was quantified using a NanoDrop spectrophotometer. 1µg RNA were used to synthesize cDNA using RETROscript kit (Ambion) Real-time reverse transcription PCR was performed with a LightCycler 480 (Roche Diagnostics) sequence detection system using LightCycler SYBR Green I. Samples were run in triplicates. Primer efficiencies were determined by using a cDNA dilution series. A 1:25 dilution of each cDNA was run. Normalization was performed using Gapdh reference gene.

Gene	Sequence	bp
GAPDH-F	GGCTGCCCAGAACATCATCCCT	278
GAPDH-R	ATGCCTGCTTCACCACCTTCTTG	278
Mouse TDP-43-F	ATTTGAGTCTCCAGGTGGGTGTGG	291
Mouse TDP-43- R	GTTTCACTATACCCAGCCCACTTTTCTTAGG	291

[222]

Table 4.1: List of primer used for Real time-PCR

### Western blotting

Equal protein amounts were loaded for each subcellular fraction (nuclear and non-nuclear fractions). 35 or 50 µg nuclear fraction, 75-µg cytoplasmic fractions, and 50 µg of total homogenate fraction were loaded on a gradient 4-15% precast protein gels (Bio-rad) and transferred to PVDF membranes (Bio-rad). Membranes were blocked in 5% powdered milk at 4°C overnight. The primary antibodies used include; rabbit anti-TDP-43 C-

terminal polyclonal antibody (1:1000; T1580, Sigma Aldrich), human specific mouse anti-TDP-43 (1:1000; ab57105, abcam), mouse anti  $\alpha$ -tubulin (1:15 000; 12G10, Developmental Studies Hybridoma Bank [DSHB], University of Iowa), Rabbit anti-HSP70 (1:1000; 4872S, cell signaling), Rabbit anti-HSP40 (C6484) (1:1000, 4871P, cell signaling). rabbit anti-HSF1 (1:1000; ADI SPA 901D, Enzo), rabbit anti-lamin B1 (1:1000; ab16048, abcam), rabbit anti-SIRT1 (1:1000; 07-131, milipore), histone H3 (D1H12) XP (1:1000; 4499S, cell signaling) mouse-gapdh MA5-1:5000; 15738, Pierce Thermo), mouse anti -gapdh (1:1000; MAB 374, milipore). Fluorescent conjugated secondary antibody, IRDye 680LT goat anti-mouse (1:15 000, LiCor) or IRDye 800CW goat anti-rabbit (1:20 000, LiCor) signals were detected with odyssey imager (LI-COR) and quantified using Image J.

### **Behavioral Analysis**

Wire-hang test was performed on WT, HSF1, TAR4/4 and TAR4/4 x HSF1 animals at post-natal day 15. Briefly, mice were placed on a wire and gently flipped upside down at about 30cm above a cage with cushion to brace the fall of the animal. Time to fall was recorded. The trials were performed with 5min rest between sessions [219].

### **Statistical Analysis**

One-way ANOVA analysis was used to determine significant differences between the four groups. Post hoc tests using bonferroni's test was used to compare measures among 4 groups. Two-tailed *t*-test was also done to compare measures between 2 groups. Values of  $p < 0.05$  were considered statistically significant. Prism 6 (GraphPad) was used for analysis.

## RESULTS

### HSF1 overexpression increases its nuclear translocation.

To investigate whether HSF1 overexpression increases its activity, brain samples from 14-day-old mice were separated into nuclear, non-nuclear, and total homogenate for biochemical analysis. As expected, the human HSF1 protein was detected in the single transgenic (HSF1) and double transgenic mice (TAR4/4 x HSF1). (Figure 4.1 A B C) Quantitative analysis showed no difference in the mouse HSF1 between the four groups, WT, HSF1, TAR4/4 and TAR4/4 x HSF1, and no difference in human HSF1 between HSF1 and TAR4/4 x HSF1 in the homogenate fraction. A trend in the increase of human HSF1 levels in the nuclear fraction, and a significant decrease in the non-nuclear fraction was seen in the TAR4/4 x HSF1 compared to HSF1. There was no change in mouse HSF1 protein levels in the non-nuclear fraction. (Figure 4.1)

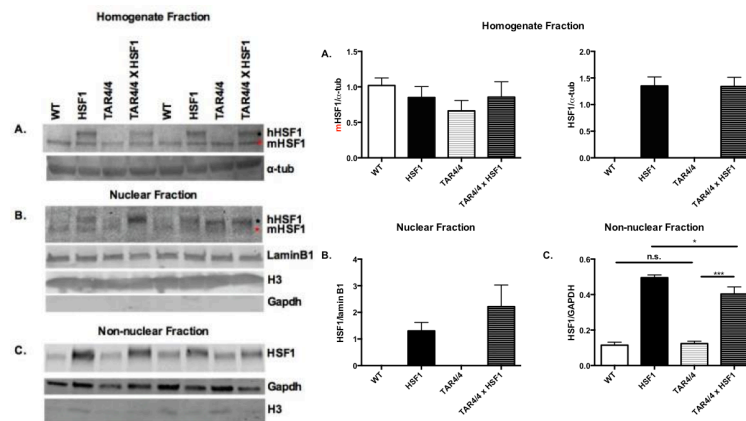


Figure 4.1: Total and subcellular localization of HSF1 in brain of TAR4/4 x HSF1 mice.

Sagittal half brain homogenized in sucrose buffer (0.125M sucrose, 10 mM Hepes, 10 mM NaCl, 1 mM  $\text{KH}_2\text{PO}_4$ , 5 mM  $\text{NaHCO}_3$ , 5 mM EDTA, 1 mM  $\text{CaCl}_2$ , 0.5 mM  $\text{MgCl}_2$ ) with protease and phosphatase inhibitor. SDS was added to total homogenate, final concentration 2% SDS. Subcellular fractionation was performed and cytoplasmic supernatant was isolated and nuclear pellet fraction dissolved in 2% SDS RIPA buffer. Immunoblot for pan-HSF1 (human and mouse) A. total homogenate B. nuclear fraction C. non-nuclear fraction, from 14day old (WT, HSF1, TAR4/4 and TAR4/4 x HSF1) mice. (n=3mice/genotype). \*  $p < 0.05$ , \*\*  $p < 0.01$ . 35 $\mu\text{g}$  nuclear fraction, 75 $\mu\text{g}$  non-nuclear fraction and 50 $\mu\text{g}$  total homogenate were loaded. Data shown are means  $\pm$  SEM.

### **HSF1 overexpression increases nuclear SIRT1 levels.**

SIRT1 is a histone deacetylase that promotes HSF1 activity [94]. To provide additional evidence that HSF1 is activated in TAR4/4 x HSF1, brain samples from 14-day-old mice were separated into nuclear and non-nuclear fractions for biochemical analysis. SIRT1 levels between WT, HSF1 and TAR4/4 mice were unchanged; however, levels in TAR4/4 x HSF1 mice were significantly increased compared to TAR4/4. There was no difference in SIRT1 levels in the non-nuclear fraction between the four groups (Figure 4.2). Alpha tubulin was used as a non-nuclear marker. We detected some alpha-tubulin was detected in the nuclear fraction. However, gapdh (non-nuclear marker) was not detected in the nuclear fraction (Figure 4.1), and this rules out any concerns about fractionation method.



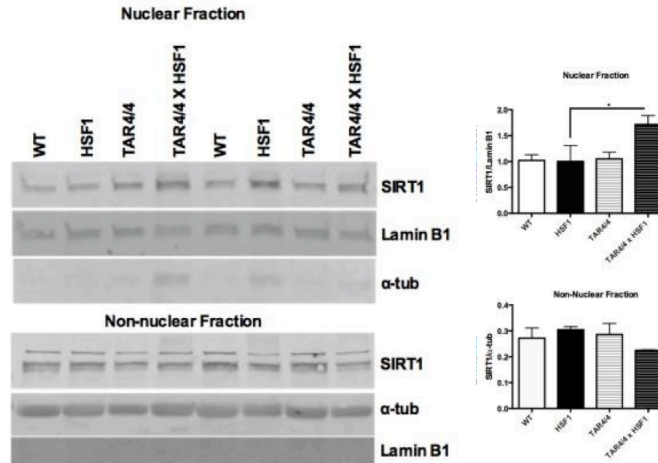


Figure 4.2: Subcellular localization of SIRT1 in brain of TAR4/4 x HSF1 mice

Sagittal half brain homogenized in sucrose buffer (0.125M sucrose, 10 mM Hepes, 10 mM NaCl, 1 mM  $\text{KH}_2\text{PO}_4$ , 5 mM  $\text{NaHCO}_3$ , 5 mM EDTA, 1 mM  $\text{CaCl}_2$ , 0.5 mM  $\text{MgCl}_2$ ) with protease and phosphatase inhibitor. SDS was added to total homogenate, final concentration 2% SDS. Subcellular fractionation was performed and cytoplasmic supernatant was isolated and nuclear pellet fraction dissolved in 2% SDS RIPA buffer. Immunoblot for SIRT1 nuclear fraction and non-nuclear fraction, from 14day old (WT, HSF1, TAR4/4 and TAR4/4 x HSF1) mice. (n=3mice/genotype). \*  $p < 0.05$ . 35 $\mu\text{g}$  nuclear fraction and 75 $\mu\text{g}$  non-nuclear fraction were loaded. Data shown are means  $\pm$  SEM.

#### Increase in TDP-43 nuclear levels in TAR4/4 x HSF1 mice.

Since the nuclear clearance of TDP-43 and its cytoplasmic aggregation is predominant to ALS and FTLN pathology, we asked whether HSF1 overexpression would drive TDP-43 into the nucleus. Brain samples from 14-day-old mice were separated into nuclear, non-nuclear, and total homogenate for biochemical analysis. To verify that TAR4/4 model was indeed overexpressing the human TDP-43, we examined TDP-43 levels in the homogenate fraction, using human-specific and pan TDP-43

antibodies. We confirmed the presence of the human TDP-43 transgene in the TAR4/4 and TAR4/4 x HSF1, and quantitative analysis showed that there was no change between them. As expected, we did not detect any human TDP-43 in the control WT or HSF1 samples. To determine the cellular distribution of TDP-43, we examined its levels in the nuclear and non-nuclear fractions. Using pan and human-specific TDP-43 antibodies we detected a significant increase (two-fold) in nuclear TDP-43, when we compared the TAR4/4 x HSF1 to TAR4/4 mice. However, no change in TDP-43 was detected in the non-nuclear fraction between the TAR4/4 x HSF1 and TAR4/4. No bands were detected in the WT or HSF1 using the human TDP-43 antibody.

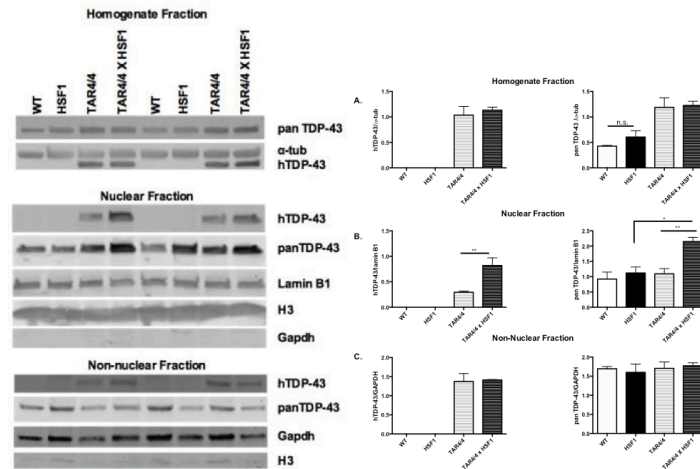


Figure 4.3: TDP-43 subcellular localization and levels in TAR4/4 x HSF1 mice

Sagittal half brain homogenized in sucrose buffer (0.125M sucrose, 10 mM Hepes, 10 mM NaCl, 1 mM  $\text{KH}_2\text{PO}_4$ , 5 mM  $\text{NaHCO}_3$ , 5 mM EDTA, 1 mM  $\text{CaCl}_2$ , 0.5 mM  $\text{MgCl}_2$ ) with protease and phosphatase inhibitor. SDS was added to total homogenate, final concentration 2% SDS. Subcellular fractionation was performed and cytoplasmic supernatant was isolated and nuclear pellet fraction dissolved in 2% SDS RIPA buffer. Immunoblot for **A.** total nuclear TDP-43 protein **B.** human nuclear TDP-43 protein levels

**C.** total TDP-43 protein levels in non-nuclear fraction **D.** human TDP-43 in non-nuclear fraction, from 14 day old (WT, HSF1, TAR4/4 and TAR4/4 x HSF1) mice. (n=3mice/genotype). \*  $p < 0.05$ . 35 $\mu$ g nuclear fraction and 75 $\mu$ g non-nuclear fraction were loaded. Data shown are means  $\pm$  SEM.

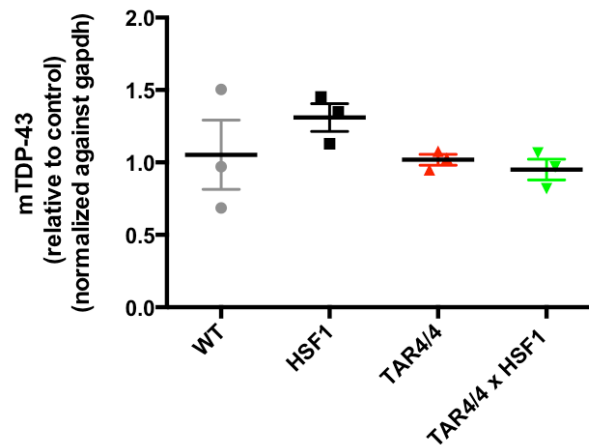


Figure 4.4: Endogenous TDP-43 mRNA expression.

Sagittal half brain homogenized in Triazol. Quantitative real time PCR (qPCR) using mTDP-43-specific primers demonstrate no change in the mTDP-43 mRNA levels in TAR4/4 x HSF1 compared to TAR4/4. Data shown are means  $\pm$  SEM from 15-day-old mice (WT, HSF1, TAR4/4 and TAR4/4 x HSF1).

#### **No change in TDP-43 mRNA levels.**

Studies have shown that TDP-43 auto-regulates itself, and keeps a tight regulation on its protein levels. Our hypothesis was that increasing the nuclear TDP-43 would reduce the endogenous levels of TDP-43 mRNA. There was no significant difference in mouse TDP-43 mRNA levels between TAR4/4 x HSF1 and TAR4/4. (Figure 4.4)

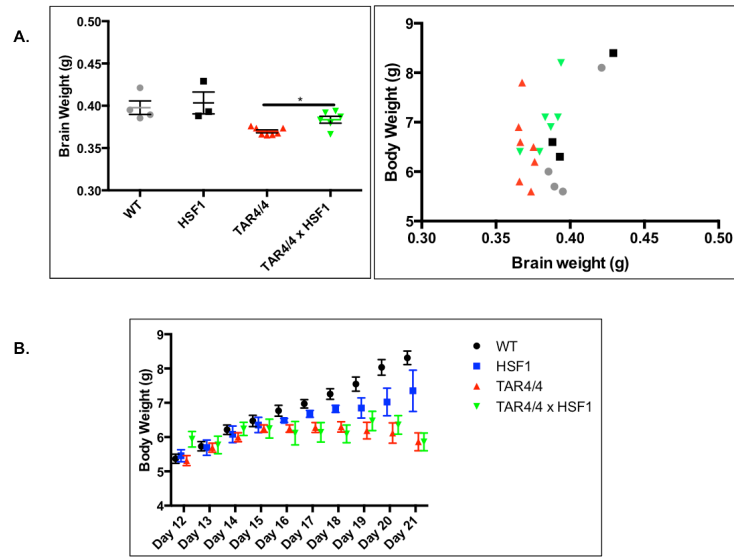


Figure 4.5: Increase in brain weight and no change in body weight.

**A.** At day 15, brain weight of TAR4/4 x HSF1 were significantly higher than age matched TAR4/4.  $n = 3-5$  mice. **B.** Body weight of WT, HSF1, TAR4/4 and TAR4/4 x HSF1 starting at day 12 to 21.  $n = 10-35$  mice per group per day.

### TAR4/4 x HSF1 show no significant rescue of phenotype

We next asked whether increasing the nuclear TDP-43 levels would improve brain and body weight loss associated with ALS or FTLT. TAR4/4 x HSF1 mice showed a significant higher brain weight in day-15 mice, and this was independent of the mice body weight. There was no difference in body weight between TAR4/4 x HSF1 compared to TAR4/4. (Figure 4.5)

We next examined the behavioral phenotype in these TAR4/4 x HSF1 mice. The wire hang test is used to measure muscle strength and detect early muscular deficits[223]. This in addition with other methods have been used to characterize ALS features in mouse models[219]. Unfortunately, due to the size and age of the animals, it was not feasible to do more tests. When we used only male's for analyses for grip strength. We

see a significant decline in the WT or HSF1 compared to the TAR4/4 or TAR4/4 x HSF1. There was no significant difference between the TAR4/4 x HSF1 and the TAR4/4 mice.

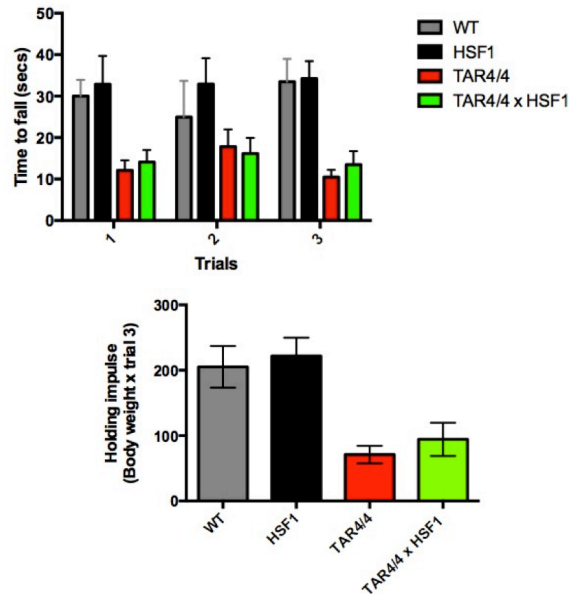


Figure 4.6: Wire hang test comparing TAR4/4 x HSF1 to TAR4/4.

At day 15, wire hang test was performed on WT, HSF1, TAR4/4 and TAR4/4 x HSF1.

$n = 3-8$  mice per group. Three trials were done with a 5 min interval after each one. Data shows mean  $\pm$  SEM

## DISCUSSION

Here, we have developed new bigenic (TAR4/4 x HSF1) mice, which overexpress human wild-type HSF1 and human wild-type TDP-43 transgenes. We have shown that in these double transgenic mice, there is an increase in HSF1 nuclear levels. This could afford it a greater or faster induction of its targets, which is supported by a trend in the increase of HSP70 mRNA levels in TAR4/4 x HSF1 compared to the TAR4/4 mice.

(Data not shown) SIRT1 plays an important role in enhancing the activation of the HSF1 induced heat shock response, by increasing the stress-induced HSF1 binding to its target DNA [94]. Our results showed a significant increase in nuclear SIRT1 in TAR4/4 x HSF1 compared to TAR4/4 or HSF1 or WT. This suggests that HSF1 activity is increased.

The key finding of this study is that HSF1 overexpression drives TDP-43 into the nucleus and rescues the brain weight phenotype. However, the changes in brain weight did not correlate to a significant increase in performance on the wire hang test.

There was no change in TDP-43 protein in the non-nuclear fraction. One reason for this could be the constitutively highly expressed human TDP-43 transgene in these mice, which might not replicate what happens in human patients. This idea is supported by the lack of change in the total TDP-43 protein levels in the TAR4/4 compared to TAR4/4 x HSF1. Another possibility is the technical difficulty in detecting small changes in TDP-43 protein due to the high total protein concentration in the non-nuclear fraction. Future studies would require other techniques such as confocal fluorescence microscopy to distinguish TDP-43 localization within the non-nuclear fraction.

We know that TDP-43 tightly regulates its protein levels [224], and our results show that endogenous TDP-43 mRNA remain the same in the TAR4/4 compared to TAR4/4 x HSF1. At late stage (day 18) in the disease progression in these mice, we do not see a significant increase in nuclear TDP-43 in the double transgenic animals. (Data not shown)

Together this data suggests that the high expression levels of TDP-43 in these mice may be too aggressive to detect robust changes in these bigenic mice. The

expression levels of TDP-43 in various mouse models correlated with the severity of phenotype seen [72]. I have also generated the hemizygous (TAR4 x HSF1) mice, which is a less aggressive model to test for HSF1 protection against TDP-43 pathology. The only draw back is that these mice take at least 14 months to develop a phenotype.

In addition, this study highlights possible behavioral phenotype differences between different sexes (data not shown), which should be further investigated.

Interestingly, we see an increasing trend in the nuclear presence of nucleocytoplasmic shuttling proteins (such as cellular apoptosis susceptibility protein CAS) and a decrease in the nuclear export protein 14-3-3 in the double transgenic (TAR4/4 x HSF1) compared to the disease mice (TAR4/4) (data not shown). This could suggest that HSF1 overexpression protects the nucleocytoplasmic transport system in TDP-43 models, however more work still needs to be done to verify this finding.

In summary, we have showed that increasing nuclear TDP-43 alone does not lead to a robust rescue of TDP-43 phenotype, and that TDP-43 levels plays a key role in pathogenicity.

## CONCLUSION

Abnormal accumulation of SOD1 and TDP-43 is a major driving force in the onset and progression of ALS and TDP-43 proteinopathies. HSPs are crucial for the maintenance of timely folding, refolding and degradation of these proteins. The age-related onset of neurological disorders implies that there is a disruption in protein homeostasis, which has been postulated to be due to a reduction in HSPs, increased cellular stress, mutations and other factors. In addition, some of these disease proteins are composed of low complexity domains (or disordered domains) that are needed for physiological functions such as phase transition during the formation of RNA granules, which can easily become pathogenic.

These studies reported here show that HSF1 overexpression upregulates HSPs in response to mutant SOD1. It shows that mutant SOD1 has exposed surface hydrophobic residues, which could be important for recognition by HSPs [109]. We show that HSF1 overexpression led to improvement of the pathological phenotype associated with ALS in mutant SOD1 mice.

In addition, this thesis work shows that overexpression of HSF1 protects against TDP-43 aggregation by enhancing the heat shock response via HSPs. HSF1 overexpression protects against cellular stress that could facilitate TDP-43 conversion into pathogenic fragments and aggregates.

I have developed a mouse model that overexpresses both the human HSF1 and human TDP-43, which can be used as a tool to study how HSF1 overexpression could protect against protein aggregation *in vivo*. I have shown that HSF1 overexpression



drives TDP-43 into the nucleus in these TAR4/4 x HSF1 mice. How overexpression of HSF1 does this is still unknown and will require future study.

These studies represent the first time that HSF1 overexpression has been shown to induce a robust increase in HSPs that protects against pathological conversion of SOD1 and TDP-43 disease-proteins. It shows that strategies that target HSF1 levels or activity could be effective in treating neurodegenerative disorders. Currently, phase II/III clinical trials are being conducted for arimoclomol- a hydroxylamine that induces HSPs under stress conditions- for the treatment of SOD1-ALS patients. Its mechanism is unknown, however, it is thought to increase the length of HSF1 activation [135].

## **FUTURE DIRECTIONS**

This work highlights the need for further investigation on how HSF1 protects against protein aggregation in ALS and other neurodegenerative diseases. We have shown that HSF1 overexpression favors inducing HSPs such as HSP70 chaperone and does not increase protein turnover by macro-autophagy. However, we have not investigated whether HSF1 overexpression increases chaperone-mediated autophagy (CMA). CMA contributes to the degradation of disease proteins involved in various neurodegenerative diseases such as TDP-43 [225, 226] [227]. More studies are needed to understand the role of CMA in TDP-43 homeostasis, and whether HSF1 overexpression enhances this system.

We have shown that HSF1 overexpression protects against TDP-43 aggregation and rescues some disease phenotype in mice. Future research will be needed to investigate whether HSF1 overexpression could protect against previously aggregated TDP-43 or SOD1 proteins seen in late stages of disease. Shorter's laboratory has

extensively studied yeast HSP104 as a disaggregase against human disease proteins such as TDP-43. They have shown that genetic engineered HSP104 restored aggregated proteins to their normal conformation [228]. More recently, the synergy between the mammalian HSP110, HSP70 and HSP40 has been found to have disaggregase activity [229]. It would be important to study whether HSF1 overexpression increases the HSP110/70/40 collaboration and solubilizes aggregated proteins. The use of viral vectors such as adeno-associated virus vectors (AAV) gene therapy could be a good strategy to investigate protein aggregates in SOD1 or TDP-43 mice. Previous work has shown that overexpression of HSF1 can be done using a lentivirus system to deliver HSF1 to different brain regions in mice [22, 230].

Recent studies have uncovered new HSF1 targets that could provide beneficial effects in neurodegenerative diseases. These targets include synaptic proteins needed for memory consolidation [87]. Memory deficit is a major facet of most of the neurodegenerative diseases. Our preliminary mass spectrometry studies from mice brains showed a decrease in the levels of some synaptic proteins in TAR4/4 mice compared to WT (data not shown). Further studies to explore whether HSF1 overexpression increases synaptic proteins levels are needed. More preliminary studies from the TAR4/4 x HSF1 bigenic mice suggest a possible effect of HSF1 overexpression on the nucleocytoplasmic transport system. Future research needs to be done to identify HSF1 targets that could provide protection to this system.

## REFERENCES

1. Bose, S. and J. Cho, *Targeting chaperones, heat shock factor-1, and unfolded protein response: Promising therapeutic approaches for neurodegenerative disorders*. Ageing Res Rev, 2016.
2. Ling, S.C., M. Polymenidou, and D.W. Cleveland, *Converging mechanisms in ALS and FTD: disrupted RNA and protein homeostasis*. Neuron, 2013. **79**(3): p. 416-38.
3. Cleveland, D.W. and J.D. Rothstein, *From Charcot to Lou Gehrig: deciphering selective motor neuron death in ALS*. Nat Rev Neurosci, 2001. **2**(11): p. 806-19.
4. Nunnari, J. and A. Suomalainen, *Mitochondria: in sickness and in health*. Cell, 2012. **148**(6): p. 1145-59.
5. Barber, S.C., R.J. Mead, and P.J. Shaw, *Oxidative stress in ALS: a mechanism of neurodegeneration and a therapeutic target*. Biochim Biophys Acta, 2006. **1762**(11-12): p. 1051-67.
6. Nixon, R.A., *The role of autophagy in neurodegenerative disease*. Nat Med, 2013. **19**(8): p. 983-97.
7. Banerjee, R., M.F. Beal, and B. Thomas, *Autophagy in neurodegenerative disorders: pathogenic roles and therapeutic implications*. Trends Neurosci, 2010. **33**(12): p. 541-9.
8. Keller, B.A., et al., *Co-aggregation of RNA binding proteins in ALS spinal motor neurons: evidence of a common pathogenic mechanism*. Acta Neuropathol, 2012. **124**(5): p. 733-47.
9. Mann, D.M., et al., *Dipeptide repeat proteins are present in the p62 positive inclusions in patients with frontotemporal lobar degeneration and motor neurone disease associated with expansions in C9ORF72*. Acta Neuropathol Commun, 2013. **1**: p. 68.
10. Menzies, F.M., A. Fleming, and D.C. Rubinsztein, *Compromised autophagy and neurodegenerative diseases*. Nat Rev Neurosci, 2015. **16**(6): p. 345-57.
11. Dantuma, N.P., et al., *Short-lived green fluorescent proteins for quantifying ubiquitin/proteasome-dependent proteolysis in living cells*. Nature biotechnology, 2000. **18**(5): p. 538-43.
12. Scotter, E.L., et al., *Differential roles of the ubiquitin proteasome system and autophagy in the clearance of soluble and aggregated TDP-43 species*. J Cell Sci, 2014. **127**(Pt 6): p. 1263-78.
13. Dawson, T.M. and V.L. Dawson, *The role of parkin in familial and sporadic Parkinson's disease*. Mov Disord, 2010. **25 Suppl 1**: p. S32-9.

14. Dantuma, N.P. and L.C. Bott, *The ubiquitin-proteasome system in neurodegenerative diseases: precipitating factor, yet part of the solution*. Front Mol Neurosci, 2014. **7**: p. 70.
15. Scotter, E.L., H.J. Chen, and C.E. Shaw, *TDP-43 Proteinopathy and ALS: Insights into Disease Mechanisms and Therapeutic Targets*. Neurotherapeutics, 2015. **12**(2): p. 352-63.
16. Kim, H.J., et al., *Mutations in prion-like domains in hnRNPA2B1 and hnRNPA1 cause multisystem proteinopathy and ALS*. Nature, 2013. **495**(7442): p. 467-73.
17. Conicella, A.E., et al., *ALS Mutations Disrupt Phase Separation Mediated by alpha-Helical Structure in the TDP-43 Low-Complexity C-Terminal Domain*. Structure, 2016. **24**(9): p. 1537-49.
18. Molliex, A., et al., *Phase separation by low complexity domains promotes stress granule assembly and drives pathological fibrillization*. Cell, 2015. **163**(1): p. 123-33.
19. Vernace, V.A., T. Schmidt-Glenewinkel, and M.E. Figueiredo-Pereira, *Aging and regulated protein degradation: who has the UPPer hand?* Aging Cell, 2007. **6**(5): p. 599-606.
20. Chen, H.J., et al., *The heat shock response plays an important role in TDP-43 clearance: evidence for dysfunction in amyotrophic lateral sclerosis*. Brain, 2016. **139**(Pt 5): p. 1417-32.
21. Chafekar, S.M. and M.L. Duennwald, *Impaired heat shock response in cells expressing full-length polyglutamine-expanded huntingtin*. PLoS One, 2012. **7**(5): p. e37929.
22. Jiang, Y.Q., et al., *Increased heat shock transcription factor 1 in the cerebellum reverses the deficiency of Purkinje cells in Alzheimer's disease*. Brain Res, 2013. **1519**: p. 105-11.
23. Hohfeld, J., D.M. Cyr, and C. Patterson, *From the cradle to the grave: molecular chaperones that may choose between folding and degradation*. EMBO reports, 2001. **2**(10): p. 885-90.
24. Akerfelt, M., R.I. Morimoto, and L. Sistonen, *Heat shock factors: integrators of cell stress, development and lifespan*. Nat Rev Mol Cell Biol, 2010. **11**(8): p. 545-55.
25. Perez, F.P., et al., *Late-onset Alzheimer's disease, heating up and foxed by several proteins: pathomolecular effects of the aging process*. J Alzheimers Dis, 2014. **40**(1): p. 1-17.
26. Yoo, B.C., et al., *Differential expression of molecular chaperones in brain of patients with Down syndrome*. Electrophoresis, 2001. **22**(6): p. 1233-41.
27. Loones, M.T., Y. Chang, and M. Morange, *The distribution of heat shock proteins in the nervous system of the unstressed mouse embryo suggests a role in neuronal and non-neuronal differentiation*. Cell Stress Chaperones, 2000. **5**(4): p. 291-305.

28. Kakkar, V., et al., *Barcoding heat shock proteins to human diseases: looking beyond the heat shock response*. Dis Model Mech, 2014. **7**(4): p. 421-34.
29. Hansen, J.J., et al., *Hereditary spastic paraplegia SPG13 is associated with a mutation in the gene encoding the mitochondrial chaperonin Hsp60*. Am J Hum Genet, 2002. **70**(5): p. 1328-32.
30. Koutras, C. and J.E. Braun, *J protein mutations and resulting proteostasis collapse*. Front Cell Neurosci, 2014. **8**: p. 191.
31. Gorman, A.M., *Neuronal cell death in neurodegenerative diseases: recurring themes around protein handling*. J Cell Mol Med, 2008. **12**(6A): p. 2263-80.
32. Levy, O.A., C. Malagelada, and L.A. Greene, *Cell death pathways in Parkinson's disease: proximal triggers, distal effectors, and final steps*. Apoptosis, 2009. **14**(4): p. 478-500.
33. Bezprozvanny, I., *Calcium signaling and neurodegenerative diseases*. Trends Mol Med, 2009. **15**(3): p. 89-100.
34. Danysz, W. and C.G. Parsons, *Alzheimer's disease, beta-amyloid, glutamate, NMDA receptors and memantine--searching for the connections*. Br J Pharmacol, 2012. **167**(2): p. 324-52.
35. Lakhan, S.E., M. Caro, and N. Hadzimichalis, *NMDA Receptor Activity in Neuropsychiatric Disorders*. Front Psychiatry, 2013. **4**: p. 52.
36. Lindholm, D., H. Wootz, and L. Korhonen, *ER stress and neurodegenerative diseases*. Cell Death Differ, 2006. **13**(3): p. 385-92.
37. Nixon, R.A. and D.S. Yang, *Autophagy and neuronal cell death in neurological disorders*. Cold Spring Harb Perspect Biol, 2012. **4**(10).
38. Kim, J., et al., *Beta-amyloid oligomers activate apoptotic BAK pore for cytochrome c release*. Biophys J, 2014. **107**(7): p. 1601-8.
39. Zarei, S., et al., *A comprehensive review of amyotrophic lateral sclerosis*. Surg Neurol Int, 2015. **6**: p. 171.
40. Liu, A.Y., et al., *Neuroprotective drug riluzole amplifies the heat shock factor 1 (HSF1)- and glutamate transporter 1 (GLT1)-dependent cytoprotective mechanisms for neuronal survival*. The Journal of biological chemistry, 2011. **286**(4): p. 2785-94.
41. Guerrero, E.N., et al., *TDP-43/FUS in motor neuron disease: Complexity and challenges*. Prog Neurobiol, 2016.
42. Souza, P.V., et al., *Clinical and genetic basis of familial amyotrophic lateral sclerosis*. Arq Neuropsiquiatr, 2015. **73**(12): p. 1026-37.
43. Cirulli, E.T., et al., *Exome sequencing in amyotrophic lateral sclerosis identifies risk genes and pathways*. Science, 2015. **347**(6229): p. 1436-41.
44. Ng, A.S., R. Rademakers, and B.L. Miller, *Frontotemporal dementia: a bridge between dementia and neuromuscular disease*. Ann N Y Acad Sci, 2015. **1338**: p. 71-93.

45. Donnelly, C.J., et al., *RNA toxicity from the ALS/FTD C9ORF72 expansion is mitigated by antisense intervention*. Neuron, 2013. **80**(2): p. 415-28.
46. Renton, A.E., A. Chio, and B.J. Traynor, *State of play in amyotrophic lateral sclerosis genetics*. Nat Neurosci, 2014. **17**(1): p. 17-23.
47. Boillee, S., C. Vande Velde, and D.W. Cleveland, *ALS: a disease of motor neurons and their nonneuronal neighbors*. Neuron, 2006. **52**(1): p. 39-59.
48. Saccon, R.A., et al., *Is SOD1 loss of function involved in amyotrophic lateral sclerosis?* Brain, 2013. **136**(Pt 8): p. 2342-58.
49. Philips, T. and J.D. Rothstein, *Rodent Models of Amyotrophic Lateral Sclerosis*. Curr Protoc Pharmacol, 2015. **69**: p. 5 67 1-21.
50. Kaur, S.J., S.R. McKeown, and S. Rashid, *Mutant SOD1 mediated pathogenesis of Amyotrophic Lateral Sclerosis*. Gene, 2016. **577**(2): p. 109-18.
51. Hayashi, Y., K. Homma, and H. Ichijo, *SOD1 in neurotoxicity and its controversial roles in SOD1 mutation-negative ALS*. Adv Biol Regul, 2016. **60**: p. 95-104.
52. Banci, L., et al., *SOD1 and amyotrophic lateral sclerosis: mutations and oligomerization*. PLoS One, 2008. **3**(2): p. e1677.
53. Subramaniam, J.R., et al., *Mutant SOD1 causes motor neuron disease independent of copper chaperone-mediated copper loading*. Nat Neurosci, 2002. **5**(4): p. 301-7.
54. Turner, B.J. and K. Talbot, *Transgenics, toxicity and therapeutics in rodent models of mutant SOD1-mediated familial ALS*. Progress in neurobiology, 2008. **85**(1): p. 94-134.
55. Joyce, P.I., et al., *SOD1 and TDP-43 animal models of amyotrophic lateral sclerosis: recent advances in understanding disease toward the development of clinical treatments*. Mamm Genome, 2011. **22**(7-8): p. 420-48.
56. Shi, P., et al., *Effects of ALS-related SOD1 mutants on dynein- and KIF5-mediated retrograde and anterograde axonal transport*. Biochim Biophys Acta, 2010. **1802**(9): p. 707-16.
57. Philips, T. and J.D. Rothstein, *Glial cells in amyotrophic lateral sclerosis*. Exp Neurol, 2014. **262 Pt B**: p. 111-20.
58. Lin, C.L., et al., *Aberrant RNA processing in a neurodegenerative disease: the cause for absent EAAT2, a glutamate transporter, in amyotrophic lateral sclerosis*. Neuron, 1998. **20**(3): p. 589-602.
59. Arai, T., et al., *TDP-43 is a component of ubiquitin-positive tau-negative inclusions in frontotemporal lobar degeneration and amyotrophic lateral sclerosis*. Biochem Biophys Res Commun, 2006. **351**(3): p. 602-11.
60. Ishihara, T., et al., *[The implications of TDP-43 mutations in pathogenesis of amyotrophic lateral sclerosis]*. Brain Nerve, 2009. **61**(11): p. 1301-7.

61. Krecic, A.M. and M.S. Swanson, *hnRNP complexes: composition, structure, and function*. Curr Opin Cell Biol, 1999. **11**(3): p. 363-71.
62. Polymenidou, M., et al., *Long pre-mRNA depletion and RNA missplicing contribute to neuronal vulnerability from loss of TDP-43*. Nature neuroscience, 2011. **14**(4): p. 459-68.
63. Ayala, Y.M., et al., *TDP-43 regulates its mRNA levels through a negative feedback loop*. EMBO J, 2011. **30**(2): p. 277-88.
64. Alami, N.H., et al., *Axonal transport of TDP-43 mRNA granules is impaired by ALS-causing mutations*. Neuron, 2014. **81**(3): p. 536-43.
65. Orru, S., et al., *Reduced stress granule formation and cell death in fibroblasts with the A382T mutation of TARDBP gene: evidence for loss of TDP-43 nuclear function*. Hum Mol Genet, 2016.
66. Shorter, J. and J.P. Taylor, *Disease mutations in the prion-like domains of hnRNPA1 and hnRNPA2/B1 introduce potent steric zippers that drive excess RNP granule assembly*. Rare Dis, 2013. **1**: p. e25200.
67. Neumann, M., et al., *Ubiquitinated TDP-43 in frontotemporal lobar degeneration and amyotrophic lateral sclerosis*. Science, 2006. **314**(5796): p. 130-3.
68. Brettschneider, J., et al., *TDP-43 pathology and neuronal loss in amyotrophic lateral sclerosis spinal cord*. Acta Neuropathol, 2014. **128**(3): p. 423-37.
69. Iguchi, Y., et al., *Loss of TDP-43 causes age-dependent progressive motor neuron degeneration*. Brain, 2013. **136**(Pt 5): p. 1371-82.
70. Sephton, C.F., et al., *TDP-43 is a developmentally regulated protein essential for early embryonic development*. J Biol Chem, 2010. **285**(9): p. 6826-34.
71. Walker, A.K., et al., *Functional recovery in new mouse models of ALS/FTLD after clearance of pathological cytoplasmic TDP-43*. Acta Neuropathol, 2015. **130**(5): p. 643-60.
72. Wils, H., et al., *TDP-43 transgenic mice develop spastic paralysis and neuronal inclusions characteristic of ALS and frontotemporal lobar degeneration*. Proc Natl Acad Sci U S A, 2010. **107**(8): p. 3858-63.
73. Caccamo, A., S. Majumder, and S. Oddo, *Cognitive decline typical of frontotemporal lobar degeneration in transgenic mice expressing the 25-kDa C-terminal fragment of TDP-43*. Am J Pathol, 2012. **180**(1): p. 293-302.
74. Dayton, R.D., et al., *Selective forelimb impairment in rats expressing a pathological TDP-43 25 kDa C-terminal fragment to mimic amyotrophic lateral sclerosis*. Mol Ther, 2013. **21**(7): p. 1324-34.
75. Liu, Y.C., P.M. Chiang, and K.J. Tsai, *Disease animal models of TDP-43 proteinopathy and their pre-clinical applications*. Int J Mol Sci, 2013. **14**(10): p. 20079-111.

76. Mitchell, J.C., et al., *Wild type human TDP-43 potentiates ALS-linked mutant TDP-43 driven progressive motor and cortical neuron degeneration with pathological features of ALS*. Acta Neuropathol Commun, 2015. **3**: p. 36.
77. Fang, Y.S., et al., *Full-length TDP-43 forms toxic amyloid oligomers that are present in frontotemporal lobar dementia-TDP patients*. Nat Commun, 2014. **5**: p. 4824.
78. Wang, W., et al., *The inhibition of TDP-43 mitochondrial localization blocks its neuronal toxicity*. Nat Med, 2016. **22**(8): p. 869-78.
79. Kim, H.J., et al., *Therapeutic modulation of eIF2alpha phosphorylation rescues TDP-43 toxicity in amyotrophic lateral sclerosis disease models*. Nat Genet, 2014. **46**(2): p. 152-60.
80. Wang, X., et al., *Activation of ER Stress and Autophagy Induced by TDP-43 A315T as Pathogenic Mechanism and the Corresponding Histological Changes in Skin as Potential Biomarker for ALS with the Mutation*. Int J Biol Sci, 2015. **11**(10): p. 1140-9.
81. Anckar, J. and L. Sistonen, *Regulation of HSF1 Function in the Heat Stress Response: Implications in Aging and Disease*. Annual Review of Biochemistry, Vol 80, 2011. **80**: p. 1089-1115.
82. Vihervaara, A. and L. Sistonen, *HSF1 at a glance*. J Cell Sci, 2014. **127**(Pt 2): p. 261-6.
83. Ritossa, F., *Discovery of the heat shock response*. Cell Stress Chaperones, 1996. **1**(2): p. 97-8.
84. Homma, S., et al., *Demyelination, astrogliosis, and accumulation of ubiquitinated proteins, hallmarks of CNS disease in hsf1-deficient mice*. J Neurosci, 2007. **27**(30): p. 7974-86.
85. Hayashida, N., *Non-Hsp genes are essential for HSF1-mediated maintenance of whole body homeostasis*. Exp Anim, 2015. **64**(4): p. 397-406.
86. Neef, D.W., A.M. Jaeger, and D.J. Thiele, *Heat shock transcription factor 1 as a therapeutic target in neurodegenerative diseases*. Nat Rev Drug Discov, 2011. **10**(12): p. 930-44.
87. Hooper, P.L., et al., *The central role of heat shock factor 1 in synaptic fidelity and memory consolidation*. Cell Stress Chaperones, 2016. **21**(5): p. 745-53.
88. Zou, J., et al., *Repression of heat shock transcription factor HSF1 activation by HSP90 (HSP90 complex) that forms a stress-sensitive complex with HSF1*. Cell, 1998. **94**(4): p. 471-80.
89. Bharadwaj, S., A. Ali, and N. Ovsenek, *Multiple components of the HSP90 chaperone complex function in regulation of heat shock factor 1 In vivo*. Mol Cell Biol, 1999. **19**(12): p. 8033-41.
90. Budzynski, M.A., et al., *Uncoupling Stress-Inducible Phosphorylation of Heat Shock Factor 1 from Its Activation*. Mol Cell Biol, 2015. **35**(14): p. 2530-40.



91. Holmberg, C.I., et al., *Phosphorylation of serine 230 promotes inducible transcriptional activity of heat shock factor 1*. EMBO J, 2001. **20**(14): p. 3800-10.
92. Wang, X., et al., *Phosphorylation of HSF1 by MAPK-activated protein kinase 2 on serine 121, inhibits transcriptional activity and promotes HSP90 binding*. J Biol Chem, 2006. **281**(2): p. 782-91.
93. Kim, S.A., et al., *Polo-like kinase 1 phosphorylates heat shock transcription factor 1 and mediates its nuclear translocation during heat stress*. J Biol Chem, 2005. **280**(13): p. 12653-7.
94. Westerheide, S.D., et al., *Stress-inducible regulation of heat shock factor 1 by the deacetylase SIRT1*. Science, 2009. **323**(5917): p. 1063-6.
95. Batulan, Z., et al., *High threshold for induction of the stress response in motor neurons is associated with failure to activate HSF1*. The Journal of neuroscience : the official journal of the Society for Neuroscience, 2003. **23**(13): p. 5789-98.
96. Kim, E., et al., *NEDD4-mediated HSF1 degradation underlies alpha-synucleinopathy*. Hum Mol Genet, 2016. **25**(2): p. 211-22.
97. Ingenwerth, M., et al., *HSF1-deficiency affects gait coordination and cerebellar calbindin levels*. Behavioural Brain Research, 2016. **310**: p. 103-108.
98. Muchowski, P.J., et al., *Hsp70 and hsp40 chaperones can inhibit self-assembly of polyglutamine proteins into amyloid-like fibrils*. Proc Natl Acad Sci U S A, 2000. **97**(14): p. 7841-6.
99. Fujimoto, M., et al., *Active HSF1 significantly suppresses polyglutamine aggregate formation in cellular and mouse models*. The Journal of biological chemistry, 2005. **280**(41): p. 34908-16.
100. Petrucelli, L., et al., *CHIP and Hsp70 regulate tau ubiquitination, degradation and aggregation*. Hum Mol Genet, 2004. **13**(7): p. 703-14.
101. Shen, H.Y., et al., *Geldanamycin induces heat shock protein 70 and protects against MPTP-induced dopaminergic neurotoxicity in mice*. J Biol Chem, 2005. **280**(48): p. 39962-9.
102. Zhang, T., et al., *Characterization of celastrol to inhibit hsp90 and cdc37 interaction*. J Biol Chem, 2009. **284**(51): p. 35381-9.
103. Paris, D., et al., *Reduction of beta-amyloid pathology by celastrol in a transgenic mouse model of Alzheimer's disease*. J Neuroinflammation, 2010. **7**: p. 17.
104. Kiaei, M., et al., *Celastrol blocks neuronal cell death and extends life in transgenic mouse model of amyotrophic lateral sclerosis*. Neurodegener Dis, 2005. **2**(5): p. 246-54.
105. Cleren, C., et al., *Celastrol protects against MPTP- and 3-nitropropionic acid-induced neurotoxicity*. J Neurochem, 2005. **94**(4): p. 995-1004.
106. Neef, D.W., M.L. Turski, and D.J. Thiele, *Modulation of heat shock transcription factor 1 as a therapeutic target for small molecule intervention in neurodegenerative disease*. PLoS Biol, 2010. **8**(1): p. e1000291.

107. Kim, S. and K.T. Kim, *Therapeutic Approaches for Inhibition of Protein Aggregation in Huntington's Disease*. Exp Neurobiol, 2014. **23**(1): p. 36-44.
108. Nakai, A., M. Suzuki, and M. Tanabe, *Arrest of spermatogenesis in mice expressing an active heat shock transcription factor 1*. EMBO J, 2000. **19**(7): p. 1545-54.
109. Lin, P.Y., et al., *Heat shock factor 1 over-expression protects against exposure of hydrophobic residues on mutant SOD1 and early mortality in a mouse model of amyotrophic lateral sclerosis*. Molecular neurodegeneration, 2013. **8**: p. 43.
110. Pierce, A., et al., *Over-expression of heat shock factor 1 phenocopies the effect of chronic inhibition of TOR by rapamycin and is sufficient to ameliorate Alzheimer's-like deficits in mice modeling the disease*. Journal of neurochemistry, 2013. **124**(6): p. 880-93.
111. Lin, P.Y., et al., *Overexpression of heat shock factor 1 maintains TAR DNA binding protein 43 solubility via induction of inducible heat shock protein 70 in cultured cells*. J Neurosci Res, 2016. **94**(7): p. 671-82.
112. Han, S., et al., *Resveratrol upregulated heat shock proteins and extended the survival of G93A-SOD1 mice*. Brain Res, 2012. **1483**: p. 112-7.
113. Watanabe, S., et al., *SIRT1 overexpression ameliorates a mouse model of SOD1-linked amyotrophic lateral sclerosis via HSF1/HSP70i chaperone system*. Mol Brain, 2014. **7**: p. 62.
114. Rosen, D.R., et al., *Mutations in Cu/Zn superoxide dismutase gene are associated with familial amyotrophic lateral sclerosis*. Nature, 1993. **362**(6415): p. 59-62.
115. Kabashi, E., et al., *TARDBP mutations in individuals with sporadic and familial amyotrophic lateral sclerosis*. Nature genetics, 2008. **40**(5): p. 572-4.
116. Valentine, J.S., P.A. Doucette, and S. Zittin Potter, *Copper-zinc superoxide dismutase and amyotrophic lateral sclerosis*. Annual review of biochemistry, 2005. **74**: p. 563-93.
117. Lelie, H.L., et al., *Copper and zinc metallation status of copper-zinc superoxide dismutase from amyotrophic lateral sclerosis transgenic mice*. The Journal of biological chemistry, 2011. **286**(4): p. 2795-806.
118. Pasinelli, P. and R.H. Brown, *Molecular biology of amyotrophic lateral sclerosis: insights from genetics*. Nature reviews. Neuroscience, 2006. **7**(9): p. 710-23.
119. Tiwari, A., et al., *Metal deficiency increases aberrant hydrophobicity of mutant superoxide dismutases that cause amyotrophic lateral sclerosis*. J Biol Chem, 2009. **284**(40): p. 27746-58.
120. Tiwari, A., Z. Xu, and L.J. Hayward, *Aberrantly increased hydrophobicity shared by mutants of Cu,Zn-superoxide dismutase in familial amyotrophic lateral sclerosis*. The Journal of biological chemistry, 2005. **280**(33): p. 29771-9.
121. Sanchez de Groot, N., et al., *Prediction of "hot spots" of aggregation in disease-linked polypeptides*. BMC structural biology, 2005. **5**: p. 18.

122. Pawar, A.P., et al., *Prediction of "aggregation-prone" and "aggregation-susceptible" regions in proteins associated with neurodegenerative diseases*. Journal of molecular biology, 2005. **350**(2): p. 379-92.
123. Chaudhuri, T.K. and P. Gupta, *Factors governing the substrate recognition by GroEL chaperone: a sequence correlation approach*. Cell stress & chaperones, 2005. **10**(1): p. 24-36.
124. Rudiger, S., et al., *Substrate specificity of the DnaK chaperone determined by screening cellulose-bound peptide libraries*. The EMBO journal, 1997. **16**(7): p. 1501-7.
125. Blond-Elguindi, S., et al., *Affinity panning of a library of peptides displayed on bacteriophages reveals the binding specificity of BiP*. Cell, 1993. **75**(4): p. 717-28.
126. Xu, X., et al., *Unique peptide substrate binding properties of 110-kDa heat-shock protein (Hsp110) determine its distinct chaperone activity*. The Journal of biological chemistry, 2012. **287**(8): p. 5661-72.
127. Kaushik, S. and A.M. Cuervo, *Chaperones in autophagy*. Pharmacological research : the official journal of the Italian Pharmacological Society, 2012. **66**(6): p. 484-93.
128. Winkler, D.D., et al., *Structural and biophysical properties of the pathogenic SOD1 variant H46R/H48Q*. Biochemistry, 2009. **48**(15): p. 3436-47.
129. Pierce, A., et al., *A Novel Approach for Screening the Proteome for Changes in Protein Conformation*. Biochemistry, 2006. **45**(9): p. 3077-3085.
130. Prosinecki, V., P.F.N. Faísca, and C.M. Gomes, *Conformational States and Protein Stability from a Proteomic Perspective*. Current Proteomics, 2007. **4**: p. 44-52.
131. Pierce, A.P., et al., *Oxidation and structural perturbation of redox-sensitive enzymes in injured skeletal muscle*. Free Radic Biol Med, 2007. **43**(12): p. 1584-93.
132. Pierce, A., et al., *GAPDH is conformationally and functionally altered in association with oxidative stress in mouse models of amyotrophic lateral sclerosis*. J Mol Biol, 2008. **382**(5): p. 1195-210.
133. Barrett, A.D., et al., *New vaccine development for chronic brain disease*. Neuropsychopharmacology : official publication of the American College of Neuropsychopharmacology, 2010. **35**(1): p. 354.
134. Sarge, K.D., S.P. Murphy, and R.I. Morimoto, *Activation of heat shock gene transcription by heat shock factor 1 involves oligomerization, acquisition of DNA-binding activity, and nuclear localization and can occur in the absence of stress*. Mol Cell Biol, 1993. **13**(3): p. 1392-407.
135. Kieran, D., et al., *Treatment with arimoclomol, a coinducer of heat shock proteins, delays disease progression in ALS mice*. Nat Med, 2004. **10**(4): p. 402-5.

136. Phukan, J., *Arimoclomol, a coinducer of heat shock proteins for the potential treatment of amyotrophic lateral sclerosis*. IDrugs : the investigational drugs journal, 2010. **13**(7): p. 482-96.
137. Yang, J., et al., *Riluzole increases the amount of latent HSF1 for an amplified heat shock response and cytoprotection*. PloS one, 2008. **3**(8): p. e2864.
138. Pierce, A., et al., *A Novel mouse model of enhanced proteostasis: Full-length human heat shock factor 1 transgenic mice*. Biochemical and biophysical research communications, 2010. **402**(1): p. 59-65.
139. Xue, H., D. Slavov, and P.E. Wischmeyer, *Glutamine-mediated dual regulation of heat shock transcription factor-1 activation and expression*. The Journal of biological chemistry, 2012. **287**(48): p. 40400-13.
140. Morley, J.F. and R.I. Morimoto, *Regulation of longevity in Caenorhabditis elegans by heat shock factor and molecular chaperones*. Mol Biol Cell, 2004. **15**(2): p. 657-64.
141. Gregory, J.M., et al., *The aggregation and neurotoxicity of TDP-43 and its ALS-associated 25 kDa fragment are differentially affected by molecular chaperones in Drosophila*. PloS one, 2012. **7**(2): p. e31899.
142. Steele, A.D., et al., *Heat shock factor 1 regulates lifespan as distinct from disease onset in prion disease*. Proc Natl Acad Sci U S A, 2008. **105**(36): p. 13626-31.
143. Pierce, A., et al., *Over-expression of heat shock factor 1 phenocopies the effect of chronic inhibition of TOR by rapamycin and is sufficient to ameliorate Alzheimer's-like deficits in mice modeling the disease*. J Neurochem, 2013. **124**(6): p. 880-93.
144. Wang, J., et al., *Fibrillar inclusions and motor neuron degeneration in transgenic mice expressing superoxide dismutase 1 with a disrupted copper-binding site*. Neurobiology of disease, 2002. **10**(2): p. 128-38.
145. Smith, R.A., et al., *Antisense oligonucleotide therapy for neurodegenerative disease*. The Journal of clinical investigation, 2006. **116**(8): p. 2290-6.
146. Hefferan, M.P., et al., *Human neural stem cell replacement therapy for amyotrophic lateral sclerosis by spinal transplantation*. PloS one, 2012. **7**(8): p. e42614.
147. Shi, L., D.R. Palleros, and A.L. Fink, *Protein conformational changes induced by 1,1'-bis(4-anilino-5-naphthalenesulfonic acid): preferential binding to the molten globule of DnaK*. Biochemistry, 1994. **33**(24): p. 7536-46.
148. Trott, O. and A.J. Olson, *AutoDock Vina: improving the speed and accuracy of docking with a new scoring function, efficient optimization, and multithreading*. Journal of computational chemistry, 2010. **31**(2): p. 455-61.
149. Di Poto, C., et al., *Optimizing separation efficiency of 2-DE procedures for visualization of different superoxide dismutase forms in a cellular model of amyotrophic lateral sclerosis*. Electrophoresis, 2007. **28**(23): p. 4340-7.

150. Munch, C. and A. Bertolotti, *Exposure of hydrophobic surfaces initiates aggregation of diverse ALS-causing superoxide dismutase-1 mutants*. Journal of molecular biology, 2010. **399**(3): p. 512-25.
151. Antonyuk, S., et al., *Structural consequences of the familial amyotrophic lateral sclerosis SOD1 mutant His46Arg*. Protein science : a publication of the Protein Society, 2005. **14**(5): p. 1201-13.
152. Wang, J., et al., *Disease-associated mutations at copper ligand histidine residues of superoxide dismutase 1 diminish the binding of copper and compromise dimer stability*. The Journal of biological chemistry, 2007. **282**(1): p. 345-52.
153. Zetterstrom, P., et al., *Proteins that bind to misfolded mutant superoxide dismutase-1 in spinal cords from transgenic amyotrophic lateral sclerosis (ALS) model mice*. The Journal of biological chemistry, 2011. **286**(23): p. 20130-6.
154. Kabuta, T., Y. Suzuki, and K. Wada, *Degradation of amyotrophic lateral sclerosis-linked mutant Cu,Zn-superoxide dismutase proteins by macroautophagy and the proteasome*. The Journal of biological chemistry, 2006. **281**(41): p. 30524-33.
155. Urushitani, M., et al., *CHIP promotes proteasomal degradation of familial ALS-linked mutant SOD1 by ubiquitinating Hsp/Hsc70*. Journal of neurochemistry, 2004. **90**(1): p. 231-44.
156. Kerman, A., et al., *Amyotrophic lateral sclerosis is a non-amyloid disease in which extensive misfolding of SOD1 is unique to the familial form*. Acta neuropathologica, 2010. **119**(3): p. 335-44.
157. Pokrishevsky, E., et al., *Aberrant localization of FUS and TDP43 is associated with misfolding of SOD1 in amyotrophic lateral sclerosis*. PloS one, 2012. **7**(4): p. e35050.
158. Bolognesi, B., et al., *ANS binding reveals common features of cytotoxic amyloid species*. ACS chemical biology, 2010. **5**(8): p. 735-40.
159. Dowjat, W.K., M. Kharatishvili, and M. Costa, *DNA and RNA strand scission by copper, zinc and manganese superoxide dismutases*. Biometals : an international journal on the role of metal ions in biology, biochemistry, and medicine, 1996. **9**(4): p. 327-35.
160. Jiang, W., et al., *DNA is a template for accelerating the aggregation of copper, zinc superoxide dismutase*. Biochemistry, 2007. **46**(20): p. 5911-23.
161. Ge, W.W., et al., *Mutant copper-zinc superoxide dismutase binds to and destabilizes human low molecular weight neurofilament mRNA*. The Journal of biological chemistry, 2005. **280**(1): p. 118-24.
162. Lu, L., et al., *Amyotrophic lateral sclerosis-linked mutant SOD1 sequesters Hu antigen R (HuR) and TIA-1-related protein (TIAR): implications for impaired post-transcriptional regulation of vascular endothelial growth factor*. The Journal of biological chemistry, 2009. **284**(49): p. 33989-98.

163. Basso, M., et al., *Characterization of detergent-insoluble proteins in ALS indicates a causal link between oxidative stress and aggregation in pathogenesis*. PloS one, 2009. **4**(12): p. e8130.
164. Jeffery, C.J., *Proteins with neomorphic moonlighting functions in disease*. IUBMB life, 2011. **63**(7): p. 489-94.
165. Pradat, P.F., et al., *Impaired glucose tolerance in patients with amyotrophic lateral sclerosis*. Amyotrophic lateral sclerosis : official publication of the World Federation of Neurology Research Group on Motor Neuron Diseases, 2010. **11**(1-2): p. 166-71.
166. Gonzalez de Aguilar, J.L., et al., *The metabolic hypothesis in amyotrophic lateral sclerosis: insights from mutant Cu/Zn-superoxide dismutase mice*. Biomedicine & pharmacotherapy = Biomedecine & pharmacotherapie, 2005. **59**(4): p. 190-6.
167. Yoshida, T. and M. Nakagawa, *Clinical aspects and pathology of Alexander disease, and morphological and functional alteration of astrocytes induced by GFAP mutation*. Neuropathology : official journal of the Japanese Society of Neuropathology, 2012. **32**(4): p. 440-6.
168. Voisine, C., J.S. Pedersen, and R.I. Morimoto, *Chaperone networks: tipping the balance in protein folding diseases*. Neurobiology of disease, 2010. **40**(1): p. 12-20.
169. Fan, H., R.S. Kashi, and C.R. Middaugh, *Conformational lability of two molecular chaperones Hsc70 and gp96: effects of pH and temperature*. Archives of biochemistry and biophysics, 2006. **447**(1): p. 34-45.
170. Lee, J.P., et al., *The role of immunophilins in mutant superoxide dismutase-linked familial amyotrophic lateral sclerosis*. Proceedings of the National Academy of Sciences of the United States of America, 1999. **96**(6): p. 3251-6.
171. Saigoh, K., et al., *Intragenic deletion in the gene encoding ubiquitin carboxy-terminal hydrolase in gad mice*. Nature genetics, 1999. **23**(1): p. 47-51.
172. Day, I.N. and R.J. Thompson, *UCHL1 (PGP 9.5): neuronal biomarker and ubiquitin system protein*. Progress in neurobiology, 2010. **90**(3): p. 327-62.
173. Liu, Y., et al., *The UCH-L1 gene encodes two opposing enzymatic activities that affect alpha-synuclein degradation and Parkinson's disease susceptibility*. Cell, 2002. **111**(2): p. 209-18.
174. Steinacker, P., A. Aitken, and M. Otto, *14-3-3 proteins in neurodegeneration*. Seminars in cell & developmental biology, 2011. **22**(7): p. 696-704.
175. Ge, W.W., et al., *14-3-3 protein binds to the low molecular weight neurofilament (NFL) mRNA 3' UTR*. Molecular and cellular neurosciences, 2007. **34**(1): p. 80-7.
176. Ge, F., et al., *Identification of novel 14-3-3zeta interacting proteins by quantitative immunoprecipitation combined with knockdown (QUICK)*. Journal of proteome research, 2010. **9**(11): p. 5848-58.

177. Johnson, C., et al., *Bioinformatic and experimental survey of 14-3-3-binding sites*. The Biochemical journal, 2010. **427**(1): p. 69-78.
178. Sluchanko, N.N., et al., *Effect of mutations mimicking phosphorylation on the structure and properties of human 14-3-3zeta*. Archives of biochemistry and biophysics, 2008. **477**(2): p. 305-12.
179. Zhou, J., et al., *Serine 58 of 14-3-3zeta is a molecular switch regulating ASK1 and oxidant stress-induced cell death*. Molecular and cellular biology, 2009. **29**(15): p. 4167-76.
180. Xu, G., et al., *Cytosolic proteins lose solubility as amyloid deposits in a transgenic mouse model of Alzheimer-type amyloidosis*. Human molecular genetics, 2013. **22**(14): p. 2765-74.
181. den Engelsman, J., et al., *Pseudophosphorylated alphaB-crystallin is a nuclear chaperone imported into the nucleus with help of the SMN complex*. PloS one, 2013. **8**(9): p. e73489.
182. Boelens, W.C., Y. Croes, and W.W. de Jong, *Interaction between alphaB-crystallin and the human 20S proteasomal subunit C8/alpha7*. Biochimica et biophysica acta, 2001. **1544**(1-2): p. 311-9.
183. Julien, J.P. and J. Kriz, *Transgenic mouse models of amyotrophic lateral sclerosis*. Biochimica et biophysica acta, 2006. **1762**(11-12): p. 1013-24.
184. Ilieva, H., M. Polymenidou, and D.W. Cleveland, *Non-cell autonomous toxicity in neurodegenerative disorders: ALS and beyond*. The Journal of cell biology, 2009. **187**(6): p. 761-72.
185. Yamanaka, K., et al., *Mutant SOD1 in cell types other than motor neurons and oligodendrocytes accelerates onset of disease in ALS mice*. Proceedings of the National Academy of Sciences of the United States of America, 2008. **105**(21): p. 7594-9.
186. Boillee, S., et al., *Onset and progression in inherited ALS determined by motor neurons and microglia*. Science, 2006. **312**(5778): p. 1389-92.
187. Sreedharan, J., et al., *TDP-43 mutations in familial and sporadic amyotrophic lateral sclerosis*. Science, 2008. **319**(5870): p. 1668-72.
188. Josephs, K.A., et al., *TDP-43 is a key player in the clinical features associated with Alzheimer's disease*. Acta neuropathologica, 2014. **127**(6): p. 811-24.
189. Rohrer, J.D., et al., *Clinical and neuroanatomical signatures of tissue pathology in frontotemporal lobar degeneration*. Brain : a journal of neurology, 2011. **134**(Pt 9): p. 2565-81.
190. Mackenzie, I.R., et al., *Pathological TDP-43 distinguishes sporadic amyotrophic lateral sclerosis from amyotrophic lateral sclerosis with SOD1 mutations*. Annals of neurology, 2007. **61**(5): p. 427-34.
191. Stalekar, M., et al., *Proteomic analyses reveal that loss of TDP-43 affects RNA processing and intracellular transport*. Neuroscience, 2015. **293**: p. 157-70.

192. Tollervey, J.R., et al., *Characterizing the RNA targets and position-dependent splicing regulation by TDP-43*. Nature neuroscience, 2011. **14**(4): p. 452-8.
193. Nonaka, T., et al., *Prion-like properties of pathological TDP-43 aggregates from diseased brains*. Cell reports, 2013. **4**(1): p. 124-34.
194. Dormann, D., et al., *Proteolytic processing of TAR DNA binding protein-43 by caspases produces C-terminal fragments with disease defining properties independent of progranulin*. J Neurochem, 2009. **110**(3): p. 1082-94.
195. Kleinberger, G., et al., *Increased caspase activation and decreased TDP-43 solubility in progranulin knockout cortical cultures*. Journal of neurochemistry, 2010. **115**(3): p. 735-47.
196. Zhang, Y.J., et al., *Progranulin mediates caspase-dependent cleavage of TAR DNA binding protein-43*. J Neurosci, 2007. **27**(39): p. 10530-4.
197. Zhang, Y.J., et al., *Aberrant cleavage of TDP-43 enhances aggregation and cellular toxicity*. Proceedings of the National Academy of Sciences of the United States of America, 2009. **106**(18): p. 7607-12.
198. Westerheide, S.D. and R.I. Morimoto, *Heat shock response modulators as therapeutic tools for diseases of protein conformation*. J Biol Chem, 2005. **280**(39): p. 33097-100.
199. Batulan, Z., et al., *High threshold for induction of the stress response in motor neurons is associated with failure to activate HSF1*. J Neurosci, 2003. **23**(13): p. 5789-98.
200. Jackrel, M.E., et al., *Potentiated hsp104 variants antagonize diverse proteotoxic misfolding events*. Cell, 2014. **156**(1-2): p. 170-82.
201. Jinwal, U.K., et al., *Cdc37/Hsp90 protein complex disruption triggers an autophagic clearance cascade for TDP-43 protein*. The Journal of biological chemistry, 2012. **287**(29): p. 24814-20.
202. Udan-Johns, M., et al., *Prion-like nuclear aggregation of TDP-43 during heat shock is regulated by HSP40/70 chaperones*. Human molecular genetics, 2014. **23**(1): p. 157-70.
203. Chang, H.Y., et al., *Heat-shock protein dysregulation is associated with functional and pathological TDP-43 aggregation*. Nature communications, 2013. **4**: p. 2757.
204. Liu, A.Y., et al., *Neuroprotective drug riluzole amplifies the heat shock factor 1 (HSF1)- and glutamate transporter 1 (GLT1)-dependent cytoprotective mechanisms for neuronal survival*. J Biol Chem, 2011. **286**(4): p. 2785-94.
205. Yang, C., et al., *The C-terminal TDP-43 fragments have a high aggregation propensity and harm neurons by a dominant-negative mechanism*. PloS one, 2010. **5**(12): p. e15878.



206. McMillan, D.R., et al., *Targeted disruption of heat shock transcription factor 1 abolishes thermotolerance and protection against heat-inducible apoptosis*. J Biol Chem, 1998. **273**(13): p. 7523-8.
207. van Eersel, J., et al., *Cytoplasmic accumulation and aggregation of TDP-43 upon proteasome inhibition in cultured neurons*. PLoS One, 2011. **6**(7): p. e22850.
208. Yoon, Y.J., et al., *KRIBB11 inhibits HSP70 synthesis through inhibition of heat shock factor 1 function by impairing the recruitment of positive transcription elongation factor b to the hsp70 promoter*. J Biol Chem, 2011. **286**(3): p. 1737-47.
209. Araki, W., et al., *Disease-associated mutations of TDP-43 promote turnover of the protein through the proteasomal pathway*. Mol Neurobiol, 2014. **50**(3): p. 1049-58.
210. Liu, Y., et al., *A new cellular model of pathological TDP-43: The neurotoxicity of stably expressed CTF25 of TDP-43 depends on the proteasome*. Neuroscience, 2014. **281C**: p. 88-98.
211. Barmada, S.J., et al., *Autophagy induction enhances TDP43 turnover and survival in neuronal ALS models*. Nat Chem Biol, 2014. **10**(8): p. 677-85.
212. Urushitani, M., et al., *Synergistic effect between proteasome and autophagosome in the clearance of polyubiquitinated TDP-43*. J Neurosci Res, 2010. **88**(4): p. 784-97.
213. Samarasinghe, B., et al., *Heat shock factor 1 confers resistance to Hsp90 inhibitors through p62/SQSTM1 expression and promotion of autophagic flux*. Biochem Pharmacol, 2014. **87**(3): p. 445-55.
214. Bentmann, E., C. Haass, and D. Dormann, *Stress granules in neurodegeneration--lessons learnt from TAR DNA binding protein of 43 kDa and fused in sarcoma*. FEBS J, 2013. **280**(18): p. 4348-70.
215. Taylor, D.M., et al., *Proteasome activity or expression is not altered by activation of the heat shock transcription factor Hsf1 in cultured fibroblasts or myoblasts*. Cell Stress Chaperones, 2005. **10**(3): p. 230-41.
216. Dasuri, K., et al., *Selective vulnerability of neurons to acute toxicity after proteasome inhibitor treatment: implications for oxidative stress and insolubility of newly synthesized proteins*. Free radical biology & medicine, 2010. **49**(8): p. 1290-7.
217. Desai, S., et al., *Heat shock factor 1 (HSF1) controls chemoresistance and autophagy through transcriptional regulation of autophagy-related protein 7 (ATG7)*. The Journal of biological chemistry, 2013. **288**(13): p. 9165-76.
218. Huang, C., et al., *Mutant TDP-43 in motor neurons promotes the onset and progression of ALS in rats*. J Clin Invest, 2012. **122**(1): p. 107-18.
219. Walker, A.K., et al., *Functional recovery in new mouse models of ALS/FTLD after clearance of pathological cytoplasmic TDP-43*. Acta neuropathologica, 2015.

220. Pierce, A., et al., *A Novel mouse model of enhanced proteostasis: Full-length human heat shock factor 1 transgenic mice*. Biochem Biophys Res Commun, 2010. **402**(1): p. 59-65.
221. Xu, Y.F., et al., *Expression of mutant TDP-43 induces neuronal dysfunction in transgenic mice*. Mol Neurodegener, 2011. **6**: p. 73.
222. Swarup, V., et al., *Pathological hallmarks of amyotrophic lateral sclerosis/frontotemporal lobar degeneration in transgenic mice produced with TDP-43 genomic fragments*. Brain, 2011. **134**(Pt 9): p. 2610-26.
223. Gunther, R., et al., *Clinical testing and spinal cord removal in a mouse model for amyotrophic lateral sclerosis (ALS)*. J Vis Exp, 2012(61).
224. Arnold, E.S., et al., *ALS-linked TDP-43 mutations produce aberrant RNA splicing and adult-onset motor neuron disease without aggregation or loss of nuclear TDP-43*. Proc Natl Acad Sci U S A, 2013. **110**(8): p. E736-45.
225. Huang, C.C., et al., *Metabolism and mis-metabolism of the neuropathological signature protein TDP-43*. J Cell Sci, 2014. **127**(Pt 14): p. 3024-38.
226. Cuervo, A.M. and E. Wong, *Chaperone-mediated autophagy: roles in disease and aging*. Cell Res, 2014. **24**(1): p. 92-104.
227. Shacka, J.J., K.A. Roth, and J. Zhang, *The autophagy-lysosomal degradation pathway: role in neurodegenerative disease and therapy*. Front Biosci, 2008. **13**: p. 718-36.
228. Torrente, M.P., et al., *Mechanistic Insights into Hsp104 Potentiation*. J Biol Chem, 2016. **291**(10): p. 5101-15.
229. Torrente, M.P. and J. Shorter, *The metazoan protein disaggregase and amyloid depolymerase system: Hsp110, Hsp70, Hsp40, and small heat shock proteins*. Prion, 2013. **7**(6): p. 457-63.
230. Kondo, N., et al., *Heat shock factor-1 influences pathological lesion distribution of polyglutamine-induced neurodegeneration*. Nat Commun, 2013. **4**: p. 1405.

## Vita

Oluwarotimi Folorunso was born on April 3, 1988 in Lagos, Nigeria to Oluwatomi (deceased) and Akanni Folorunso.

### Education

Towson University, Towson, MD  
Double Major, Chemistry and Biochemistry  
Bachelor of Science, Summa Cum laude May 2009

Newcastle University, Newcastle upon Tyne, United Kingdom  
TU Exchange – U.K Study Abroad Program Fall 2007

University of Texas Medical Branch (UTMB), Galveston, TX  
PhD Program: Biochemistry and Molecular Biology  
Principal Investigator: Anson Pierce

### Teaching/Mentoring Responsibilities

Teaching responsibility at University of Texas Medical Branch

**Course Co-Director:** Summer Methods and Techniques Series for students of the  
Biochemistry and Molecular Biology Program, 2015

**Instructor:** Introduction to Biological Systems (PREP program) 2014, 2015

**Small Groups Facilitator:** Biochemistry (BBSC 6401) 2012, 2014

### *Mentee*

Marcy Hanson, Ball High school Bench Program, 2014-2015

Teaching responsibility at College of the Mainland

**Lecturer:** Developmental Psychology, 2015

Teaching responsibility at Texas A & M Galveston

**Lecturer:** Fundamentals of Toxicology (MARB 414) 2015

Teaching responsibility at Towson University

**Teaching Assistant:** Chemistry for Health Professions, Towson University 2008

## **Publications**

### Peer-reviewed Manuscripts

Lin, P.-Y.\*, **Folorunso, O.\***, Taglialatela, G. and Pierce, A. (2016), Overexpression of heat shock factor 1 maintains TAR DNA binding protein 43 solubility via induction of inducible heat shock protein 70 in cultured cells. *Journal of Neuroscience Research*, 94: 671–682. doi:10.1002/jnr.23725. \* Equal contribution.

Lin PY, Simon SM, Koh WK, **Folorunso O**, Umbaugh CS, Pierce A. Heat shock factor 1 over-expression protects against exposure of hydrophobic residues on mutant SOD1 and early mortality in a mouse model of amyotrophic lateral sclerosis. *Molecular Neurodegeneration* 2013 Nov 21;8:43.

Permanent address: 921 marine drive, apt 219. Galveston, TX 77550

This dissertation was typed by Oluwarotimi Folorunso